Spring 4-10-2019

# The Influence of Process Variables on Physical and Mechanical Properties in Laser Powder Bed Fusion

Joshua Robert Koepke
*University of New Mexico*

Bradley Jared
*Sandia National Laboratories*

Yu-Lin Shen
*University of New Mexico*

## Recommended Citation

Koepke, Joshua Robert; Bradley Jared; and Yu-Lin Shen. "The Influence of Process Variables on Physical and Mechanical Properties in Laser Powder Bed Fusion." (2019). https://digitalrepository.unm.edu/me_etds/164

Joshua Koepke
*Candidate*

Mechanical Engineering
*Department*

This dissertation is approved, and it is acceptable in quality and form for publication:

*Approved by the Dissertation Committee:*

Yu-Lin Shen , Chairperson

Mehran Tehrani

Bradley Jared

# The Influence of Process Variables on Physical and Mechanical Properties in Laser Powder Bed Manufacturing

By

Joshua R. Koepke

B.S., Chemical Engineering, University of New Mexico, 2017

THESIS

Submitted in Partial Fulfillment of the
Requirements for the Degree of

Masters of Science
Mechanical Engineering

The University of New Mexico
Albuquerque, New Mexico

May 2019

# Acknowledgements

I would like to acknowledge everyone who supported me with this study and my journey through my master's degree.  My family and friends provided the encouragement to keep going when times got tough.  Dr. Bradley Jared for being my mentor at Sandia on this project. Dr.  Deidre Hirschfeld for helping with research guidance and for reviewing my thesis.  Dr. Yu-Lin Shen for guidance through my master's degree and being the chair of my defense committee.  Dr Mehran Tehrani for being part of my defense committee.  David Saiz for all his help with programming the experimental builds and assisting with the machine characterizations.  I couldn't have finished this study without all the others that helped with the testing of experiments, reviewing my paper, and supporting me in this project including, Michael Heiden, Shawn Whetton, Samantha Taylor, Andrew Kustas, Aron Robbins, Todd Huber, Ben Martinez, Ryan Hill, and to anyone else I may have inadvertently left out.

Sandia National Laboratories is a multimission laboratory managed and operated by National Technology & Engineering Solutions of Sandia, LLC, a wholly owned subsidiary of Honeywell International Inc., for the U.S. Department of Energy's National Nuclear Security Administration under contract DE-NA0003525. SAND2019-3991 T

The Influence of Process Variables on Physical and Mechanical Properties in Laser Powder Bed Fusion

By

Joshua Koepke

B.S., Chemical Engineering, University of New Mexico, 2017

M.S., Mechanical Engineering, University of New Mexico, 2019

# Abstract

Laser powder bed fusion additive manufacturing consists of a process that incorporates many process variables into fabricating parts. This study investigated several of these process variables and determined their influence on part properties. The process variables investigated include laser power, velocity, focus offsets, layer thickness, and powder particle size. Physical properties will be compared including surface roughness, form, and density. Tensile testing provided mechanical properties including unloading Young's modulus, ultimate tensile strength, yield strength, uniform elongation, and ductility. Process maps will be developed that will provide recommendations for these process settings. It will be shown that these laser settings can be used to maximize physical properties and manipulate the mechanical properties. Several samples had their grains analyzed showing that laser settings also have an influence on grain sizes. Two simple models were tested for accuracy against experimental results. The results from the models showed they can be used as a starting point for future process optimization studies.

## Table of Contents

# Table of Figures

# Table of Equations

# List of Tables

# Chapter 1: Introduction

Additive manufacturing (AM) has been around for decades and with continual research, the impact of AM on the manufacturing industry has continued to grow [1]. AM is the method for fabricating parts, layer-by-layer, directly from a three-dimensional digital model [2]. Using the AM method allows for complex, topologically optimized parts to be produced that may not be possible with traditional manufacturing processes. Certain AM processes have even be used to repair parts, to extend the part's lifetime [3]. Other advantageous applications of AM are for use with one-off parts, rapid manufacturing of test specimens, and reduction of waste materials. Almost any material can be used in AM printers today including plastics, ceramics, and metals. Metal AM was reported by the US Navy to have the potential to enhance operational readiness, reduce cost, reduce energy consumption, and to enable parts-on-demand manufacturing [4]. Because of the potential AM has with metal parts, this study explored the influence of process variables on physical and mechanical properties for a metal AM laser powder bed fusion printer.

## Section 1.1 Directed Energy

There are two commonly used types of metal powder AM printers. One is laser engineered net shaping (LENS™) which is a directed energy metal powder AM printer. The LENS process consists of a powder delivery system where the powder is delivered in a gas stream through nozzles. The nozzles focus the metal powder into a stationary focused laser beam, seen in Figure 1. The laser beam creates a molten melt pool on a substrate that travels by the movement of a motion stage that the substrate is attached to

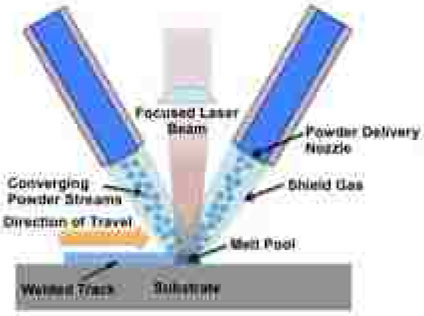

[redacted]

(not shown). A part is fabricated by the motion stage moving the substrate to desired locations to build up a layer. After the first layer is complete the laser and the nozzle assembly move up, and the next layer of the part is fabricated. This process continues on a layer by layer basis until the part is complete [5].

Each type of metal AM process has its advantages and disadvantages. Some advantages for the LENS process are its use of multi-materials and the ability to repair parts. The LENS process uses a set of powder hoppers for the powder delivery system which provides an opportunity to fabricate parts with multiple material types. The U.S Army has used LENS to repair parts in its Mobile Parts Hospital (MPH) which provides battlefield repair and replacement capabilities [3]. LENS provides a smaller and more controlled “heat affected zone” because of highly targeted deposition resulting in less damage to the underlying part [3].

Disadvantages of the LENS process include high residual stresses, poor surface finishes, and the inability to produce topologically optimized (TO) parts. A high temperature gradient between the fabricated part and the surrounding air can cause high residual stresses in fabricated parts [6]. The poor surface roughness is likely caused by the size of the powder particles used in the process. TO is difficult in the LENS process unless many supports are used. Whereas the powder bed fusion process is best for fabricating TO parts because the powder can be used as supports.

## Section 1.2: Powder Bed Fusion

The other common type of metal powder AM process is powder bed fusion (PBF). There are two types of PBF printers: one that uses an electron beam with a vacuum environment and one that uses a laser with an inert environment to melt the metal powder. The fabrication process is practically identical besides the heat source and the environment. The laser-PBF (L-PBF) process will be discussed because it was the type of AM printer used in this study. A schematic of the L-PBF process can be seen in Figure 2. The process begins with a metal powder in the powder delivery system, for this study stainless steel 316L was used. The next steps involve the powder delivery piston rising and a roller moving the powder from the delivery system to the fabrication plate on top of the fabrication piston. The roller evenly spreads a layer of powder across the fabrication plate, layer thicknesses are typically in the tens of microns range. After the roller returns to the starting point the laser fires. The laser fires only on the selected areas

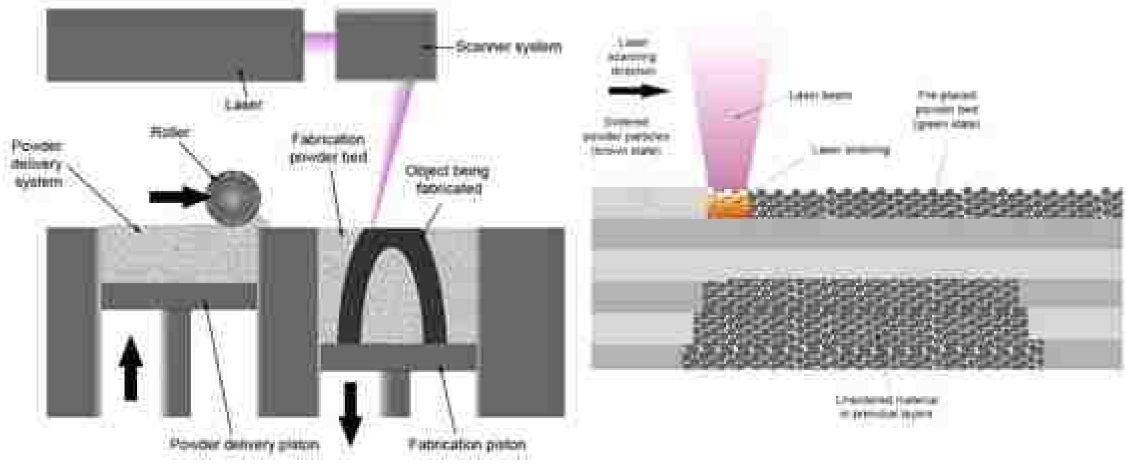

Source: https://commons.wikimedia.org/w/index.php?curid=4032088

[redacted]

[redacted]

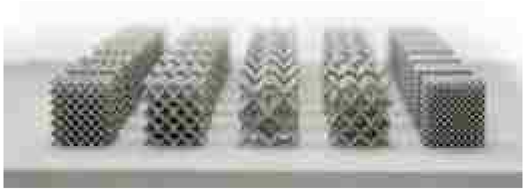

[redacted]

[redacted]

according to the design, melting the metal powder where desired while leaving nonmelted powder elsewhere. After sintering on this layer is complete the fabrication piston moves down, and the process is repeated until a final part is produced.

An advantage of L-PBF is that it offers an opportunity to fabricate parts that cannot be machined or fabricated using common manufacturing techniques. Some examples include topology optimized (TO) parts and lattice structures. TO and lattices, if manufactured correctly, can provide desired mechanical properties with reduced weight of cast or wrought material. Examples of TO and lattice parts can be seen in Figure 3.

L-PBF does have its limitations. Some disadvantages include fabricating parts with defects and a high variability in mechanical properties. Types of defects include porosity, balling, geometric defects, surface defects, residual stress, cracks, and delamination [7]. Porosity is the most studied defect and can be caused by lack of fusion, balling, keyholing, and entrapped gas. Examples of porosity can be seen in Figure 4. Lack of fusion porosity is the result of insufficient overlap of successive melt pools [8]. Keyholing is when the melt pool is heated to a high enough temperature to create a recoil momentum produced by the vaporized material exerting a force on the molten material, forming a cavity [9]. Entrapped gas is can be caused by keyholing or porosity in the

[redacted]

[redacted]

[redacted]

[redacted]

feedstock powder. Variability in mechanical properties has also been shown to be caused by defects in the parts [10].

## Section 1.3: Need for Study

For AM to become a commercial manufacturing technology the disadvantages need to be addressed. Specifically, the reduction of defects needs to be accomplished for the L-PBF process. One strategy is to optimize a set of process variables in L-PBF printers. Selecting a set of process variables can be difficult because more than 50 can be enumerated easily [11]. The process variables that have been investigated most are the laser power and laser velocity. The laser velocity is the speed the laser moves across the

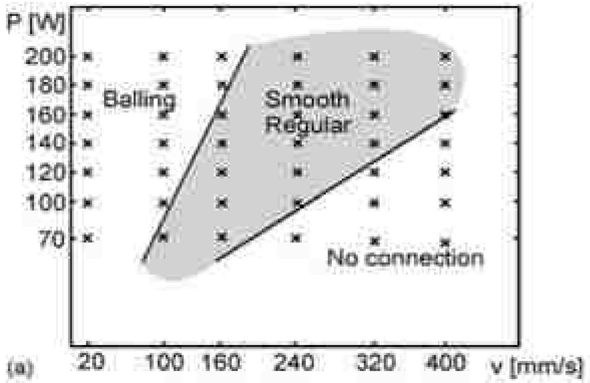

[redacted]

surface being melted. Process maps have been used to understand the regimes in the laser power and velocity process window, an example from Kruth et al. [11] can be observed in Figure 5 [11]. The process map shows three distinct regions; balling, smooth regular, and no connection. The balling region is a result of two different phenomena, the first is low laser power and the second is caused by too high of laser velocity [12]. In low laser power regimes, balling is the result of the lack of liquid formation and a low under cooling [12]. Balling from high laser velocity is caused by high capilary instability of the melt pool [12]. The no connection region is because the energy generated isn't enough to melt the powder, failing to fusing it together. The region in which the process should be running is obivously the smooth, regular region. Because the process map developed by Kruth et al. [11] shows many laser power and velocity combinations finding a set to produce high quality parts should be easy. The problem is the effect of other process variables on the process. As stated earlier, there are at least 50 that can be easily counted and possibly up to 130 [13]. This study focused on narrowing down the the number of variables to a set that has the most impact on the process.

## Section 1.4: Study Overview

This study investigated process variable optimization for the ProX 200 metal L-PBF printer from 3D Systems (Rock Hill, South Carolina). The ProX 200 uses a 300 W continuous wave 1070 nm laser with a beam diameter of approximately 100 μm. The build volume is approximately 140 x 140 x 100 mm with an argon atmosphere. The baseline settings for 316L stainless steel is ~107 W power, 1400 mm/s velocity, 30 μm layer thickness, 0 mm laser focus offset, 50 μm hatch spacing, and using a 316L powder with a particle size distribution of 5 – 30 μm in diameter.

A metric that was used to compare the influence of several process variables to physical and mechanical properties was volumetric energy density (VED) [13]. The equation for VED can be seen in Equation 1 where P is power, $v$ is velocity, σ is beam diameter, and $t$ is layer thickness.

$$VED = \frac{P}{v\sigma t}$$

*Equation 1: Volumetric energy density*

First investigating the operations of the laser beam in the system was needed, before experiments began. The laser power was the first variable to be studied. The input for laser power into the software required a percentage, so knowing the actual wattage delivered to the powder layer was crucial for calculations. After measuring the laser power, understanding how the laser beam size changes over time was needed. Measuring the beam diameter over time not only provided when the laser beam was in focus but also how the laser beam changed over time at different offsets.

The first set of experiments in this study involved simple line scans both on a 316L plate without powder and on an AM 316L pad covered with powder. The line scans provided information on the melt pool geometry. Line scans have been investigated by many researchers to develop process maps [13]–[19]. The variables investigated in this study included laser power, velocity, and focus offsets. Comparisons were made between the observed melt pool dimensions and a model based on process variables.

The next set of experiments were AM fabricated area scans which explained how lines next to and on top of each other interact. Area scans are more representative of real process conditions than line scans because the flatness of powder spreading becomes critical to fabrication stability [17]. Process variables investigated were laser power, velocity, and focus offsets. Area scans provided data from surface roughness and form measurements for comparisons across the process map.

After area scans, cube experiments provided information on how the area pad responds to continued fabrication. Cubes provided the opportunity to generate density data along with surface roughness on the sides of the cubes. Process variables that were explored for the cubes other than laser power and velocity include laser focus offsets, layer thickness, and powder particle size. Besides the laser settings having an influence on physical and mechanical properties it has been shown that particle size and distributions can also have an influence [20], [21]. Experimental data from the cube experiments were used to validate a density model.

The final set of experiments included fabrication of tensile arrays. Tensile arrays are a group of dog bones printed together for high throughput tensile testing. The tensile arrays not only provided information about building detailed parts but also provided the mechanical properties. The variables investigated for the tensile arrays were only laser power and velocity to reduce the number of samples needed. The mechanical properties provided from tensile testing included unloading modulus, ultimate tensile strength (UTS), yield strength, ductility, and strain at UTS.

This study included many samples which investigated the influence of process variables on physical and mechanical properties of fabricated 316L stainless steel parts. The process parameters varied included laser power, laser velocity, laser focus offsets, layer thickness, and powder lots. The goal of this study was to provide a set of variables maximizing density, ductility, and/or strength to develop simple models for process optimization. The following chapters include characterization of the laser and powder, introduction to the models, a detailed description of the experiments performed, the results and discussion of the experiments, and recommended variables for part fabrication.

# Chapter 2: Parameter Characterization

Before attempting any process optimization, an understanding of the laser and the 316L stainless steel was needed. The characterization of the laser beam was the first to be investigated. The characterization included measuring the laser power provided to the powder and not the percentage of the max laser power provided by the manufacturer. The laser focus was characterized by measuring the laser beam diameter over time to determine shifts in the focal point of the laser during operation. The laser focus characterization also quantified beam diameter due to variations in laser focus offset. A basic Rosenthal Model was developed to estimate melt pool geometry and a basic density model was developed to predict density. The final characterization was of the powder used for the parts fabricated for this study.

## Section 2.1: Laser Power Validation

The first step in characterizing the laser was to measure the actual laser power that was provided at the fabrication plate. Using the baseline power setting of 43% with a 300-watt laser in the ProX 200, the energy being deposited into the part should have been 129 watts. To test this, the laser power was measured using the Ophir (Jerusalem, Israel)

[redacted]

L50(300)A-LP1 power meter. The power meter was placed inside the fabrication chamber on the fabrication plate as seen in Figure 6. The yellow arrow denotes the direction of travel for the laser beam. The fabrication plate was then raised to its maximum height to measure the beam while the laser beam was out of focus, to prevent damage to the power meter. The power was measured from 15 – 100% at 5% increments and at 43% to validate the baseline laser power setting.

The results showed, as seen in Figure 7, that the actual laser power does not match the output commanded power. The actual laser power was approximately 20 W less than the commanded up to 80%. After 80% the difference increases, this was likely caused by thermal lensing of the optics [22]. The knowledge gained from knowing the actual laser power delivered to the fabrication plate was crucial for understanding machine operation. Actual laser power is also important because of its use in the Rosenthal model because the estimations and experimental results of the melt pool geometries would not be comparable.

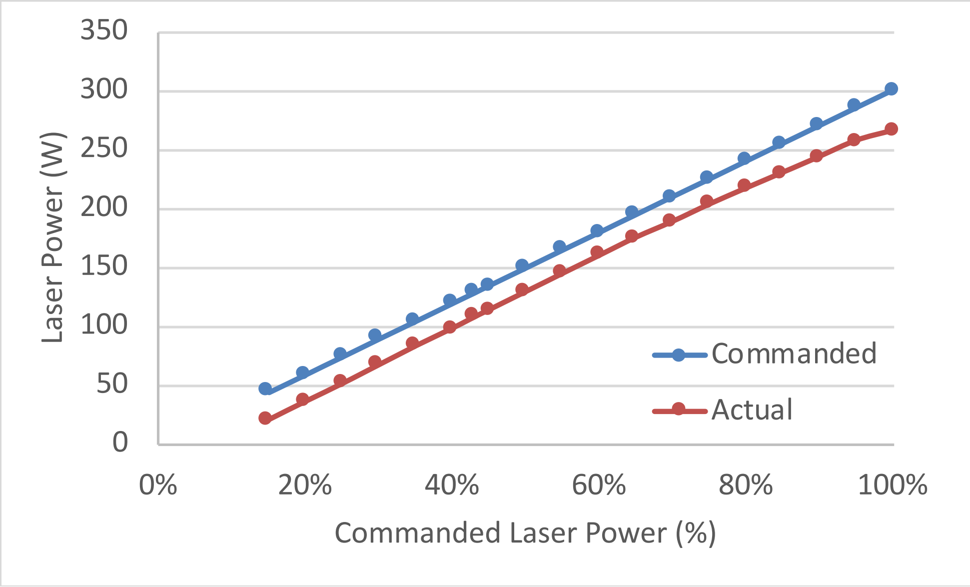

[redacted]

## Section 2.2: Laser Focus

Characterization of how the laser beam changed over time and determination of the focal point of the laser beam was the emphasis of this experiment. The ProX 200 runs a setup process before each build that finds a zero-sintering location for the fabrication plate relative to the position of the powder roller. Ideally the laser beam's focal position would be at the zero-sintering location. The build software does provide the opportunity to add an offset to the fabrication plate in case the laser focal point is not at the zero-sintering location. This set of experiments measured the beam diameter over time to determine the focal plane of the laser beam.

The laser beam diameter was measured using a laser beam attenuator from Ophir model LBS 300 that was attached to a beam profiler from Ophir model SP 928. The beam attenuator and profiler were placed on the fabrication plate inside the ProX 200, as seen in Figure 8. The travel distance of the Ophir components was known to an accuracy of 50 μm which allowed for an accurate determination of the focal point of the laser beam. The laser beam was measured for both one-minute and ten-minute durations at build platform locations from 3.0 mm below the expected focal point to 3.5 mm above.

[redacted]

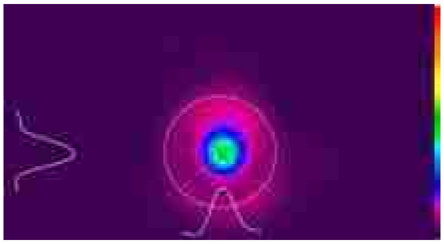

[redacted]

The one-minute measurements were measured in 0.25 mm height increments of the fabrication plate and the ten-minute measurements were with 1.0 mm height increments of the build platform. The beam diameter was measured using the Beam Gauge software that was provided with the Ophir components, a screenshot of a typical image can be seen in Figure 9. To find the beam focal point an image was taken every two seconds for a total of thirty-one images for the one-minute measurements. The laser focal point was selected by the location of the build platform with the lowest average beam diameter and the smallest standard deviation.

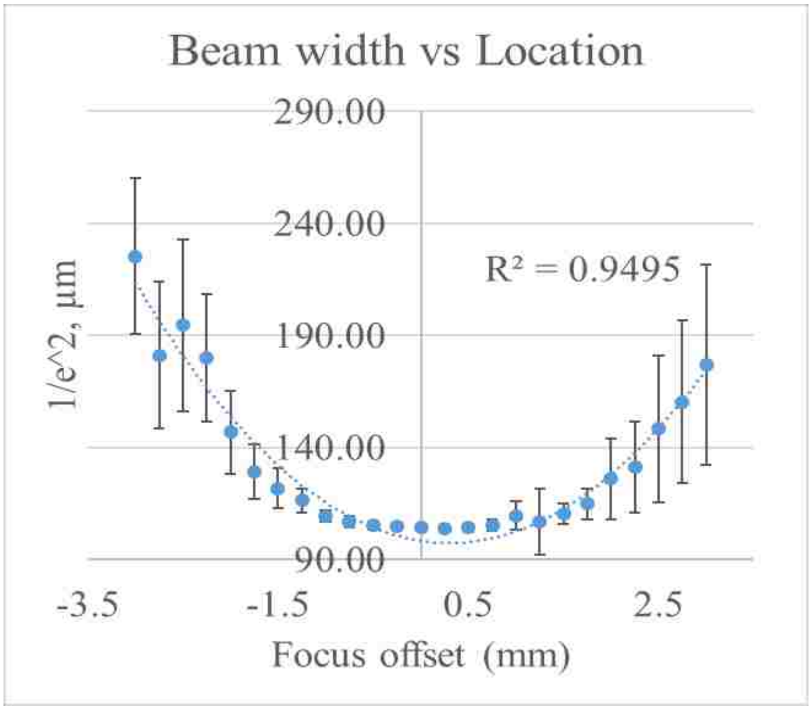

[redacted]

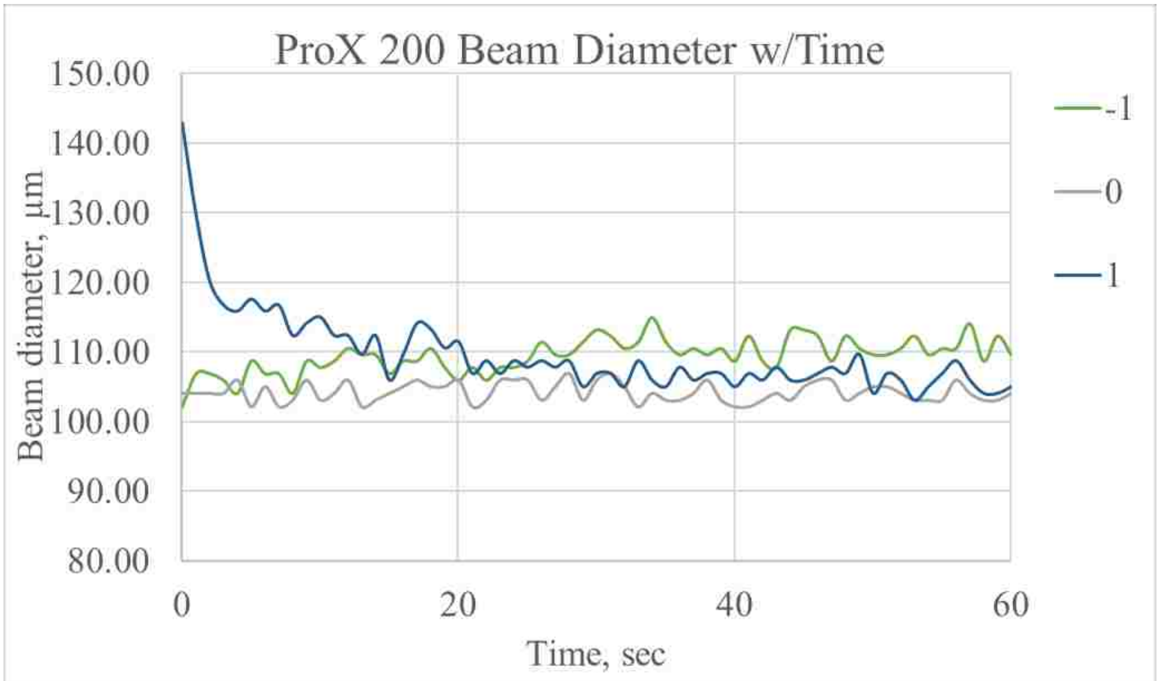

[redacted]

The results from the one-minute runs shows an accurate parabolic trendline, as seen in Figure 10. The parabolic trend line showed there was a Gaussian distribution in the laser. Figure 10 plots the average diameter for each of the offset locations, where the error bars are the standard deviation of the thirty-one measurements over one-minute spans. The focal point of the laser beam should have been at the minimum of the trendline, but several of the measurements, approximately 2.0 mm worth, were found near the focal position. This showed there was room for error when determining the focal point of the laser. The results from the most focused and 1.0 mm above and below focus runs can be seen in Figure 11. The results also showed when the laser was run below the focal point the beam started in focus and then moved out of focus. When the laser was run above the focal point the opposite is shown, the laser started out of focus then moved into focus. These results provided an opportunity to investigate if the focal point

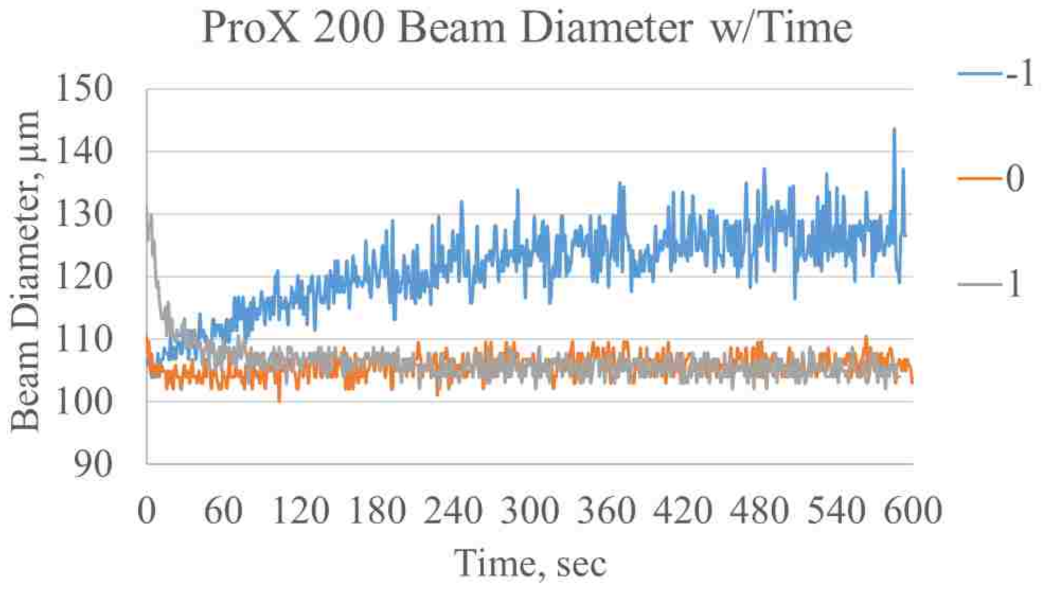

[redacted]

eventually moved out of focus at all offsets. To answer this, the ten-minute measurements were conducted around the focal point.

Measuring the laser beam diameter for ten-minutes provided an understanding how the laser beam changed over a long-time period. For the ten-minute runs the build platform was only measured at the focal point and 1.0 mm above and below the focal point. The results showed the same results as the one-minute runs with the focal point having the lowest average diameter and standard deviation. The location below focus once again moved out of focus within the one-minute and becomes erratic as time increased. The location of the fabrication plate above the focal point again started out of focus but between the two and ten-minute marks the location appeared to be as stable as the focal point. The results for the ten-minute runs can be seen in Figure 12. The knowledge gained from these experiments allowed for the investigation of the effects of offsets on part fabrication.

## Section 2.3: Simple Models

The Rosenthal model was developed in the 1940s by Daniel Rosenthal. The model predicts the heat distribution from a moving heat source during welding [23]. The melt pool dimensions include depth and width were predicted using the Rosenthal equation, Equation 2 [23]. The inputs included $T_f$ (the final temperature), $T_0$ (initial temperature), q (laser power * absorptivity), *k* (thermal conductivity), *v* (laser velocity), α (thermal diffusivity), R (distance from the heat source), and *w* (x-direction distance). R was the distance from the heat source, seen in Equation 3, and *w* provided the distance in the x-direction in a moving coordinate system, seen in Equation 4. Where x, y, and z are Cartesian coordinates and *t* is time.

$$T_f - T_0 = \frac{q}{2\pi kR} e^{-\frac{v(w+R)}{2\alpha}}$$

*Equation 2: Rosenthal heat distribution equation*

$$R = (w^2 + y^2 + z^2)^{\frac{1}{2}}$$

*Equation 3: Distance from heat source equation*

$$w = x - vt$$

*Equation 4: Distance in x-direction in a moving coordinate system*

The Rosenthal equation can be modified to approximate the shape of the melt pool which can be used to predict lack of fusion voids. To estimate the width of the melt pool for a given material Equation 2 was modified to solve for width represented by W, as seen in Equation 5. The Rosenthal model results will be compared with the experimental results in chapter 5. This modification used the melting point of the material as $T_f$ which provided an estimated melt pool width [8]. The inputs not included in Equation 2 are e (Euler's number) and ρ (the density of the material of interest). The Rosenthal model results will be compared in the line scan experiments results section.

$$W = 2\sqrt{\frac{2q}{e\pi\rho C_p\left(T_f - T_0\right)v}}$$

*Equation 5: Modified Rosenthal equation*

[redacted]

[redacted]

Using the melt pool widths and depths provided by the Rosenthal model a prediction was made for density. Equation 6 was developed by Tang et al for predicting lack-of-fusion density where H is hatch spacing, W is width, L is layer thickness, and D is depth [8]. If the solution of the inputs is less than or equal to 1 a full dense part is expected. Using the width and depths from the Rosenthal and the hatch spacing and layer

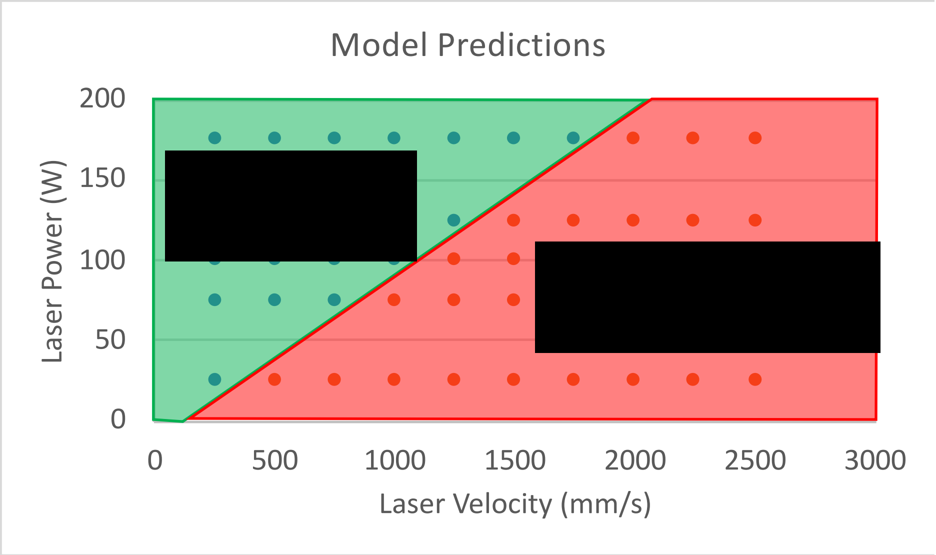

[redacted]

[redacted]

[redacted]

thickness from the process settings, a process map was modeled showing what parts of the process map should have fully dense material based solely on lack-of-fusion void formation. The results from the model are shown in Figure 13. The model does not predict actual density and ignores void formation mechanisms such as keyholing and balling.

## Section 2.4: Powder Characterization

This study used 316L stainless steel from three different powder lots to fabricate parts for this study. All three of the lots of powder were supplied by 3D Systems, two of the lots had similar particle size distributions and the other was significantly different. Each powder lot was characterized using a scanning electron microscope (SEM) from FEI (Hillsboro, Oregon). The characterization provided an average diameter, aspect ratio, and particle volume fraction distribution for each powder lot.

The powder characterization process included sampling 50,000 particles from virgin powder after the powder was mixed using a powder roller. The powder was then blown onto carbon tape attached to an aluminum stub by an argon gas flow. The powder was blown onto the stubs to provide an even distribution of powder across the stub. For each powder, five stubs were used with 10,000 powder particles analyzed on each stub. The samples were then analyzed overnight in the SEM using an automated feature analysis (AFA) procedure that was provided within the FEI's Perception software. The averaged results from the five stubs were used to determine the powder's characteristics.

The first lot of powder will be referred to as powder lot #1 for simplicity. The average diameter for powder lot #1 was 15.5±7.1 μm and had an aspect ratio of 1.43±0.6.

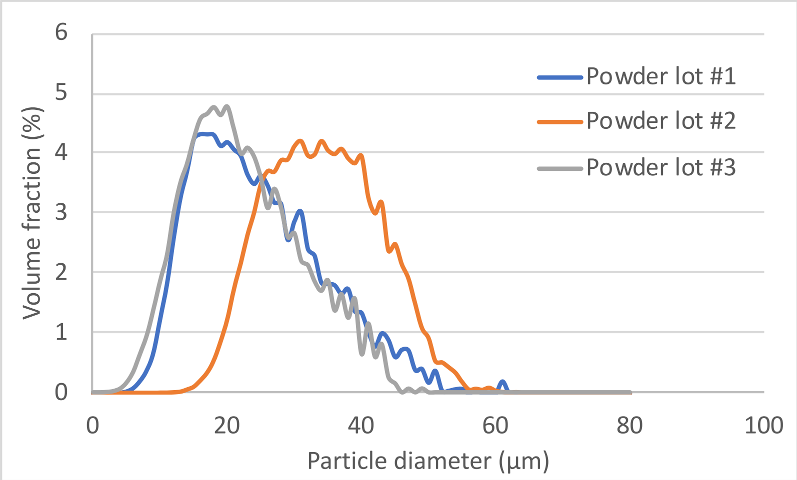

[redacted]

The volume fraction distribution can be seen in Figure 14 along with the volume fraction distribution of the other two powder lots. The second powder lot used will be referred to as powder lot #2. The average diameter for powder lot #2 was 25.5±8.9 µm with an aspect ratio of 1.36±0.5. The final powder lot will be referred to as powder lot #3. The average diameter of powder lot #3 was 11.6±5.4 µm with an aspect ratio of 1.51±0.7.

The powder characterization was important for fully understanding the process. Knowing the powder sizes also provided an idea about estimating the layer thickness, which was investigated as a parameter of interest in this study. After the characterization of the laser, estimating melt pool dimensions, and characterizing the powder experiments were performed to determine the effects of these process varaibles on part fabrication.

# Chapter 3: Experimental Procedure

To develop an understanding of the process space for the ProX 200 several types of experiments were performed. Experiments focused on the process variables that were believed to have the largest influence on the process. The two variables most studied were laser power and laser velocity. Laser power and velocity were used as the axis of process maps. These process maps have been used in past research by Kruth et al and Beuth et al. [14], [15]. Other process variables investigated were laser focus offsets, layer thickness, and powder particle size distributions. Experiments ranged from simple line scans to complex tensile dog bone arrays which will be covered in more detail.

## Section 3.1: Line Scans

The simplest experiments performed were laser line scans on a bare 316L stainless steel plate. The 316L stainless steel plate had an as-machined surface and was free of any 316L powder. These experiments have been performed by many to develop a starting point in process development for their printers [13]–[18]. This study not only performed laser line scans on plate but also performed laser line scans with powder on an AM 316L pad. Both the on plate and on AM pad laser line scan experiments used the same laser settings for the ability to compare the differences. The settings used five different laser power inputs with ten laser velocities for each power setting. Laser powers used were 25, 75, 100, 125, and 175 W. Laser velocities used were 250, 500, 750, 1000, 1250, 1500, 1750, 2000, 2250, and 2500 mm/s. Laser focus offsets were also compared using the 100 W, 1500 mm/s setting. The offsets used were from 3.5 mm above focus to 1.5 mm below focus in 0.5 mm increments. These experiments each

[redacted]

consisted of 60, 1.0 cm long lines for comparisons. The lines were spaced 1.0 mm apart and consisted of a single laser pass.

The purpose of the laser line scans was to understand the melt pool width and depth generated by a moving heat source. The melt pool width was measured using a Keyence microscope model VK-X100 for the lines on bare plate and model VR-3100 for the lines on the AM pad. Line width was measured at 3 locations at approximately 25, 50, and 75% of the line length, see Figure 15. An average and standard deviation on the three width measurements were used to assign a width to each line. To determine depth, metallography was conducted on each of the samples. The metallography process consisted of cutting the samples approximately at the center on each line transverse to the direction of the line. The samples were then mounted, ground, polished, etched, and imaged using a Keyence microscope. A width measurement was also determined from the metallography results to compare to the top measurements to determine if the method's measurements were realistic, which was found to be true. Examples of the metallography images can be seen in Figure 16. The depth was measured from the top of

[redacted]

the plate to the bottom of the half semi-circle and the width in measured at the top of the plate from the left side of the semi-circle to the right side for the lines on plate (shown in red dashes on the left image in Figure 16). The lines on pad measured the width approximately 30 µm above the surface above the pad, the depth was measured from this point to the bottom of the line, and the area included the entire melt area (shown in red dashes in the right image of Figure 16*)*.

## Section 3.2: Area Pads

Twenty-four AM pads were built on a 140 mm by 140 mm build plate. The pads were arranged in four columns with six rows, and the arrangement was kept constant for eight total plates, an example fabrication plate can be seen in Figure 17. The pads on six of the eight plates varied laser power and velocity, while keeping all other variables constant. One plate was fabricated using baseline settings to determine if there are any locations on the fabrication plates that effected the experimental results. The final plate

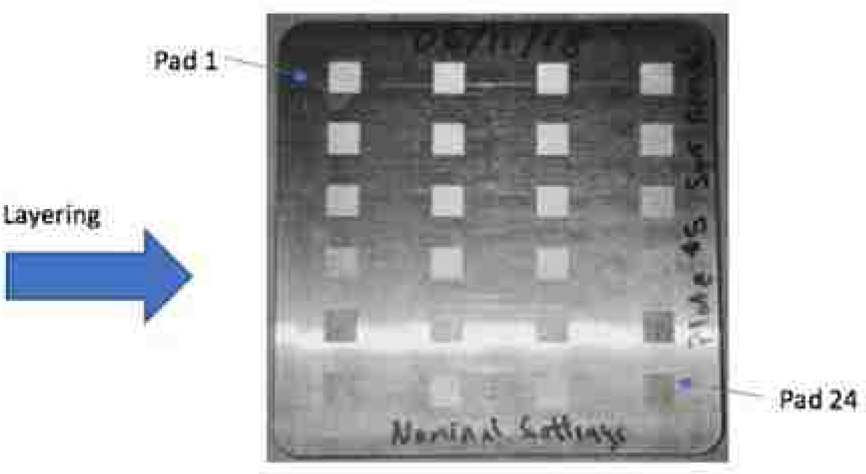

[redacted]

used five laser parameter settings in conjunction with five different laser focus offsets to determine if the focus offsets had any effects on surface roughness.

The pads were all twenty layers thick with a 30 µm thickness per layer for a 0.6 mm total thickness. The material used from powder lot #1. The laser focus offset was +1.0 mm for all plates except the one that compared the focus offsets. The pads were designed to be a 10 mm by 10 mm square, but pads with slower laser velocities were over built. The pads were over built because the colinear start and stop settings were not adjusted. The colinear start and stop controls how fast the laser starts and stops and was not fully understood until this study.

Surface roughness data was measured using a Keyence VR-3100 at 180x zoom. The 180x zoom provided a measurement area of approximately 4 $mm^2$ on the top of the pad. The form of the top surface was also measured using the Keyence at a 12x zoom. The 12x zoom provided a measurement area of nearly the entire pad surface of 1 $cm^2$ but excluded the edges. The edges were avoided to prevent skewing of the data. The surface roughness and form values were measured only on the top of each pad because the sides were inaccessible.

## Section 3.3: Cubes

Cubes were built with approximate measurements of 1.0 cm x 1.0 cm x 1.0 cm. There were 10 plates used for this study; 1 plate with 9 cubes, 1 plate with 10 cubes, and 9 plates with 24 cubes. An example of a density cube plate can be seen in Figure 18. This provided ~210 cubes to be tested for density, surface roughness on the top and side, form, and grain structure. Density was measured using Archimedes density method [24]. The measurement process includes first measuring the cube in air (A), then measuring the cube after being saturated with water (B), then measuring the cube for a third time suspended in water. Shows the equation used for calculating density where D is density and ρ is density of water. Surface roughness and form were measured using a Keyence

$$D = \frac{A * \rho}{B - F}$$

*Equation 7: Archimedes density calculation*

VR-3100 with a high magnification to measure surface roughness and a low magnification to measure form. Process variables were selected on a plate by plate basis and will be described below. Plates were fabricated using powder from powder lots #1 and #2 for selected plates.

The first plate of cubes was built to determine the best laser focus offset to be used for the remainder of the plates. There was a total of 9 cubes built on this plate using baseline process settings of 107 W laser power, 1400 mm/s laser velocity, 30.0 μm layer thickness, and powder from batch #1. The laser focus offsets explored were in 0.5 mm increments starting at 2.0 mm below the focal point of the laser and moving up to 2.0 mm above the focus point. Determining the focal point was discussed in chapter 2.

Density cube plate #1 (DC1) included 24 cubes as seen in Figure 18. The process settings for DC1 included varied laser power and velocity while keeping the focus offset constant. The layer thickness was 30.0 μm and the powder used was from powder lot #1. The process settings for DC1 used laser power and velocity settings that had volumetric energy density (VED) inputs near what is used for the baseline settings (23.3 J/mm$^3$) for most of the cubes. Three cubes with outlying energy value cubes were also printed; 1 had a low VED (3.8 J/mm$^3$), 1 had a high VED (59.2 J/mm$^3$), and 1 had a very high VED (105.9 J/mm$^3$). The 3 outliers are marked with a red circle in Figure 18. The low VED

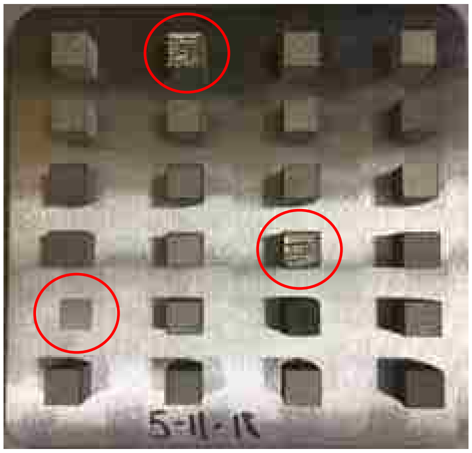

[redacted]

cube did not print, the high VED cube had bad form on top, and the very high VED cube has even worse form. This plate helped develop a plan for where to attempt to build on the laser power and velocity process map, Figure 19 shows the initial process map for the first plate of cubes with the outliers again marked with a red circle.

The remainder of the plates continued to fill in the process map but some also investigated the effects of other process variables on density. Plate DC2 used the same layer thickness, focus offset, cube layout, and powder batch as DC1 but continued

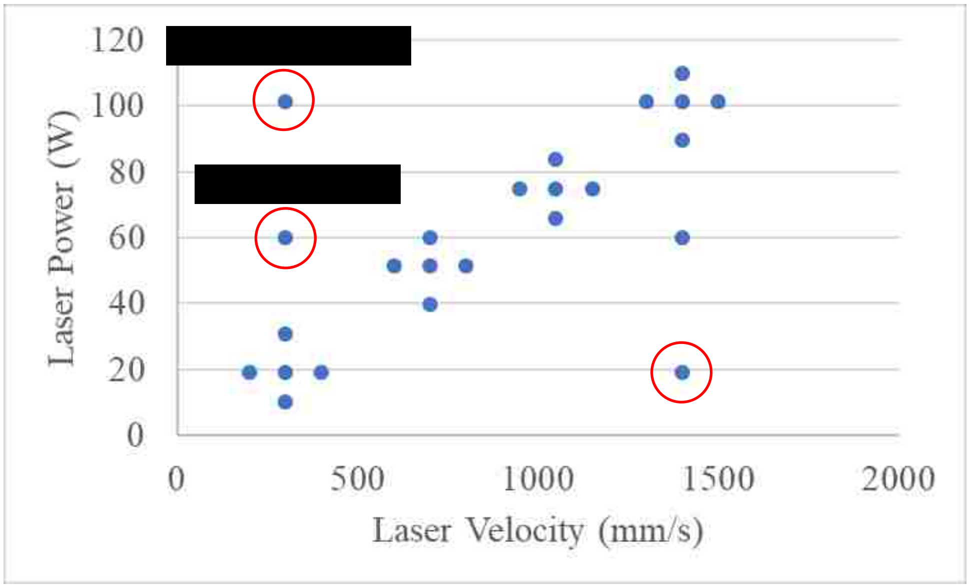

Low VED

[redacted]

varying laser power and velocity. The only change with DC3 from the first 2 plates were only 10 cubes were built on this plate. DC4 looked at the effect of changing the layer thickness form 30.0 μm to 40.0 μm while repeating the other settings for 24 cubes from the first 2 plates. DC5 was the first plate to use powder lot #2, layer thickness was 30.0 μm, and used power and velocity settings used on other plates with powder lot #1. DC6 again used powder lot #2 but with a layer thickness of 40.0 μm and many cubes had power and velocity settings used on DC5. The only plate to fail was DC7, this plate had many cubes with very high VED values and had to be stopped because of the roller contact with the cubes. To determine if location on the plate was having any effects on the results DC8 used all baseline settings and powder lot #1. DC9 used powder batch #1 and a layer thickness of 40.0 μm with laser power and velocity settings set to match VED values from previous plates. The final plate, DC10, explored more of the process space that had been missed using powder from powder lot #1 and a layer thickness of 30.0 μm.

Table 1 has an overview of all the cube fabrication plates. The results and comparisons of the density cubes across all plates will be covered in the next chapter.

*Table 1: Cube fabrication plate overview*

| Plate (#) | Power (W) | Velocity (mm/s) | Focus offset (mm) | Layer thickness (μm) | Powder lot (#) |
|---|---|---|---|---|---|
| FDC | 107 | 1400 | Varied | 30 | 1 |
| 1 | 10 to 110 | 200 to 1500 | +1 | 30 | 1 |
| 2 | 90 to 140 | 800 to 2000 | +1 | 30 | 1 |
| 3 | 140 to 180 | 600 to 1400 | +1 | 30 | 1 |
| 4 | 75 to 160 | 300 to 2000 | +1 | 40 | 1 |
| 5 | 85 to 180 | 600 to 1800 | +1 | 30 | 2 |
| 6 | 100 to 180 | 300 to 1800 | +1 | 40 | 2 |
| 7 | failed | | | | |
| 8 | 107 | 1400 | +1 | 30 | 1 |
| 9 | 85 to 175 | 225 to 1800 | +1 | 40 | 1 |
| 10 | 130 to 240 | 1400 to 2800 | +1 | 30 | 1 |

## Section 3.4: Dog Bone Arrays

The first three sets of experiments provided information on physical properties in the process space but did not provide any information about mechanical properties. To gather mechanical data, dog bone arrays were printed across the proven process space developed by area and cube experiments. At Sandia National Laboratories the opportunity to quickly test many tensile specimens is possible using the high throughput tensile (HTT) system, as seen in Figure 20. The HTT system allows for 50 dog bones to be tested in less then 10 minutes. Tensile testing provided mechanical property data including unloading Young's Modulus, ultimate tensile strength (UTS), ductility, Yield Strength, and uniform elongation. The focus of this set of experiments was to examine how laser power and velocity has an infuence on mechanical properties and if there was a set of parameters that can maximize specific mechanical properties.

A total of 5 plates were printed for this set of experiments with a total of 67 dog bone arrays and over 700 individual tensile tests. The variables investigated for the tensile testing only included varying laser power and velocity. The first three plates used powder from powder lot #1 and the last two used powder from powder lot #3. The first three plates also did not consider the colinear and noncolinear start and stop settings.

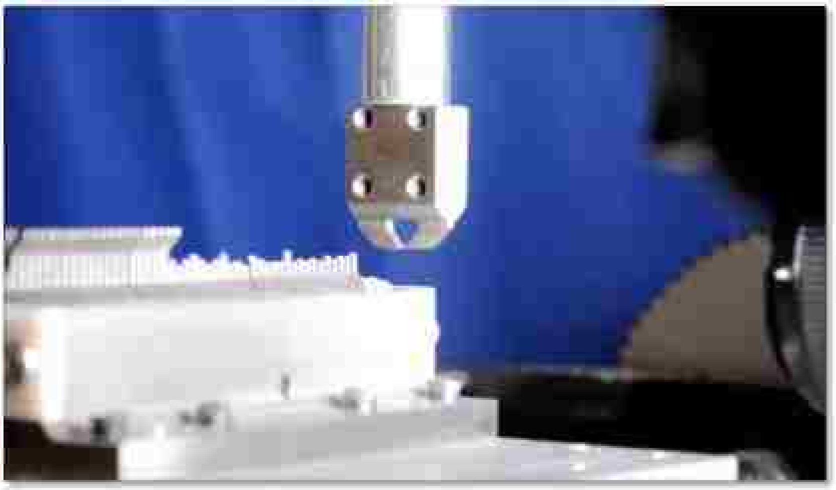

[redacted]

This caused the cross-sectional areas to vary, but the actual areas were accounted for in the strength properties calculations. The dog bones' nominal cross-sectional area was 1.0

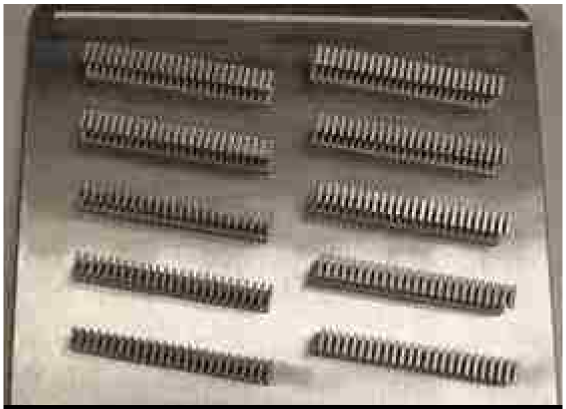

[redacted]

mm$^2$ with a gauge height of 5.0 mm.  The dog bone arrays also provided an opportunity to examine how part fabrication can be affected by varying process settings because of the fine features.

The laser settings of the first three plates were selected on a plate by plate basis. The first plate, tensile sample #1 (TS1), consisted of ten dog bone arrays with twenty-five tensile specimens per array, the plate layout from TS1 can be seen in Figure 21.  The laser settings for TS1 were chosen because of their high densities from the cube results. The next two plates, TS2 and TS3, used laser settings to investigate more of the process space that was not included in TS1.  TS2 and TS3 used tensile arrays of ten tensile samples instead of twenty-five tensile samples that were fabricated on TS1.  Printing ten tensile samples to an array provided an opportunity to explore more of the process space

[redacted]

without using so many fabrication plates. TS2 can be seen in Figure 22 and includes arrays that were stopped because they were possibly going to cause the build to fail and other arrays that were damaged by the roller. Damaged arrays were tested if possible, even if it was only a couple samples printed correctly.

The final two plates were printed to test the repeatability of the results. These two plates used a different powder, powder lot #3, but the size distribution was comparable to the original lot. These plates also used corrected colinear and non colinear start and stop settings since they were now understood, this provided a gauge section closer to the 1.0 mm that was requested. TS4 consisted of sixteen arrays with ten tensile samples to each array. The laser settings used were deemed the four best from the original three plates. Each parameter setting consisted of four arrays that were randomized on the plate to minimize plate location effects from the results. TS4 also included a Charpy sample for each setting which will be discussed in the next section. The final plate, TS5, consisted of twenty dog bone arrays with ten tensile samples each. The laser settings for this plate consisted of samples where the colinear and non colinear start and stop settings may have had an influence on the mechanical properties caused by the variation in cross-sectional areas.

## Section 3.5: Charpy Samples

One of the final plates from the tensile samples included four Charpy bars. The dimensions of the Charpy samples are 10.0 mm x 10.0 mm x 50.0 mm. One Charpy bar was fabricated for each of the laser power and velocity settings that was deemed the possible optimal settings from the original set of tensile plates. The Charpy bars provided a means to conduct Archimedes density and Rockwell B hardness in addition to

Charpy impact testing.  A notch was machined into the Charpy sample for testing.  The decision to add Charpy bars to the final set of parameters was deemed important to understand other experiments ongoing in the group which are beyond the scope of this study.

# Chapter 4: Experimental Results

This chapter covers the results from all the experiments introduced in the previous chapter. The line scans section includes the lines on plate and lines on pad results. The area pads section covers the surface roughness and form measurements for process variables to determine a process window. The cubes results section covers the surface roughness, form, and density across the process space and compares how the process space differs as other process variables are varied besides just the laser settings. The cubes section also includes the microstructure comparisons. The tensile section will discuss how the mechanical properties vary across the process space. The Charpy samples will demonstrate how laser settings have an influence on hardness and Charpy impact testing.

## Section 4.1: Line Scans

The line scans experiments were designed to cover a large area of the process space for the ProX 200. The first results were from a visual inspection of the lines which included if the lines existed (printed), if there was bead up, or if the lines were solid. After the visual inspection, the results from metallography provided the width and depth of the line to understand the melt pool across the process space.

The first line scan experiment examined a total of fifty lines across the laser power and velocity process space. Ten more lines were included to investigate the laser focus effects on the geometry of the lines. The visual inspection of the lines on plate showed continuous lines for all except the lowest power, 25 W, with velocities over 1500

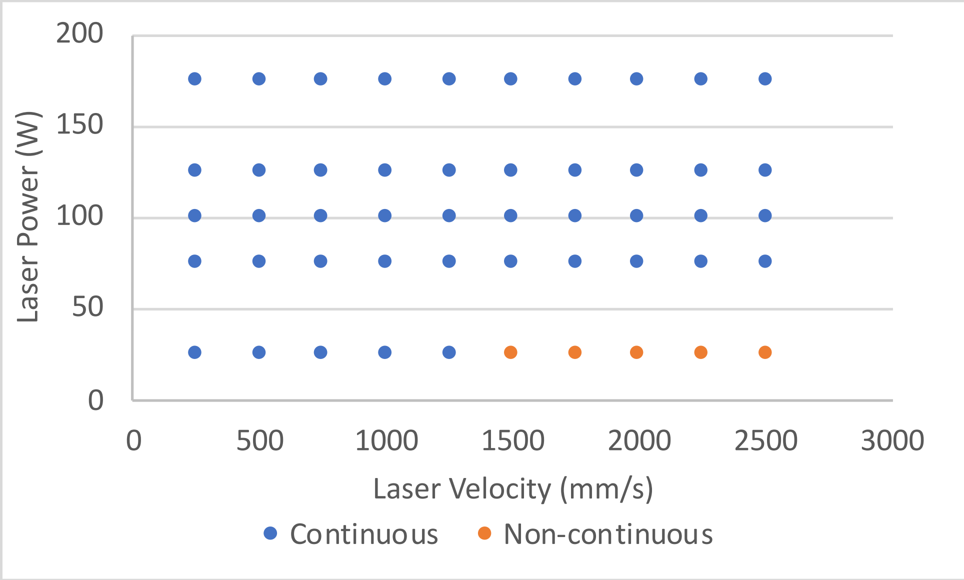

[redacted]

mm/s.  A plot showing where the continuous and non-continuous lines fall on the process map can be seen in Figure 23.

To determine the geometry of the melt pool, metallography was conducted.  The results show an increase in the melt pool area as power was increased at a constant velocity.  For example, the images for the five power settings at a constant velocity of 1500 mm/s can be seen in Figure 24.  The results showed when holding power constant and varying velocity the melt pool area decreases.  The images for 125 W laser power and velocities of 500, 1000, 1500, 2000, and 2500 mm/s can be seen in Figure 25.  The increase in the melt area was seen to be more of a result of increased melt pool depth than

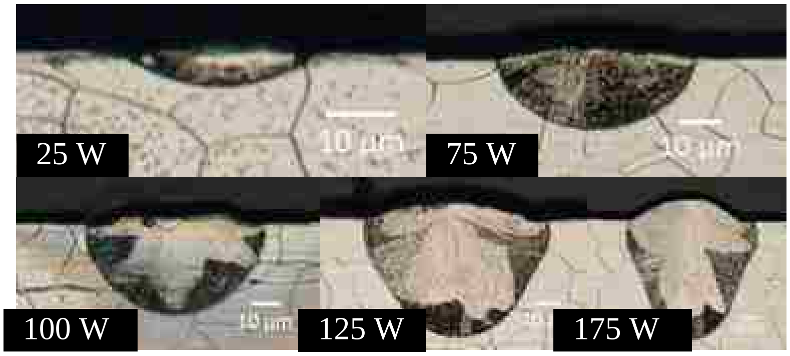

[redacted]

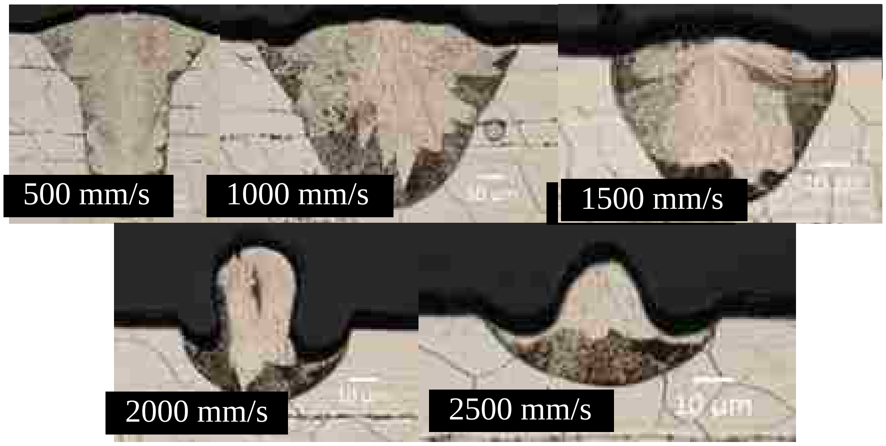

[redacted]

increased width. The 125 W images showed a transition from keyholing to bead up with increased velocity. Plotting the melt pool widths on the process maps shows regions with comparable width regions as shown in Figure 26.

The effects of laser focus on melt pool geometry was also investigated. Eleven focus offsets were investigated using 125 W power and 1500 mm/s velocity. The focus offsets ranged from 3.5 mm above focus to 1.5 mm below focus in 0.5 mm increments. The results showed the width of each line was not being affected much and no clear trend

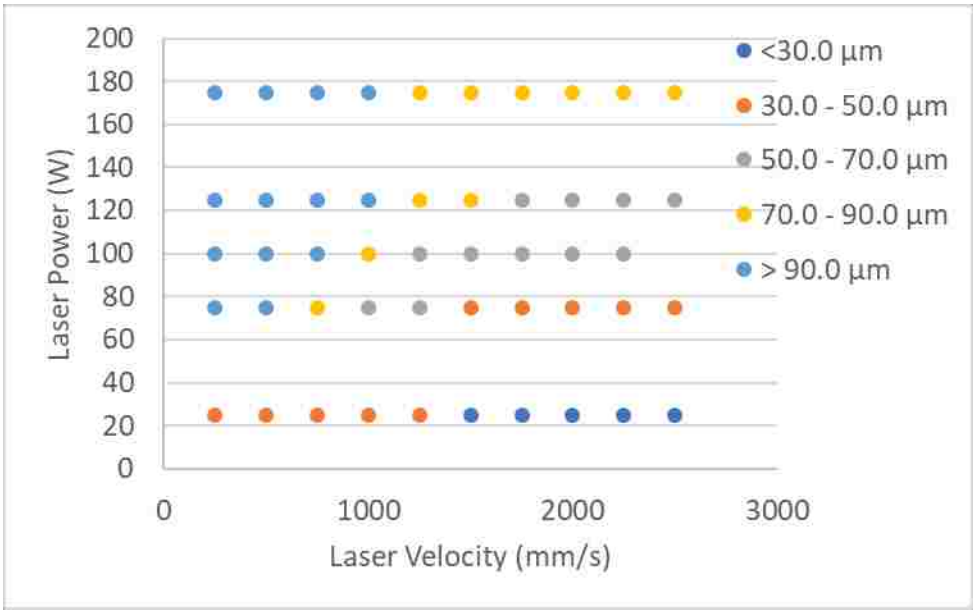

[redacted]

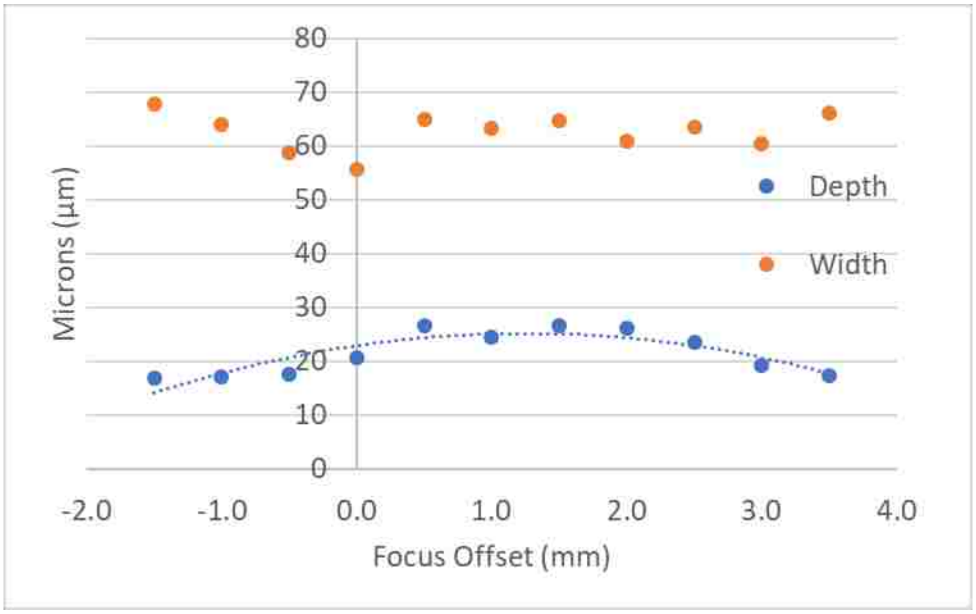

[redacted]

in the effects on the focus offset, as seen in Figure 27. The focus offsets did appear to have an influence on the depth of each line, also seen in Figure 27. The depth appeared to follow a strong trend with a maximized depth at offsets of 1.0 – 2.0 mm above focus. Line scans on plate provided information on how the laser settings influenced the melt pool on a flat, solid material. The lines on pad experiment provided a "real world" AM experiment.

To understand the interaction of lines on a fabricated pad which is more realistic, the lines on pad experiment was performed. The visual inspection of the lines was noticeably different from the on-plate lines. The lines on pad showed solid lines, lines where balling was dominant, and where the lines did not connect. While the no connection zone was identical to the process maps produced by Kruth and Beuth developed using lines on plates, the balling and smooth zones are flipped. A possible reason for the difference between what was seen in literature and this experiment was the lines of powder in literature are produced on a machined plate, not an AM pad. The AM

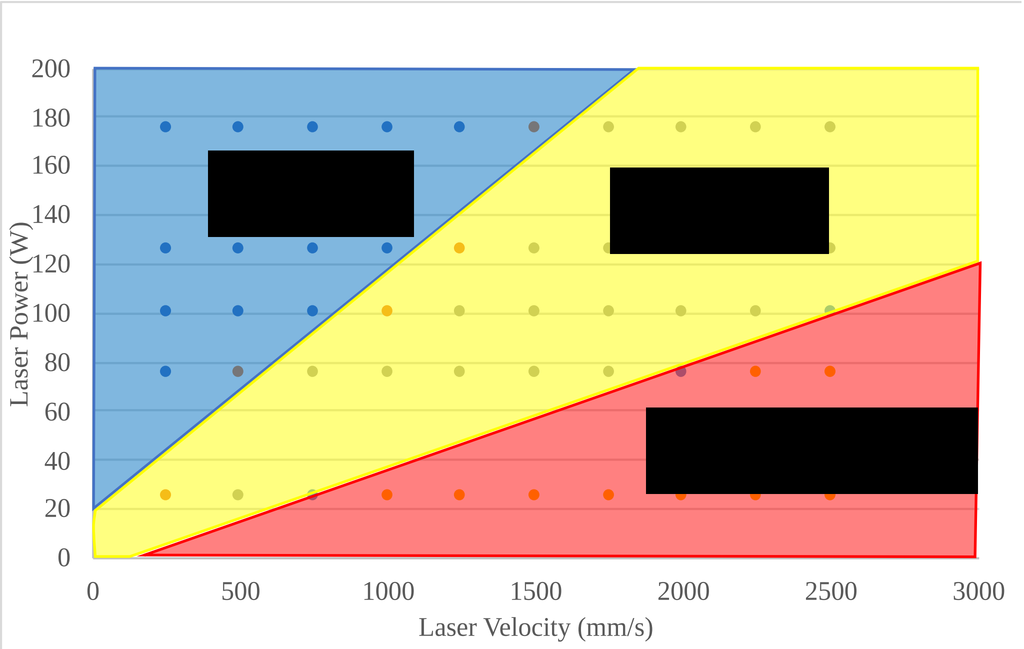

[redacted]

pad naturally has a larger surface roughness then a machined plate which more than likely influenced the results. A graph showing where the three zones fall on the process map from this experiment are shown in Figure 28.

To determine the melt pool areas for the lines on pad experiment metallography was performed. Because of the large number of lines that were seen balling or missing, performing metallography to capture all the lines in one cut was impossible. The line widths and depths were also difficult to determine because of the roughness of the top of the AM pad. For the lines on pad only the cross-sectional area of the lines that were found were used in the analysis.

The melt pools for the lines on pad did show similar trends across changing laser settings in the metallography, like what was seen in the lines on plate. The lines on pad that used a constant velocity of 1500 mm/s only had two lines found in the metallography, at 125 and 175 W. The 175 W line did appear to have an increased depth from the 125 W line, the metallography images can be seen in Figure 29. The lines that

[redacted]

had a laser power of 125 W showed the influence of velocity on the melt pool geometry. The metallography on four of the lines with a laser power of 125 W can be seen in Figure 30. Although the surface of the pad is uneven, the reduction in depth of the lines is noticeable with increased velocity. After analyzing all the Keyence and metallography data a process map showing the regions was produced, as seen in Figure 31. The process map shows four regions, keyholing, smooth, balling and no connection. Most of the lines that were considered smooth from the Keyence images were found to be keyholing in the metallography. Also, many that appeared to ball from the Keyence images were found to have a regular looking melt pool shape in the metallography, so they were labeled as being in the smooth region. A reason for why the lines appeared to be balling in the

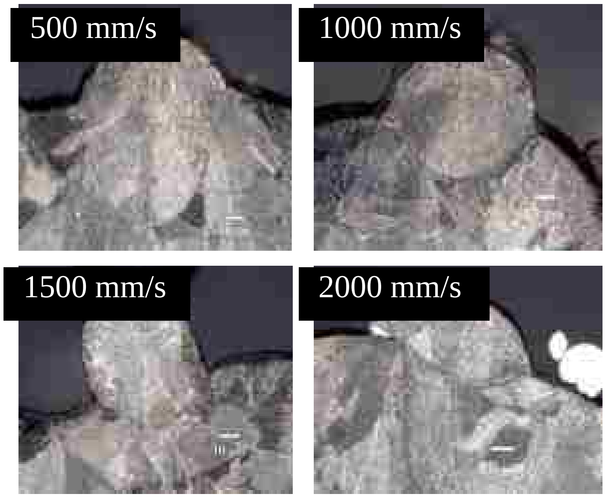

[redacted]

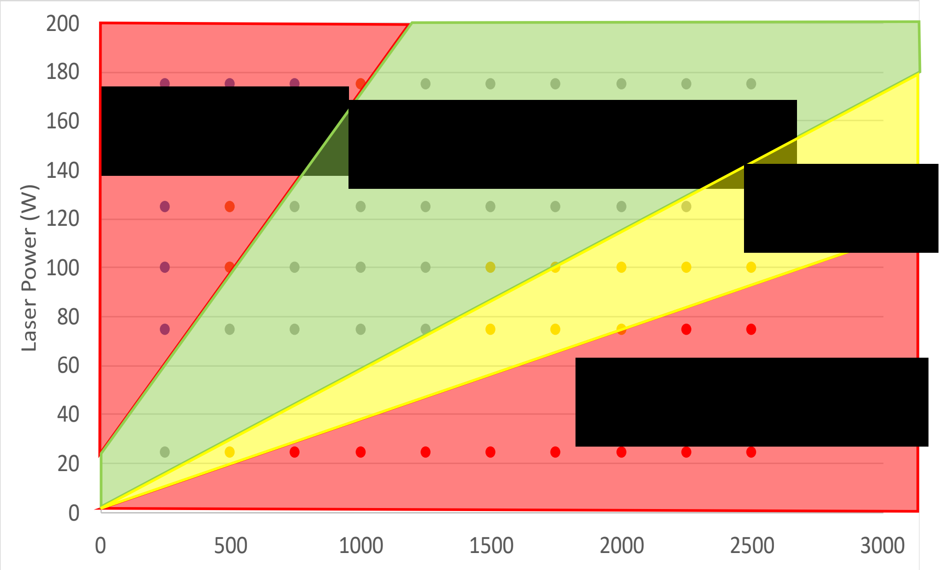

[redacted]

Keyence image could be because of the surface roughness of the pad influenced the height of the lines.

The last group of lines were the set of 10 that investigated the laser focus offset. These lines showed all the lines with a focus offset from 1.5 mm below focus to 1.0 mm above focus were balling and were missed in metallography. As the focus offset went further below the focus point the balling became worse. The lines that were found in metallography from 1.5 mm to 3.5 mm above focus showed similar shapes as seen in

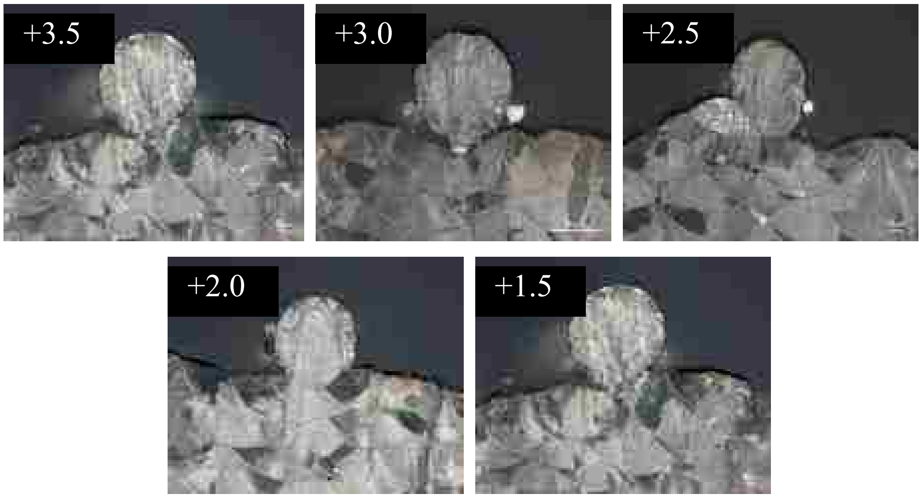

[redacted]

Figure 32. The only thing that could be concluded from the focus offset lines on pad was that offsets below focus should be avoided, because of an increase in balling the further the distance below the focal point.

## Section 4.2: Area Pads

For the area pads a range of laser settings were selected to produce a comprehensive process map. The process map in Figure 33 included the settings for six plates built for this experiment. To determine the regions of the process space, pads were measured for surface roughness and form. The area pads also included plates that investigated differences in location on the fabrication plate and the influence of focus offsets on laser power and velocity settings.

The first, and easiest, part of the analysis was to first identify area pads that did not connect to the fabrication plate. There were four settings that failed to print, this provided the no connection zone on the process map. The common trend of the four

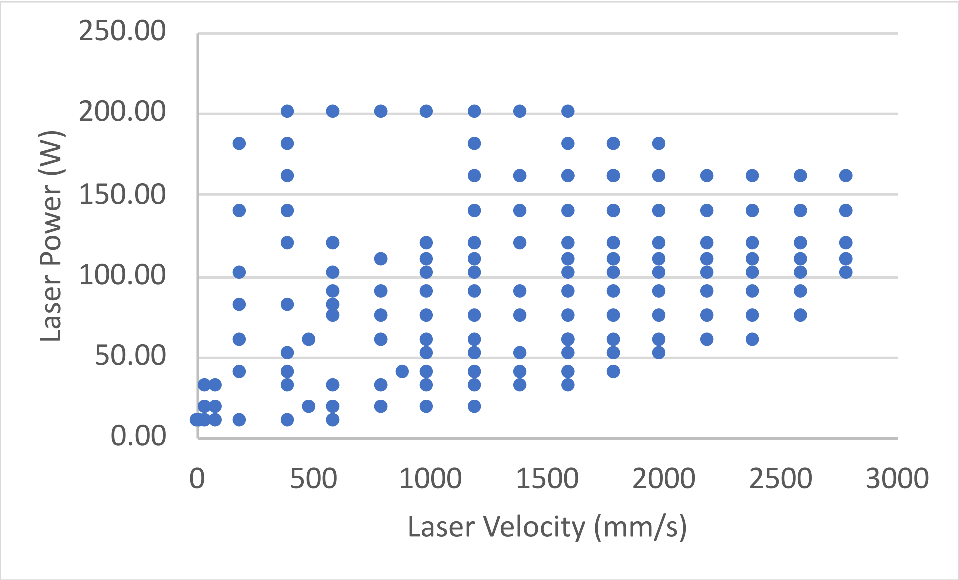

[redacted]

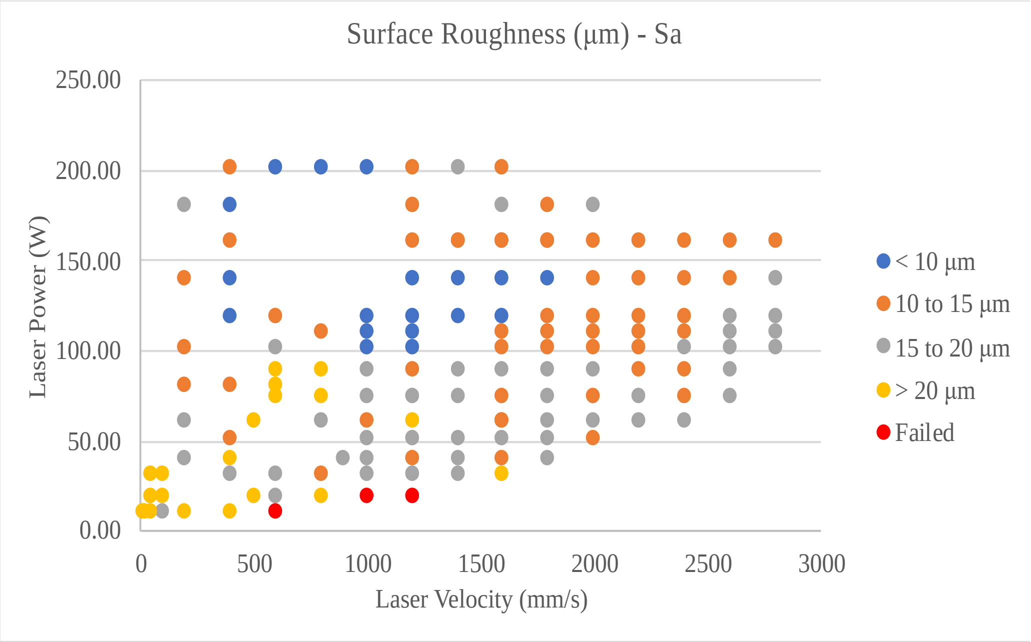

[redacted]

settings was they all had a VED below 7.1 J/mm$^3$. This demonstrated there was a minimum amount of energy needed to fuse the powder together.

The next step in the analysis was to identify trends in the surface roughness data of the remaining pads. The surface measurement parameter used for this study was $S_a$, arithmetical mean height. A surface roughness threshold of 15.0 µm, the average diameter of the powder, was used to compare the results. The surface roughness values are shown on a process map in Figure 34. There were four pads that did not print, which produced a no connection region at low power and high velocity. The pads with the highest surface roughness values, above 20.0 µm, were all found in powers less than 100 W and velocities less than 1000 mm/s. The pads with surface roughness's between 15.0 and 20.0 µm were mostly found below 100 W power but at all velocities. The remainder of the pads that fall into the 15.0 – 20.0 µm surface roughness category that were above 100 W had very fast velocities, 2250 mm/s and above. The process map showed that almost every pad above 100 W produced a surface roughness below the threshold value

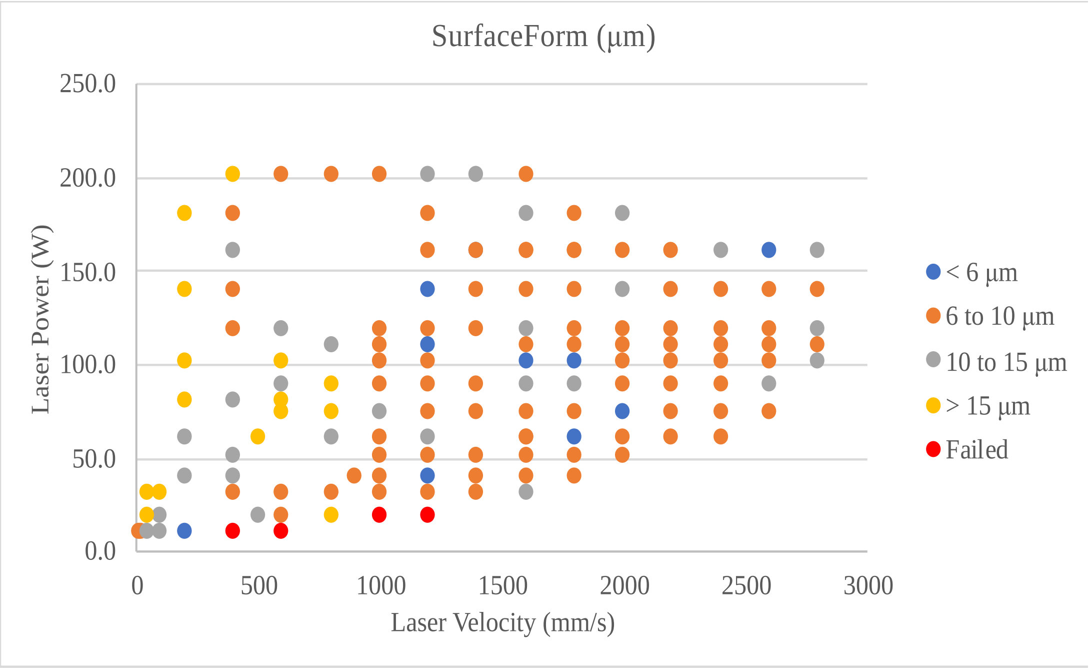

[redacted]

of 15.0 µm.  The best surface roughness pads, less than 10.0 µm, were found in an area in the middle of the process map with a few outliers found at high powers and/or low velocities.  The group of pads with the best surface roughness's were found from 100 – 140 W and 1000 – 1600 mm/s.

The area pads were also measured for surface form.  Surface form uses the same $S_a$ value but measures the entire surface of the pad.  Form is a measurement of how flat the surface was.  Most pads with the worst form, above 10.0 µm, were found at velocities below 800 mm/s, as seen in Figure 35.  All the pads above 15.0 µm were all found in this range.  This showed that there may have been too much energy being deposited into these pads, causing their form to be poor.  The pads with the best form, 6.0 µm or less, were spread out across the process map above 800 mm/s with no strong correlations in laser settings.  Since there wasn't a strong correlation in the pads with the best form measurements, form may only be useful for regions of the process map to avoid.

[redacted]

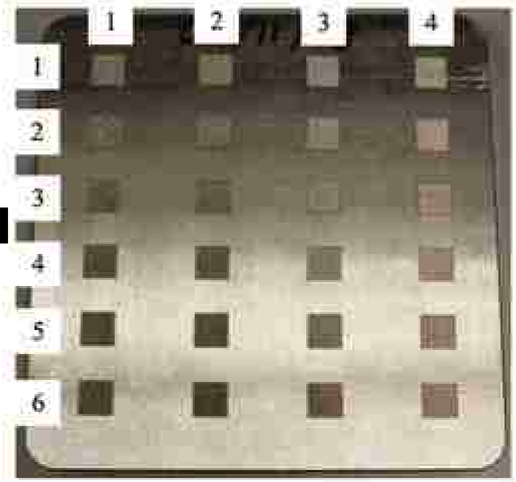

[redacted]

[redacted]

To determine if there were any effects on the pad measurements due to the location on the fabrication plate, a baseline parameter plate was printed. This plate included the same layout as the previous plates but repeated the process settings for all twenty-four pads. The average surface roughness of the pads was 9.87±1.37 µm. and the average form was 5.62±0.44 µm. The results showed there was a small difference in both measurements when looking at the entire plate. The plate was split up into four columns and six rows for comparisons, as seen in Figure 36. The surface roughness values in the four columns differed by about one standard deviation. The results also show the two columns closer to the powder supply (left side of the plate) had the best surface roughness and decrease towards the edge of the plate, away from the powder supply. The form measurements, while minimal, do show an increase across the plate from the powder supply (left) side to the (right) edge of the plate. The results for the column and row measurements can be seen in Table 2. The rows again showed a trend in

[redacted]

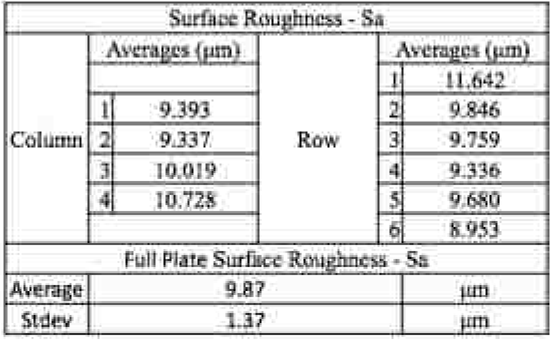

| Surface Roughness - Sa | | | | | |
|---|---|---|---|---|---|
| | Averages (µm) | | | Averages (µm) | |
| Column | | | Row | 1 | 11.642 |
| | 1 | 9.393 | | 2 | 9.846 |
| | 2 | 9.337 | | 3 | 9.759 |
| | 3 | 10.019 | | 4 | 9.336 |
| | 4 | 10.728 | | 5 | 9.680 |
| | | | | 6 | 8.953 |
| Full Plate Surface Roughness - Sa | | | | | |
| Average | 9.87 | | | µm | |
| Stdev | 1.37 | | | µm | |

measurements with both the surface roughness and form being poorest at the top of the plate and increased as the rows progress toward the bottom of the plate. While there was variation across the plate, it was minimal and will not be considered in this study.

[redacted]

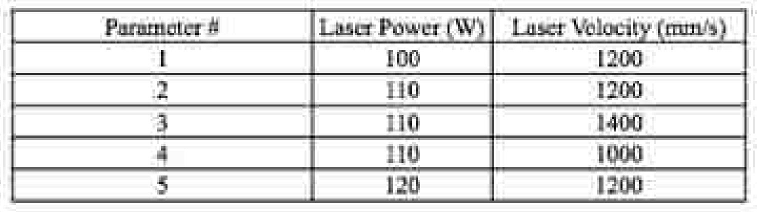

| Parameter # | Laser Power (W) | Laser Velocity (mm/s) |
|---|---|---|
| 1 | 100 | 1200 |
| 2 | 110 | 1200 |
| 3 | 110 | 1400 |
| 4 | 110 | 1000 |
| 5 | 120 | 1200 |

The final plate of area pads for this study investigated the influence of varying the laser focus. This plate used five different laser power and velocity settings and compared them at five different offsets from focus. The offsets include 0.0 mm (focus) to 2.0 mm

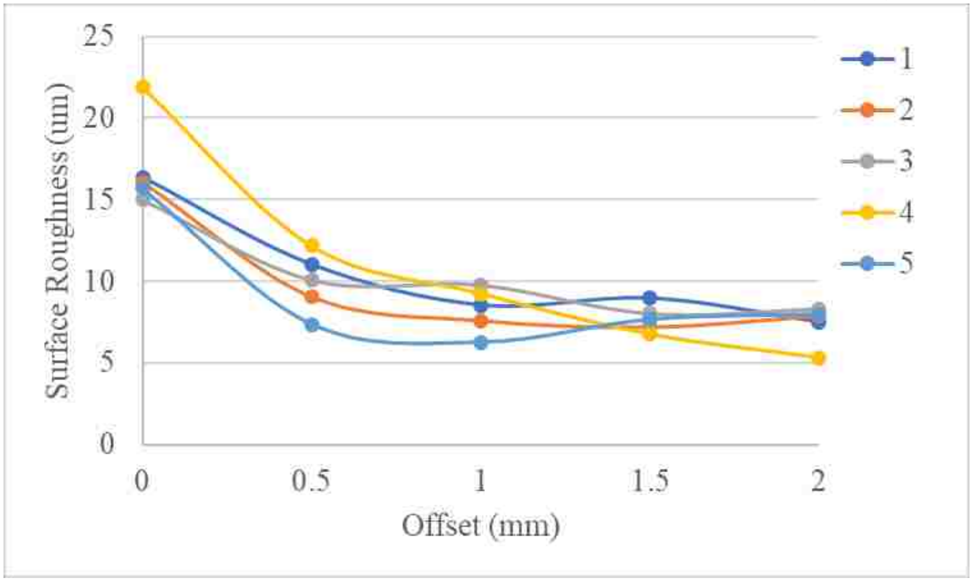

[redacted]

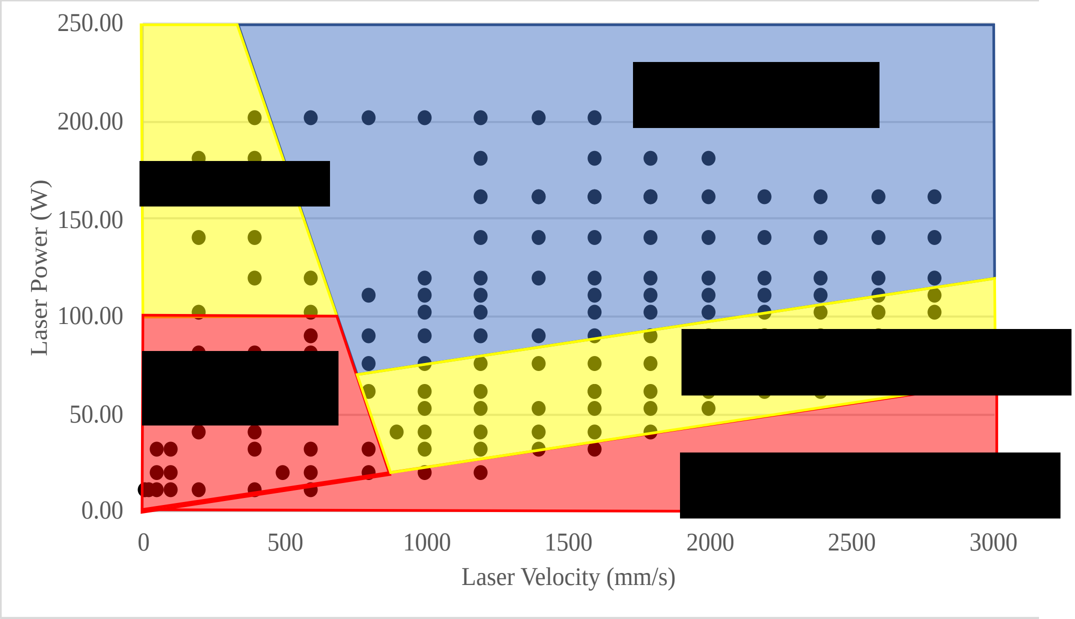

[redacted]

above focus in 0.5 mm increments.  The five parameter settings can be seen in Table 3. The results from the surface roughness measurements showed as the focus offset increased above focus, the surface roughness increased in quality.  While four of the five settings improve the quality of the surface roughness by almost 2x, setting #4 shows improvement by 4x, shown in Figure 37.  These results showed that using a laser focus offset above focus can be beneficial to providing parts with a quality surface finish.

Much was learned from the area pads including generating a process map, plate location effects, and laser focus offset effects.  A process map marking the regions of interest can be seen in Figure 38.  Location effects on surface roughness was found to be minimal but should be explored more.  Laser focus offsets also showed it can be a used as a setting to increase surface finish.  While the process window appeared large from the area pads other experimental results from the next section, cubes, should provide a narrowing of the window.

## Section 4.3: Cubes

The cubes section included the most extensive set of results for the entire study. They provided an opportunity to fabricate parts that could be measured for the effects of process settings on porosity. Measuring porosity was performed using Archimedes density which was a simple way of calculating the density of the cubes. The cubes were also measured for form on top and surface roughness on the top and sides. About thirty cubes were sectioned for EBSD to study grain orientation. The process variables investigated for the cubes are laser power and velocity, laser focus offsets, plate location, two-layer thicknesses, and two 316L powder lots. To better explain the results the cubes are separated into six groups as followed: laser focus offsets, powder lot #1 with a 30.0 μm layer thickness, baseline plate, powder lot #1 with a 40.0 μm layer thickness, powder lot #2 with a 30.0 μm layer thickness, and powder lot #2 with a 40.0 μm layer thickness. Results for cube will be discussed in each section and compared across sections when available.

The first group, group #1, of cubes were the laser focus cubes. Group #1 consisted of 9 cubes that used the baseline settings except for varying the laser focus offset. The laser focus was offset from 2.0 mm below the focus point to 2.0 mm above the focus point for this group of cubes. The results showed the cubes built above focus have much better physical qualities than the cubes built below the focus point. When both surface roughness and density were plotted against the focus offsets, a polynomial trend was noticeable with an $R^2$ value over 0.97 as seen in Figure 39. The results showed that both surface roughness and density were maximized around 1.0 – 1.5 mm above

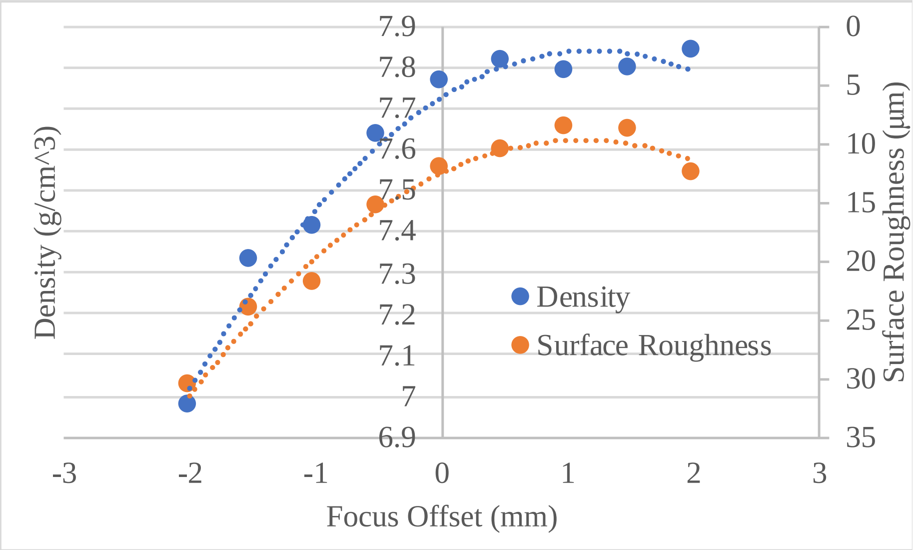

[redacted]

focus. The remainder of the plates used the results from this group and used a laser focus offset of 1.0 mm above focus to fabricate the remainder of the cubes.

To determine if there were any focus offsets influence on grain size and orientations, two cubes from group #1 were cross-sectioned and EBSD imaged. The cubes that were selected for EBSD had the highest and lowest density. The cube with the highest density had a focus offset of 2.0 mm above focus and the cube with the lowest density had a focus offset of 2.0 below focus. The EBSD results showed a lot of voids (black areas) in the 2.0 mm below focus cube which would be expected from the low density but also appeared to have larger grains. The 2.0 mm above focus showed a fully

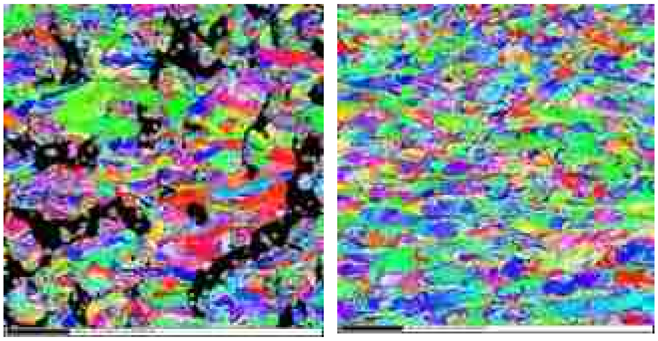

[redacted]

dense image with smaller grains. The EBSD images can be seen in Figure 40. With only the laser focus offset being varied in these two cubes, a laser focus offset appeared to have an influence on the grain size.

The next group, group #2, of cubes that were analyzed used powder lot #1 at a 30.0 μm layer thickness. Group #2 was by far the largest with over eighty cubes fabricated and analyzed. Laser settings for group #2 included laser power ranging from 10 – 240 W and laser velocity from 200 – 2800 mm/s. These laser settings were used to build cubes with densities from 3.89 – 7.89 g/cm$^3$, surface roughness values of 5.7 – 109.2 μm, and form measurements of 4.8 – 173.3 μm. Literature values for 316L stainless steel state the density can vary depending on the composition but typically 8.0 g/cm$^3$ is used [25]. Archimedes density can be accurate but also has many sources of error [24]. The highest density for a cube in this study was 7.895 g/cm$^3$, this provided an assumption which was this was this cube was fully dense.

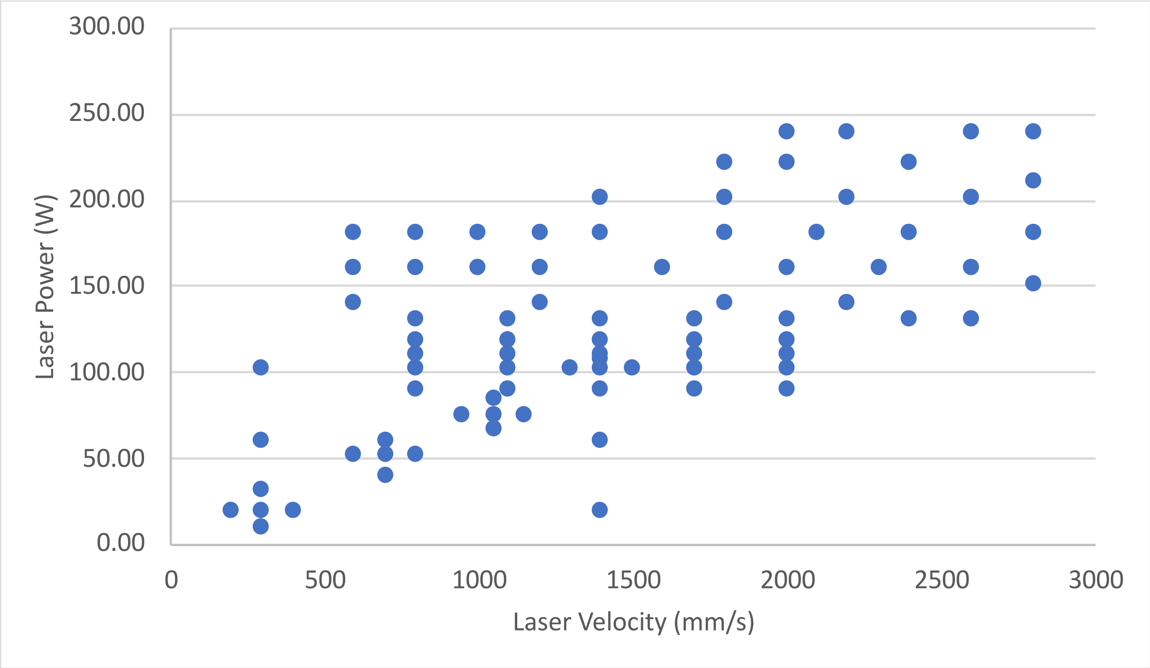

[redacted]

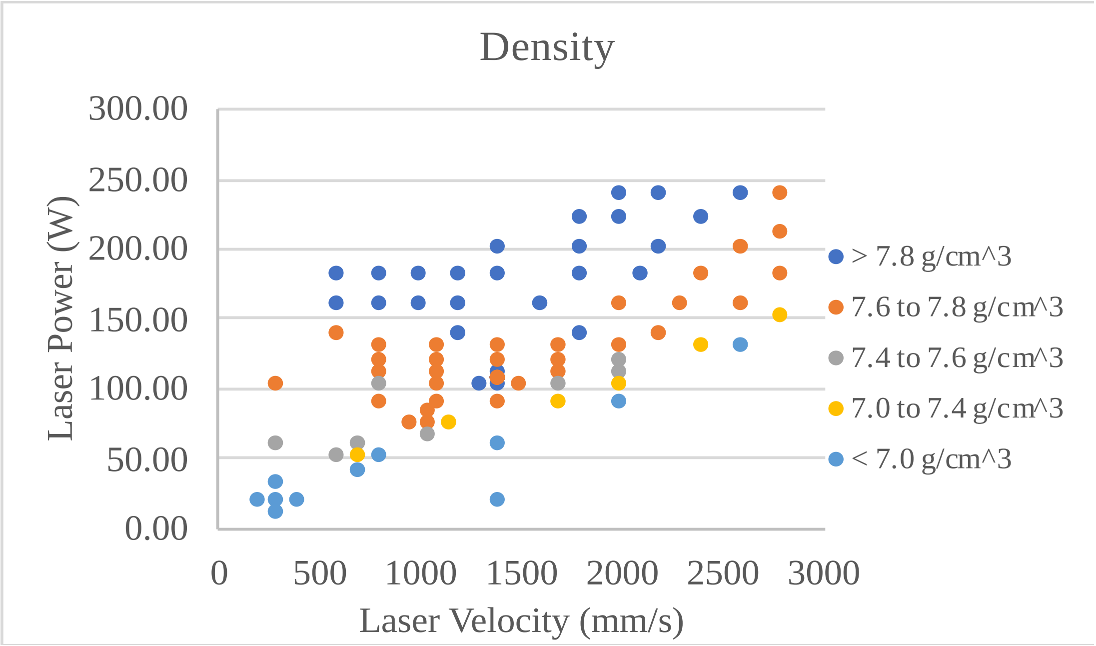

[redacted]

The process map for group #2 shows there was a large number and variation in power and velocity settings used, as seen in Figure 41. There were many cubes fabricated using power and velocity settings in the center on the map and lesser as the settings moved away from the center. This distribution allowed for focusing the study around the baseline settings but still allowed for a broad range of settings being explored. The density results for group #2 showed that many power, and velocity settings can produce cubes with densities over 7.6 g/cm$^3$, as seen in Figure 42. Cubes that had a laser power of over 140 W at most velocities had densities over 7.8 g/cm$^3$. The results showed when using laser powers below 100 W, cubes typically had low densities. This 100 W threshold was also seen in the area pads where surface roughness was poor when using a laser power under 100 W. The process map also showed as laser velocity is increased the density decreased with constant power.

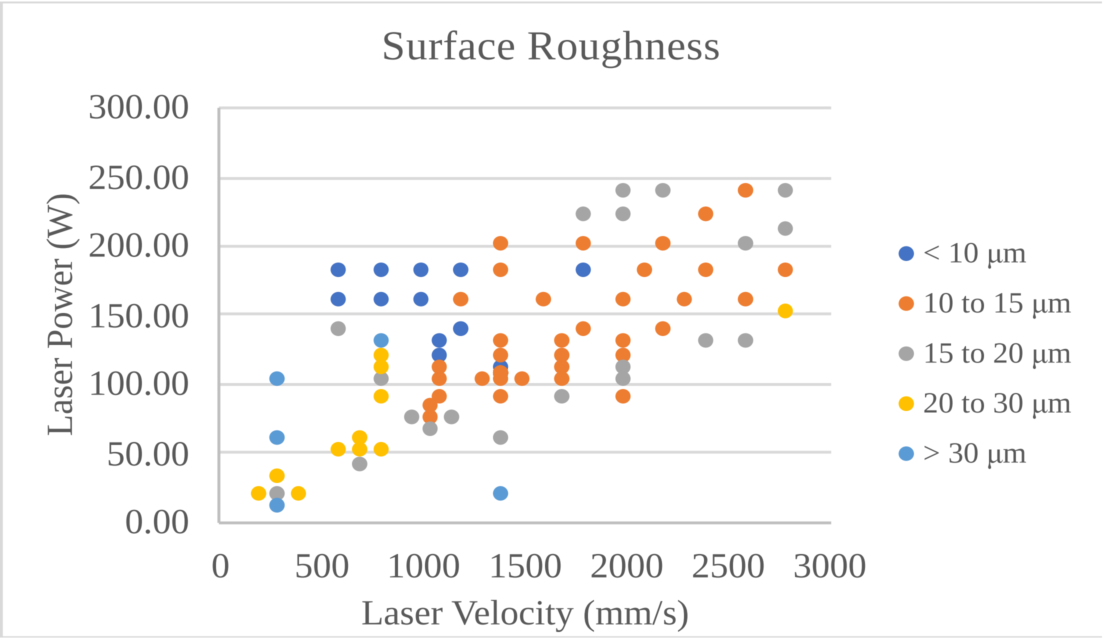

[redacted]

The surface roughness on the tops of the cubes showed similar trends to the area pads with the 100 W threshold, as seen in Figure 43. Most of the cubes with powers above 100 W have a surface roughness below 15.0 µm. Laser velocities play a role in the cube’s surface roughness in powers over 100 W, low velocities provided the best results and as velocities increase the surface quality diminished.

The surface roughness on the sides of the cubes provide information about how well the edges of each cube melts on each layer. The process map in Figure 45 shows the results from the side surface roughness measurements. Again, there was a trend in the cubes with laser powers above 100 W producing a lower surface roughness. The cubes with laser power over 100 W and velocities less than 1400 mm/s provided the best results.

The final measurement performed on this set of cubes was the form on the top side of the cube. The majority of the cubes provided a form measurement of less than 15.0 µm as seen in Figure 44. The region of the process map that produced cubes with

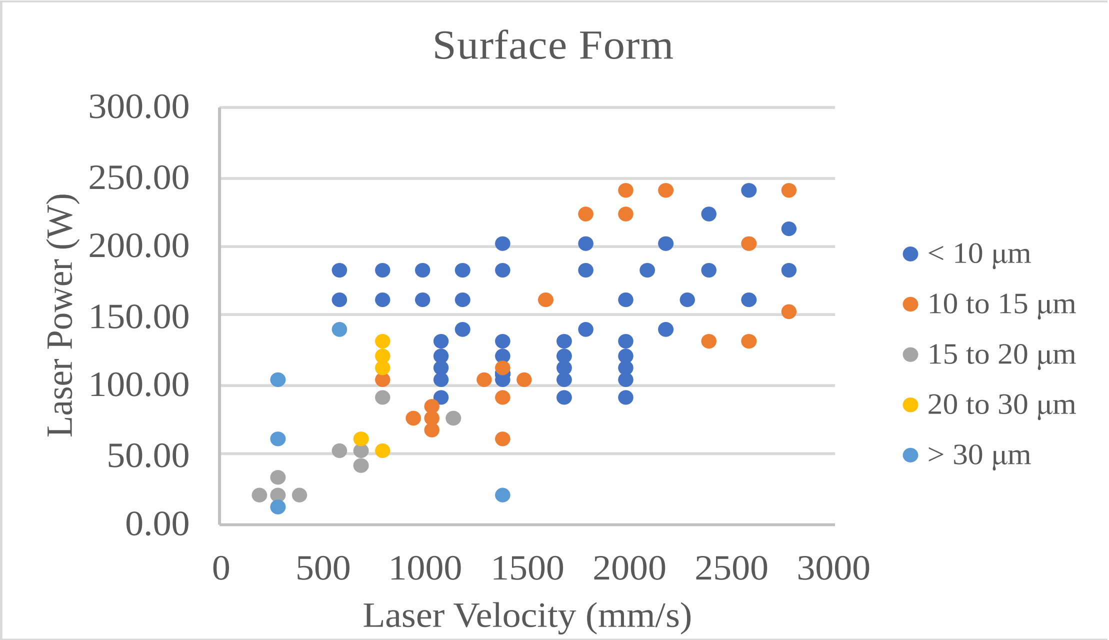

[redacted]

poor form was seen with velocities under 800 mm/s in all powers below 140 W. The results from the four different measurements was combined to produce a process window for fabricating dense parts, with quality surface finish, with powder lot #1, a 30.0 µm

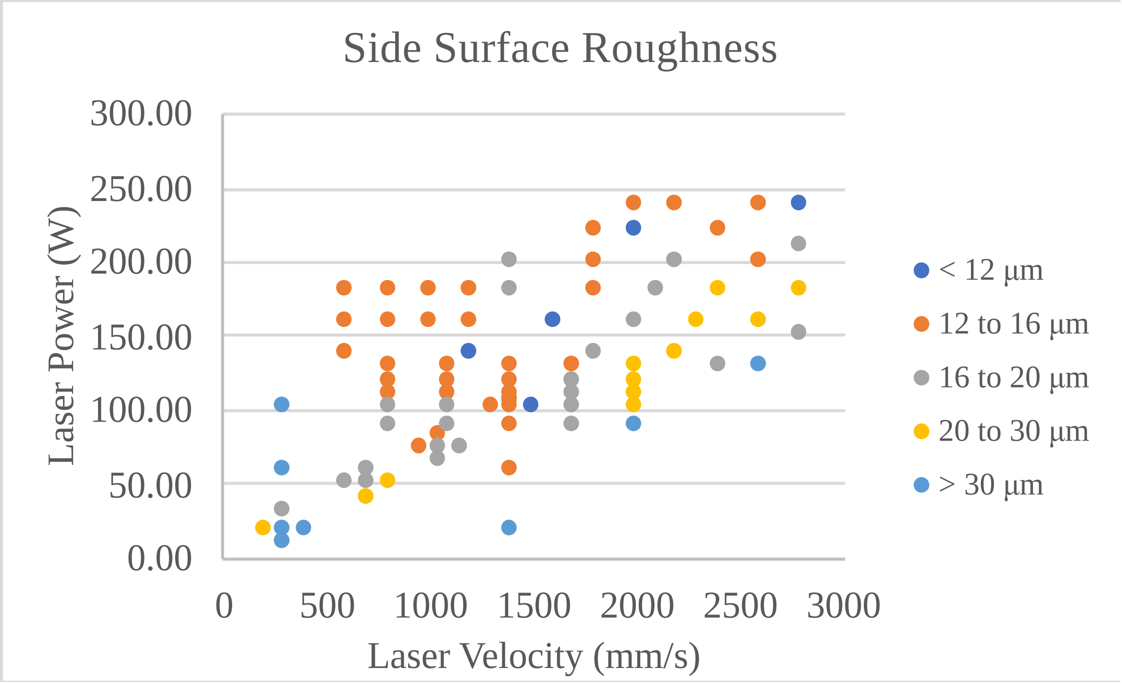

[redacted]

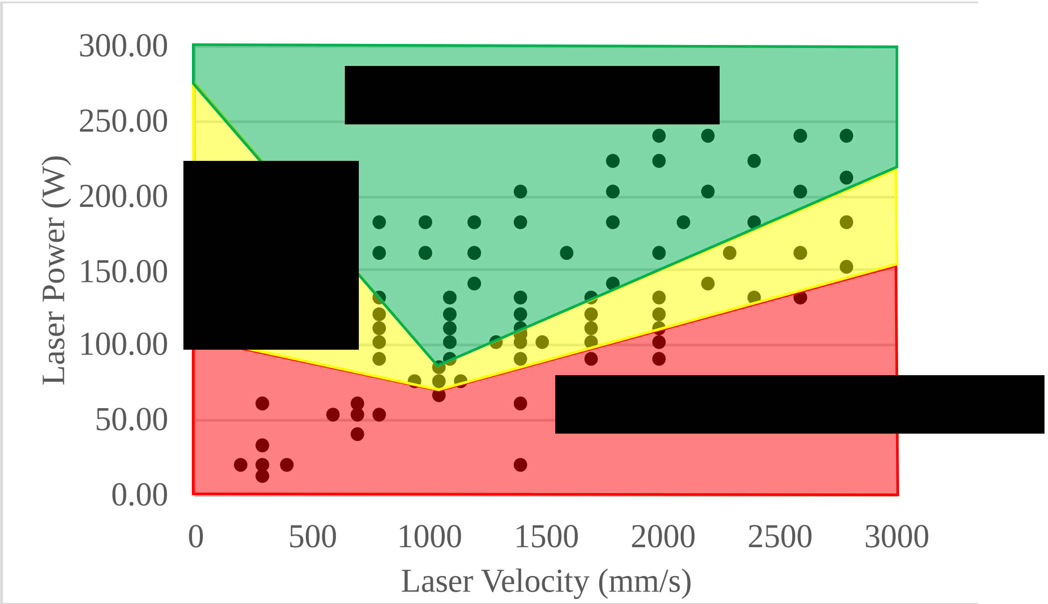

[redacted]

layer thickness, and a 1.0 mm above laser focus, the process window can be seen in Figure 46.

Eleven cubes from cube group #2 were selected for EBSD imaging. These cubes were investigated for grain size variations across laser power and velocity settings. There were five cubes that had a laser power of 120 W with laser velocities of 800, 1100, 1400, 1700, and 2000 mm/s. These cubes showed as laser velocity was increased the grain size decreased, as seen in Figure 47. The next set that was investigated used a constant velocity and varied power for comparison in grain size as power as varied. The velocity used was 1400 mm/s and the powers were 60, 90, 107, 120, 180, and 200 W, the grain

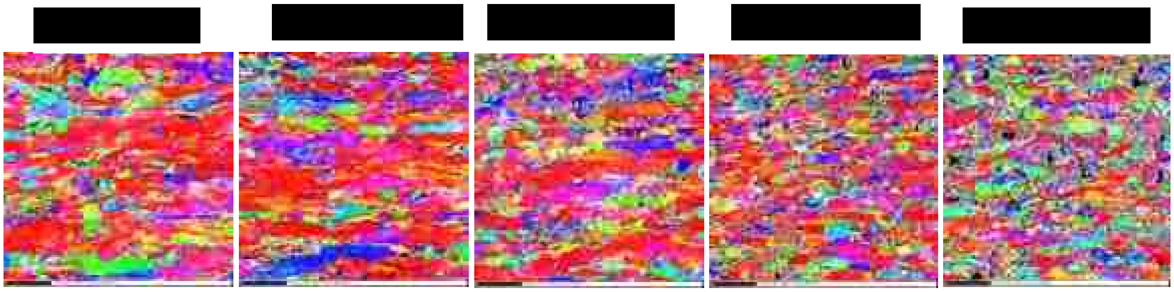

[redacted]

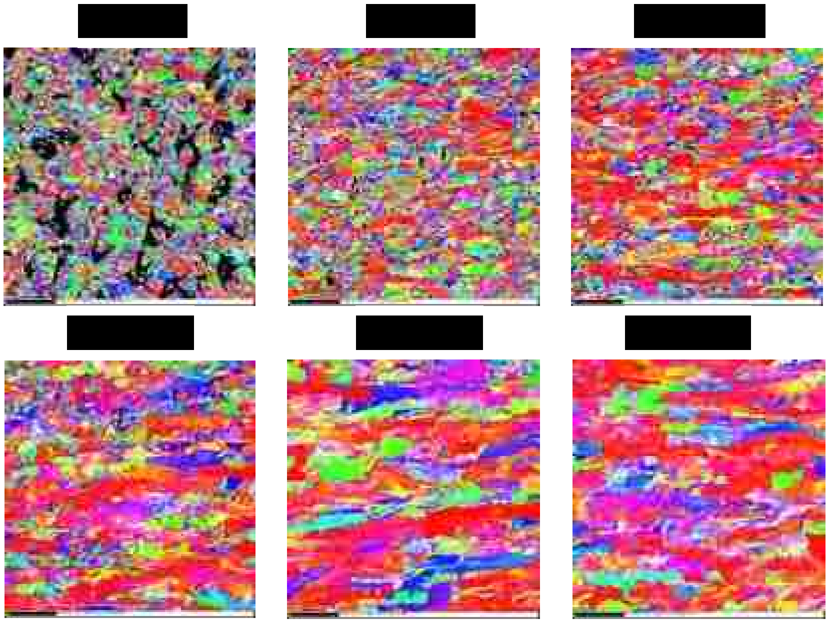
[redacted] [redacted] [redacted]
[redacted] [redacted] [redacted]

[redacted]

size increased with increasing power shown in Figure 48. The results from EBSD has shown laser power and velocity settings can influence grain sizes.

Before moving onto other layer thicknesses and effects of powder size, plate location on physical properties needed to be investigated. For this group, cube group #3, a baseline setting plate was fabricated using powder lot #1, 30.0 μm layer thickness, and a 1.0 mm laser focus offset. For this analysis the cubes were examined individually, by

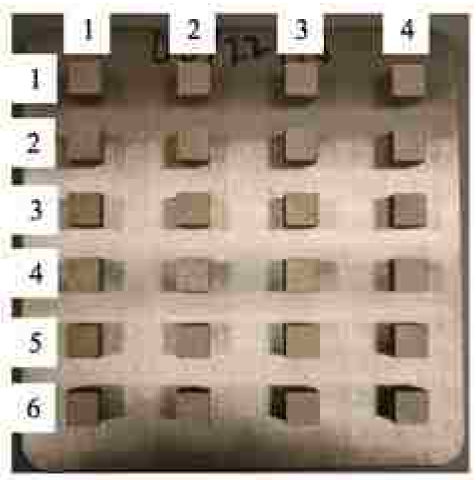

[redacted]

[redacted]

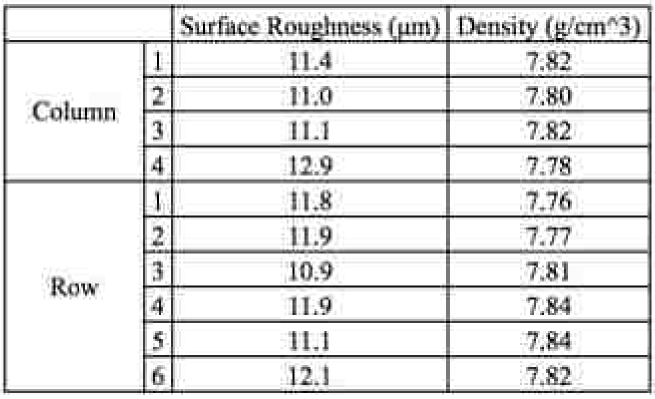

| | | Surface Roughness (μm) | Density (g/cm^3) |
|---|---|---|---|
| Column | 1 | 11.4 | 7.82 |
| | 2 | 11.0 | 7.80 |
| | 3 | 11.1 | 7.82 |
| | 4 | 12.9 | 7.78 |
| Row | 1 | 11.8 | 7.76 |
| | 2 | 11.9 | 7.77 |
| | 3 | 10.9 | 7.81 |
| | 4 | 11.9 | 7.84 |
| | 5 | 11.1 | 7.84 |
| | 6 | 12.1 | 7.82 |

the column, by the row, and the plate as a whole. Figure 49 shows the layout of the group #3 fabrication plate. The cubes were built from left to right starting in row 1 so that the cube in row 1 column 1 was built first and the cube in row 6 column 4 was built last. The cube with the highest denstity was found in row 5 column 2 and had a density of 7.87 g/cm$^3$. The cube with the lowest density was found in row 1 column 4 and had a density of 7.68 g/cm$^3$. It was suprising to see the difference of 0.21 g/cm$^3$ between the two cubes since they were built with the exact same parameters. The average density of all 24 cubes was 7.81±0.04 g/cm$^3$. This showed while there may be a large difference between the most and least dense cube, the rest of the cubes were rather constistant. When examining the the rows and columns, it was shown there was some vairiability but it was pretty consistant. The column with the lowest average density is column 4 and the row with the highest average density is row 1. The results from the the baseline setting plate can be seen in Table 4. The results from this plate showed there was some plate location effects on the cubes but it is minimal. For this study the plate locations effects will be ignored but this plate provided infromation for when building parts, avoid the top right corner of the build plate.

As stated earlier the most and least dense cube had a difference of 0.21 g/cm$^3$. To investigate if there was any differences in the grain structure that may have caused this difference, these two cubes had EBSD imaging performed. Visually there was a minimal differnce in grain size between the two, as seen in Figure 50. The cube with the highest density appears to have larger grains than the cube with the lowest density. To detemine if this is actually the case the grains sizes should be measured.

The next group, group #4, of cubes increased the layer thickness to 40.0 μm from 30.0 μm with powder from lot #1. There were two plates built with twenty-four cubes on each for this group for a total of forty-eight cubes. The first plate used laser power and velocity setting from group #2 to compare cubes with a layer thickness of 30.0 μm to cubes with a layer thickness of 40.0 μm. The results showed only nine of twenty-four cubes had an increased density at a 40.0 μm layer thickness and only two of the twenty-four had an improved surface roughness, the results can be seen in Table 5. The only

[redacted] [redacted]

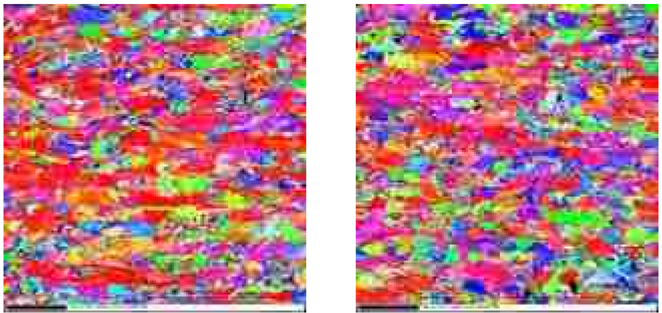

[redacted]

noticeable trend for the nine cubes with a higher density in the 40.0 μm was these cubes all had velocities less than 1400 mm/s.  The two with better surface roughness values also had lower velocities, 300 and 800 mm/s.  A suspected reason why the cubes with a 40.0 μm layer thickness had a lower density than the cubes with a 30.0 μm layer thickness is the reduction in the VED for the 40.0 μm cubes.

[redacted]

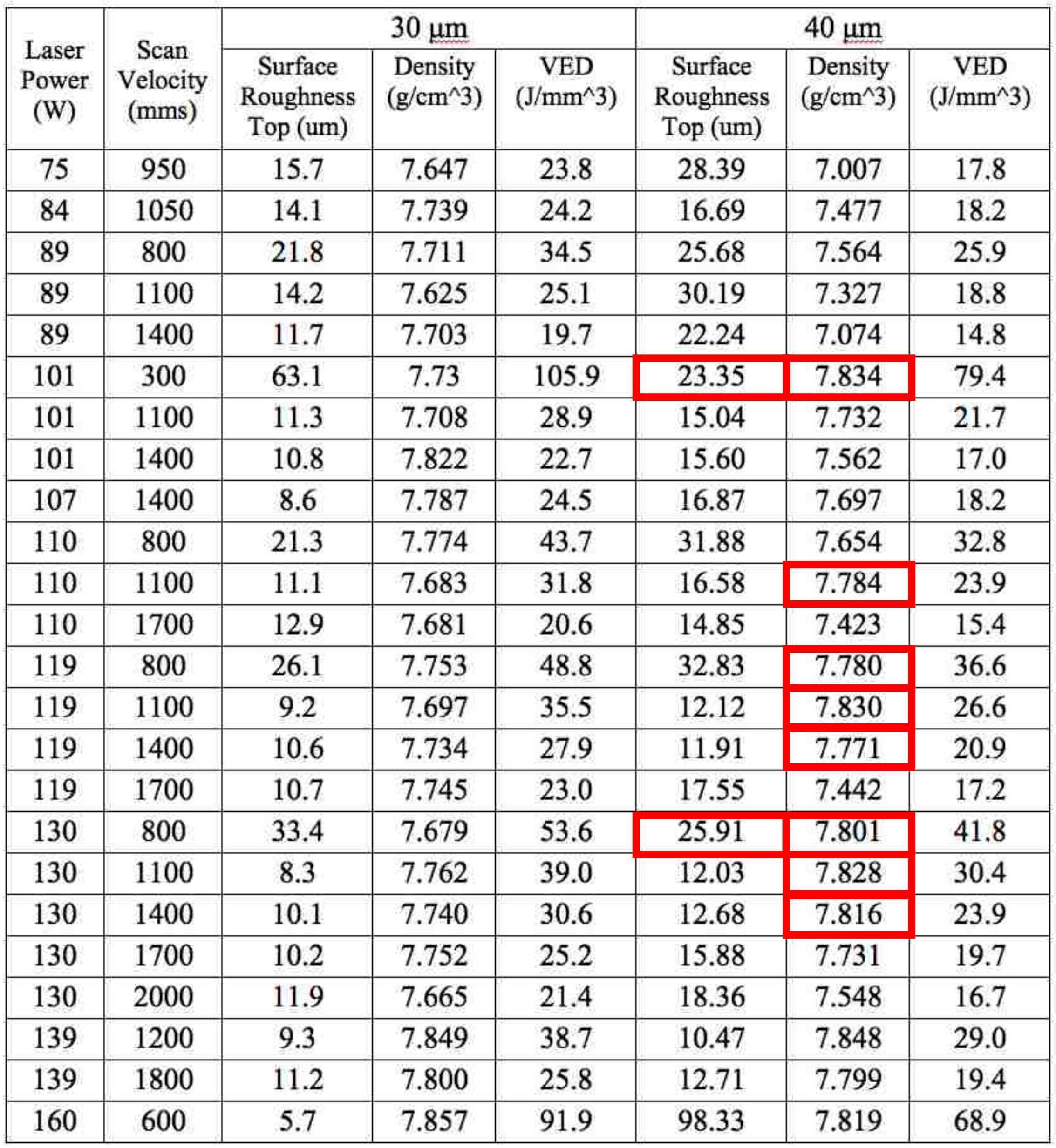

| Laser Power (W) | Scan Velocity (mms) | 30 µm | | | 40 µm | | |
|---|---|---|---|---|---|---|---|
| | | Surface Roughness Top (um) | Density (g/cm^3) | VED (J/mm^3) | Surface Roughness Top (um) | Density (g/cm^3) | VED (J/mm^3) |
| 75 | 950 | 15.7 | 7.647 | 23.8 | 28.39 | 7.007 | 17.8 |
| 84 | 1050 | 14.1 | 7.739 | 24.2 | 16.69 | 7.477 | 18.2 |
| 89 | 800 | 21.8 | 7.711 | 34.5 | 25.68 | 7.564 | 25.9 |
| 89 | 1100 | 14.2 | 7.625 | 25.1 | 30.19 | 7.327 | 18.8 |
| 89 | 1400 | 11.7 | 7.703 | 19.7 | 22.24 | 7.074 | 14.8 |
| 101 | 300 | 63.1 | 7.73 | 105.9 | 23.35 | 7.834 | 79.4 |
| 101 | 1100 | 11.3 | 7.708 | 28.9 | 15.04 | 7.732 | 21.7 |
| 101 | 1400 | 10.8 | 7.822 | 22.7 | 15.60 | 7.562 | 17.0 |
| 107 | 1400 | 8.6 | 7.787 | 24.5 | 16.87 | 7.697 | 18.2 |
| 110 | 800 | 21.3 | 7.774 | 43.7 | 31.88 | 7.654 | 32.8 |
| 110 | 1100 | 11.1 | 7.683 | 31.8 | 16.58 | 7.784 | 23.9 |
| 110 | 1700 | 12.9 | 7.681 | 20.6 | 14.85 | 7.423 | 15.4 |
| 119 | 800 | 26.1 | 7.753 | 48.8 | 32.83 | 7.780 | 36.6 |
| 119 | 1100 | 9.2 | 7.697 | 35.5 | 12.12 | 7.830 | 26.6 |
| 119 | 1400 | 10.6 | 7.734 | 27.9 | 11.91 | 7.771 | 20.9 |
| 119 | 1700 | 10.7 | 7.745 | 23.0 | 17.55 | 7.442 | 17.2 |
| 130 | 800 | 33.4 | 7.679 | 53.6 | 25.91 | 7.801 | 41.8 |
| 130 | 1100 | 8.3 | 7.762 | 39.0 | 12.03 | 7.828 | 30.4 |
| 130 | 1400 | 10.1 | 7.740 | 30.6 | 12.68 | 7.816 | 23.9 |
| 130 | 1700 | 10.2 | 7.752 | 25.2 | 15.88 | 7.731 | 19.7 |
| 130 | 2000 | 11.9 | 7.665 | 21.4 | 18.36 | 7.548 | 16.7 |
| 139 | 1200 | 9.3 | 7.849 | 38.7 | 10.47 | 7.848 | 29.0 |
| 139 | 1800 | 11.2 | 7.800 | 25.8 | 12.71 | 7.799 | 19.4 |
| 160 | 600 | 5.7 | 7.857 | 91.9 | 98.33 | 7.819 | 68.9 |

To test this theory, another plate of cubes was built at 40.0 μm. This plate kept either laser power or velocity constant for each cube and varied the other to keep the VED constant to match the VED for the 30.0 μm cubes. By only varying one of the laser settings was a chance to investigate if power or velocity, had a greater influence on the density. The selection of which setting was changed, and which one wasn't, for each cube was selected at random. This provided twelve cubes with a new power setting and twelve cubes with a new velocity setting. The cubes that used the same power but changed the velocity had mixed results with six cubes having a better density at a 40.0 μm layer thickness. There was a noticeable trend in this set of cubes when comparing the density to the VED value. The cubes with a VED value above 30.0 J/mm$^3$ showed an increase in density in five of the six 40.0 μm layer thickness cubes. The opposite can be said for the cubes with a VED value below 30.0 J/mm$^3$, the results can be seen in Figure 51. The twelve 40.0 μm cubes where the power was increased to match the VED on the

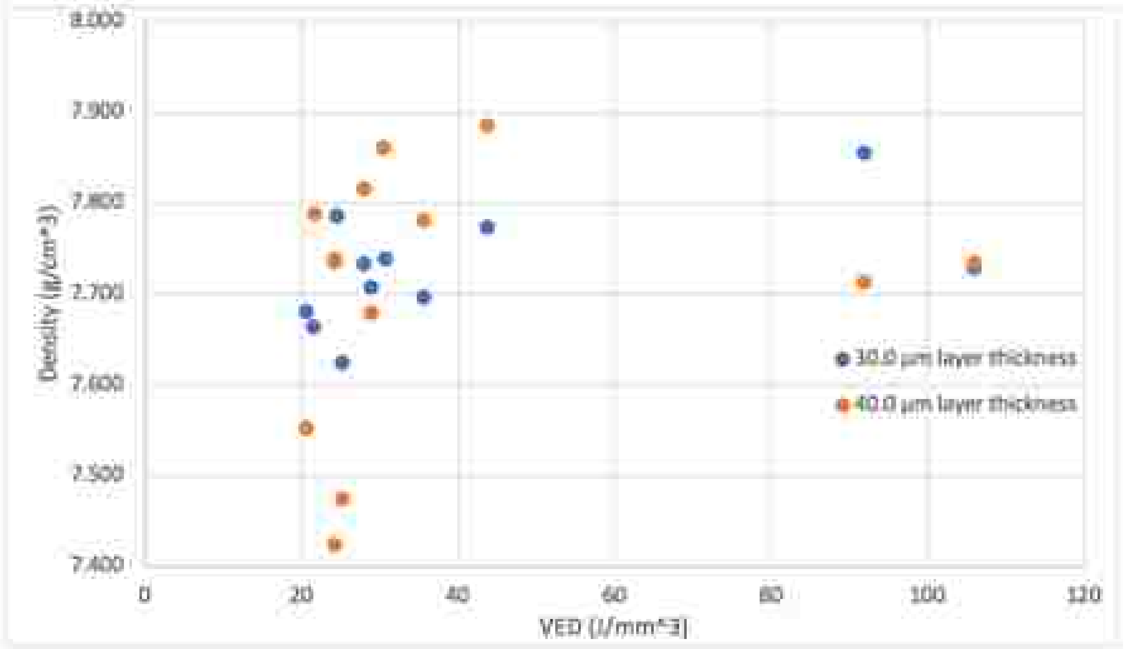

[redacted]

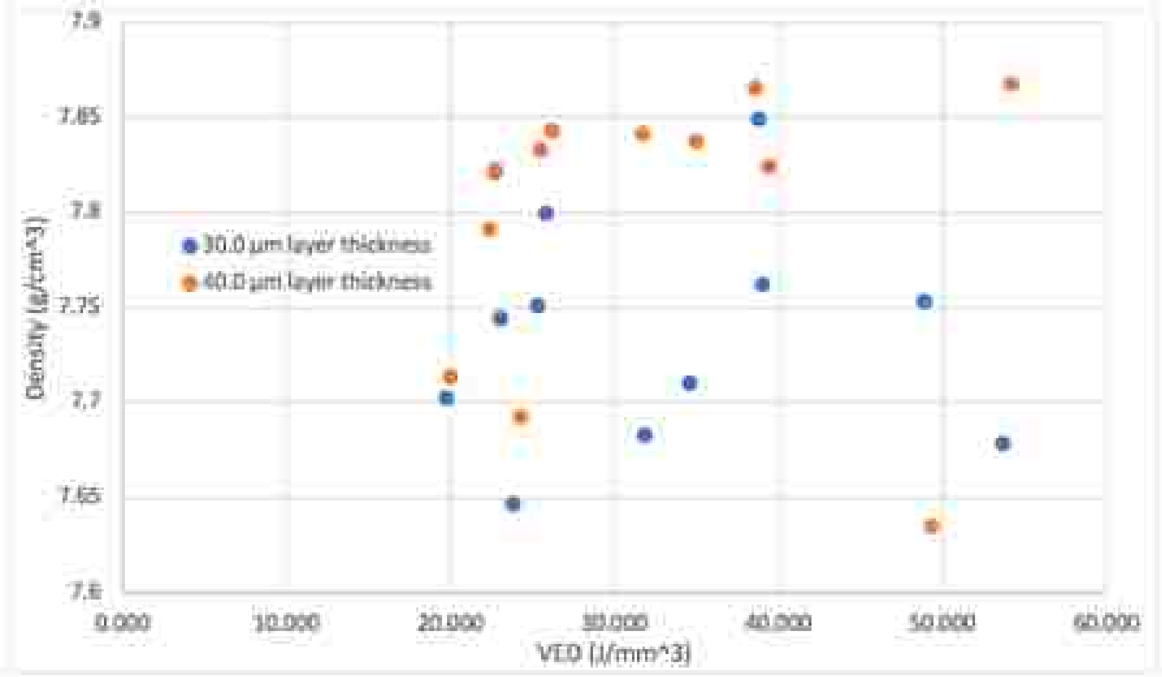

[redacted]

30.0 µm layer thickness cubes was more promising. This set of cubes had ten of twelve that displayed an increased density, when compared to the 30.0 µm layer thickness cubes. This indicated power may have a greater influence on density than the velocity does. The result comparison for the power set can be seen in Figure 52. Overall the plate where VED was held constant for the two-different layer thickness demonstrated an increased density for two-thirds of the cubes at a 40.0 µm layer thickness when compared to the cubes with 30.0 µm layer thickness. The downfall of group #4 was that the surface roughness quality was reduced at the 40.0 µm layer thickness with twenty-two of the twenty-four cubes having a better surface finish on the 30.0 µm layer thickness cubes.

Group #4 had 5 cubes EBSD imaged to investigate the changes of the grain sizes. One cube was used for both the constant power and velocity settings, three others were used for constant power, and only one other for constant velocity. First comparing the four cubes with 120 W power and velocities of 800, 1100, 1400, and 1700 mm/s. The [redacted] [redacted] [redacted] [redacted]

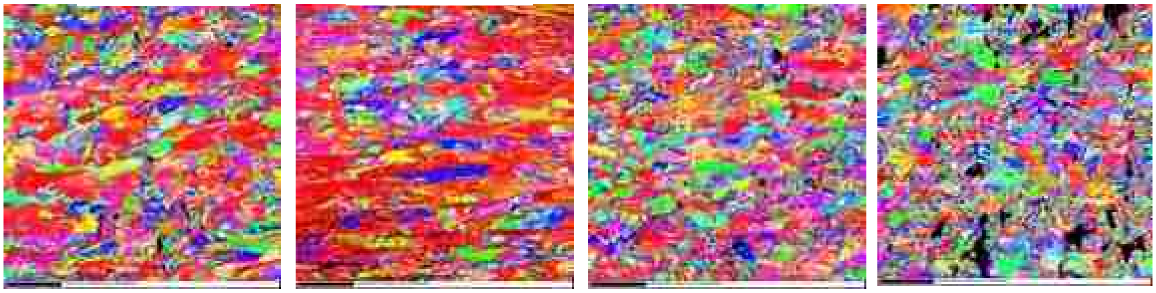

[redacted]

results showed similarity with group #2 as when velocity was increased at constant power the grain size decreases.  The constant power EBSD images can be seen in Figure 53. Only two cubes were compared at 1400 mm/s per second for group #4, as seen in Figure 54.  The differences in grain sizes are hard to determine in the two cubes, mostly because the number of voids in the 90 W cube.  If the same trend was followed in group #4 that was seen in group #2 the 120 W cube would have a larger grain size.

The next groups of cubes investigated how a different 316L powder would react to the same process settings.  The first group, group #5, of cubes used power and velocity process settings from group #2 but used powder lot #2 at a 30.0 μm layer thickness.  The focus of this plate was to understand if a larger particle size would require a larger VED to completely melt the powder.  Another question was how an average particle size of

[redacted] [redacted]

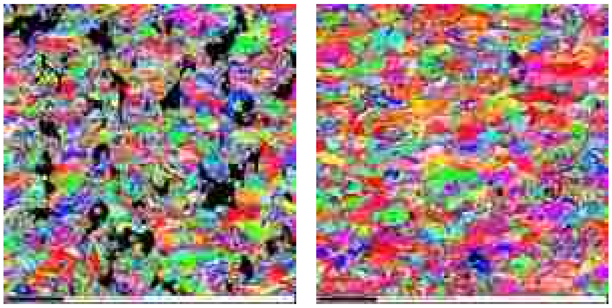

[redacted]

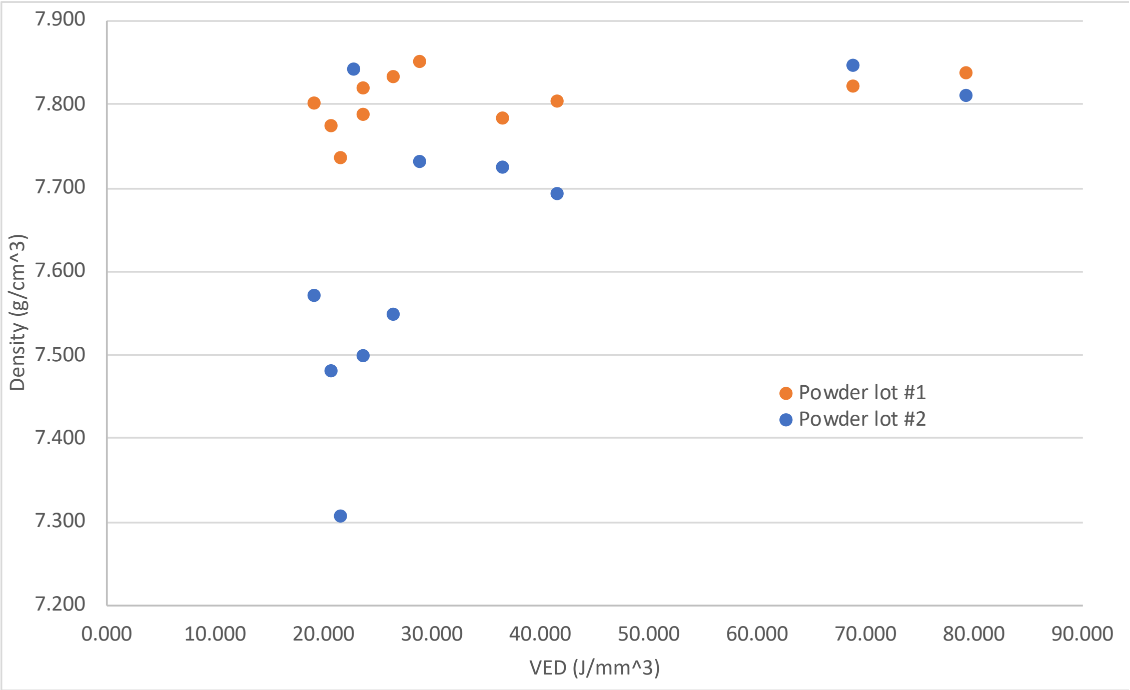

[redacted]

~25.0 µm would affect density when the layer thickness was at 30.0 µm. The results showed that VED did have a large influence of cube group #5. The ten cubes with a VED less than ~30.0 J/mm$^3$ had a higher density in cube fabricated using powder lot #1, as seen in Figure 55. Of the fourteen cubes remaining above the 30.0 J/mm$^3$ VED threshold nine of them have a higher density with powder lot #2. Only one of the five cubes had a substantially higher density leaving the other 4 cube's differences minimal and was viewed as equal. The results from this cube group #5 showed that powder with a larger particle size needed an increase in VED to provide dense parts.

In cube group #5 there were 5 cubes imaged using EBSD. One was used for both constant power and constant velocity, two for constant power, and two for constant velocity. The constant power cubes were at 120 W and velocities of 800, 1400, and 1700 mm/s. Similar trends were once again seen with the grain size decreasing as velocity is increased, as seen in Figure 56. The constant velocity cubes used 1400 mm/s at 100, [redacted] [redacted] [redacted]

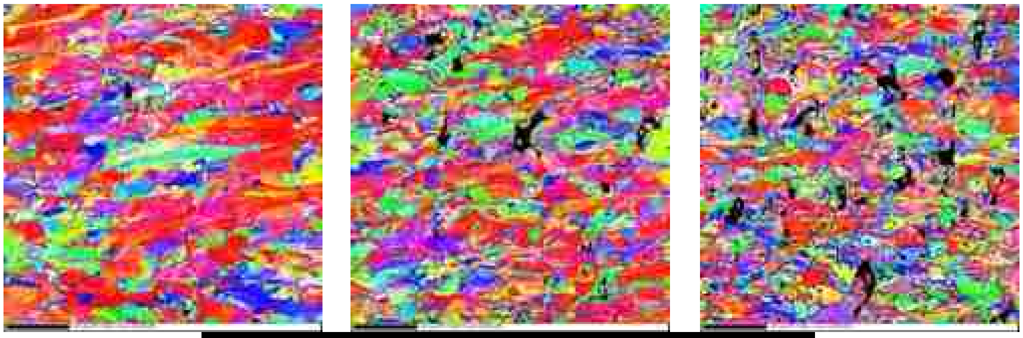

[redacted]

120, and 180 W. The same trend from previous groups with the grain size getting larger as power is increased at constant velocity is also seen in this group, Figure 57.

The final plate of cubes, cube group #6, for this study again used powder lot #2 but at a 40.0 µm layer thickness. This plate included seventeen laser power and velocity settings that were used in cube group #5. The results showed that cubes from cube group #5 had a higher density in fifteen of seventeen cubes, as seen in Figure 58. Only four of the cubes compared was over the ~30.0 J/mm$^3$ threshold seen in the comparisons of 30.0 and 40.0 µm layer thicknesses in powder lot #1. Only one of the four cubes over 30.0 J/mm$^3$ had a higher density. This showed the powder lot B performed better at a 30.0 µm layer thickness when using similar laser settings. Adjusting the laser settings to match the VED was not performed in powder lot #2.

[redacted] [redacted] [redacted]

[redacted]

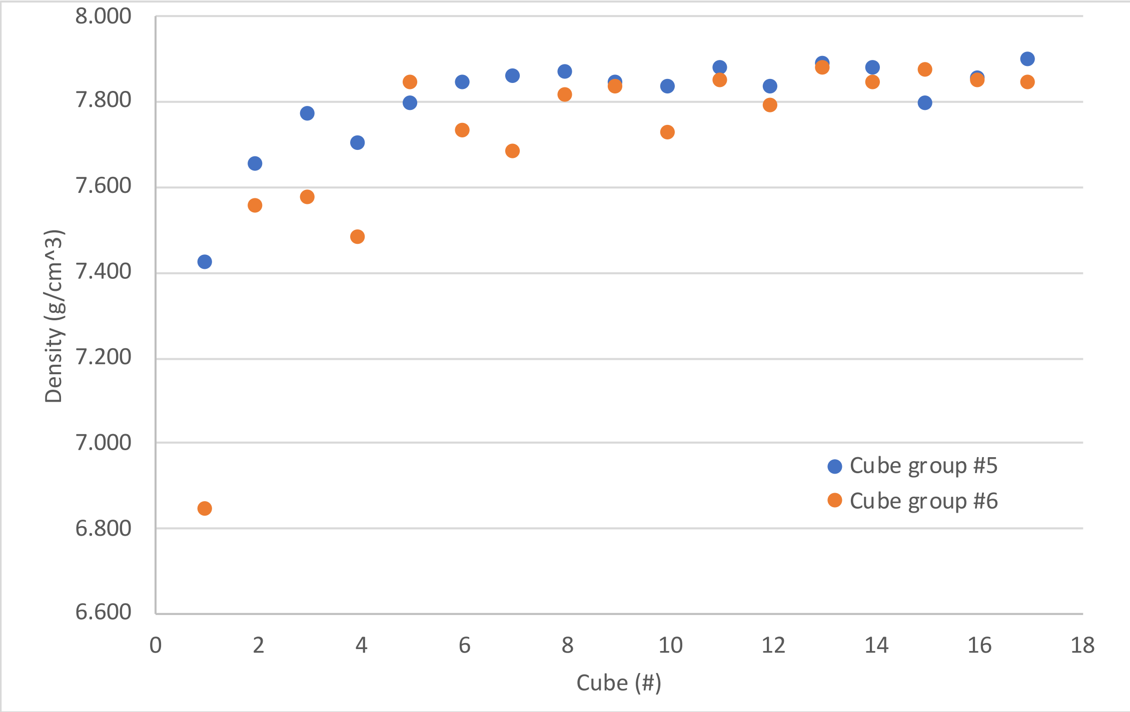

[redacted]

Cube group #6 also used five cubes for EBSD comparisons same as group #5. One was used for constant power and velocity, two for constant power, and two for constant velocity. The constant velocity cubes had a power setting of 120 W with velocities of 800, 1100, and 1400 mm/s. The results were the same seen in all other constant power cubes with as velocity was increased the grain size got smaller, the results can be seen in Figure 59. The cubes used for the constant velocity of 1400 mm/s used

[redacted] [redacted] [redacted]

[redacted]

[redacted] [redacted] [redacted]

[redacted]

powers at 100, 120, and 180 W. The comparisons of changes in power at constant velocities displayed increased grain size as power was increased, as seen in Figure 60.

Cubes fabricated using different process variables have been compared with a focus of optimizing surface roughness and density. Grain sizes were also compared within the groups of cubes they were assigned to, investigating how the grain size changed when changing either laser power or velocity. To determine if the layer thickness or the powder size had an influence on grain size or density cubes between groups were compared. Comparisons were made between groups when the laser power and velocity settings were held constant and either the layer thickness or powder lot varied. As a reminder cube group #2 used a 30.0 µm layer thickness and powder lot #1, cube group #4 used a 40.0 µm layer thickness and powder lot #1, cube group #5 used a 30.0 µm layer thickness and powder lot #2, and cube group #6 used a 40.0 µm layer thickness and powder lot #2.

There was a total of five laser power and velocity settings that were used to fabricate at least three cubes from different cube groups and had EBSD images. The first set of laser settings were 120 W power and 800 mm/s velocity, the EBSD images can be seen in Figure 61. EBSD showed similarities in grain size in cube group #2 and #5, and [redacted] [redacted] [redacted] [redacted]

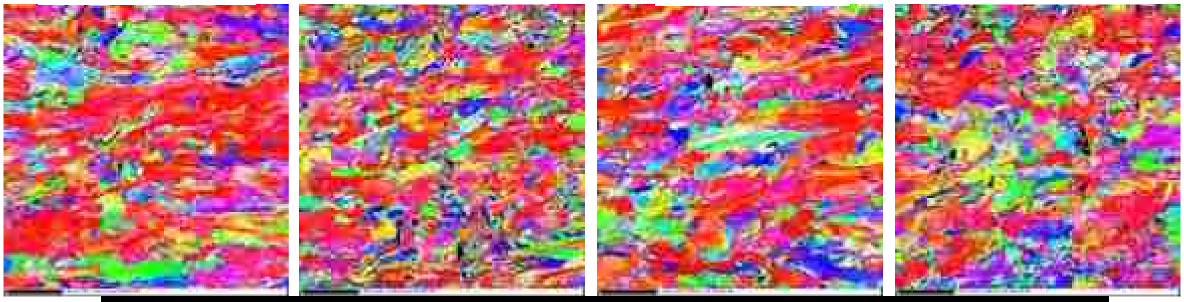

[redacted]

in group #4 and #6. The other common trend between the groups with similar grain sizes was the layer thickness. This showed that layer thickness may have more of an influence on grain sizes than powder size did. The densities for each cube showed similarity across the four groups with this set of laser settings.

The next laser settings again used 120 W for the power but 1100 mm/s for the velocity. The results showed the layer thickness may not have the influence on grain size as thought from the first set of laser settings. The EBSD images showed similarities between the two-powder lot #1 groups, groups #2 and #4, as seen in Figure 62. The grains in group #2 and #4 not only have similar grain sizes but the orientations were also similar in that they are running horizontally. The densities between these three cubes did not have any similarities.

[redacted] [redacted] [redacted]

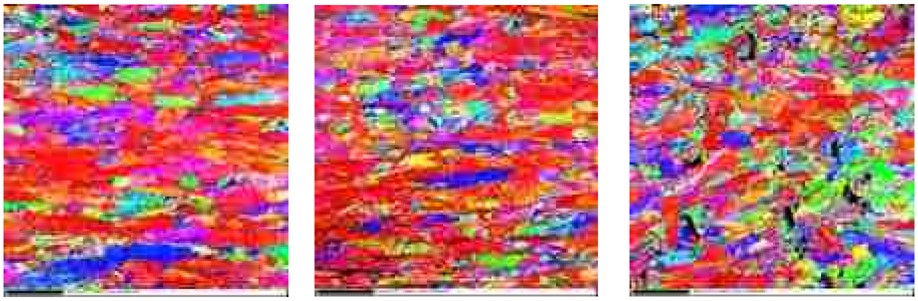

[redacted]

[redacted]

[redacted]

[redacted]

[redacted]

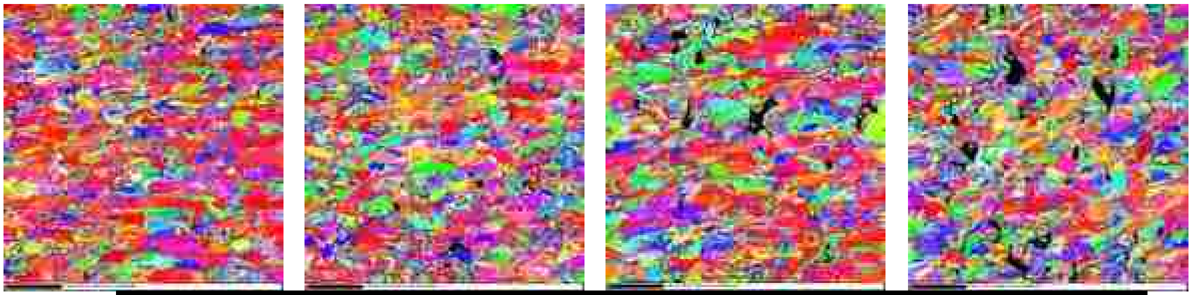

[redacted]

The next set of laser settings again used a laser power of 120 W but a laser velocity of 1400 mm/s. The EBSD images from this set of laser settings show similarities in grain size across all four cubes, as seen in Figure 63. These similarities in grain size may be because as velocity was increased in each group, the grain size got smaller, as shown earlier when cubes were compared in individual groups. For the density comparisons only, the cube from group #6 showed a large difference in density from the other three.

The final set of cubes that used 120 W for power used 1700 mm/s as velocity. These ESBD images showed similarities, again, in the powder lot used, as seen in Figure 64. Group #2 did show some similarities in grain size with group #5 and #6 but there

[redacted]

[redacted]

[redacted]

[redacted]

[redacted]

[redacted]

[redacted]

[redacted]

were larger grains found in group #2 which made it appear different. Interestingly the densities in group #5 and #6 were almost identical, and group #2 had a higher density.

The final set of laser parameters that was compared was 180 W power and 1400 mm/s velocity. This set of laser settings not only provided similar grain sizes but also nearly identical densities, as seen in Figure 65. These results showed that laser power is probably the most influential parameter because as the laser power was increased the grain sizes and densities became similar while all other variables were kept constant.

In this summary, many process variables were varied and their influences on surface roughness, form, density, and grain size were investigated. The variables investigated were laser power, velocity, and focus offsets along with layer thickness and particle size. It was found that laser focus and laser power were the most influential on density. Laser power can have a negative effect on form if velocities are too slow. Velocities appeared to have the most influence on grain sizes, with slower velocities creating larger grains and as velocity was increased the grains became smaller.

## Section 4.4: Dog Bone Arrays

The dog bone arrays were the first parts built that provided mechanical properties. There were five plates of dog bone arrays fabricated for tensile testing. The first three plates explored the effects of laser power and velocity settings on mechanical properties and the last two plates were used for validation and repeatability. The mechanical properties provided from tensile testing are yield strength, unloading Young's modulus, ultimate tensile strength (UTS), ductility, and uniform elongation (strain at UTS). For comparing mechanical properties for AM fabricated 316L parts, AISI type 316L stainless steel annealed bar was used. Two sets of data are shown in Table 6, the first is from literature and the second is from wrought 316L which was machined into a twenty-five dog bone array and tested at Sandia using the HTT to use as a baseline for 316L in house [25]. The in-house tested wrought 316L mechanical properties were used for comparisons against the AM 316L mechanical properties generated from this study. Each property was compared against laser settings for developing a process map for mechanical properties.

The laser setting used for the first dog bone arrays' plate were chosen based on data from the cube data, where laser settings produced dense cubes. The next two plates' laser settings were chosen by filling in the gaps inside of the process map and to test the

[redacted]

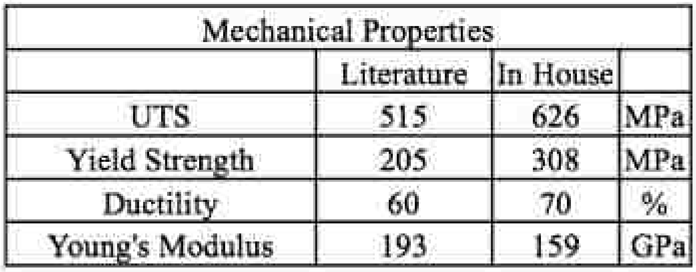

| Mechanical Properties | | | |
|---|---|---|---|
| | Literature | In House | |
| UTS | 515 | 626 | MPa |
| Yield Strength | 205 | 308 | MPa |
| Ductility | 60 | 70 | % |
| Young's Modulus | 193 | 159 | GPa |

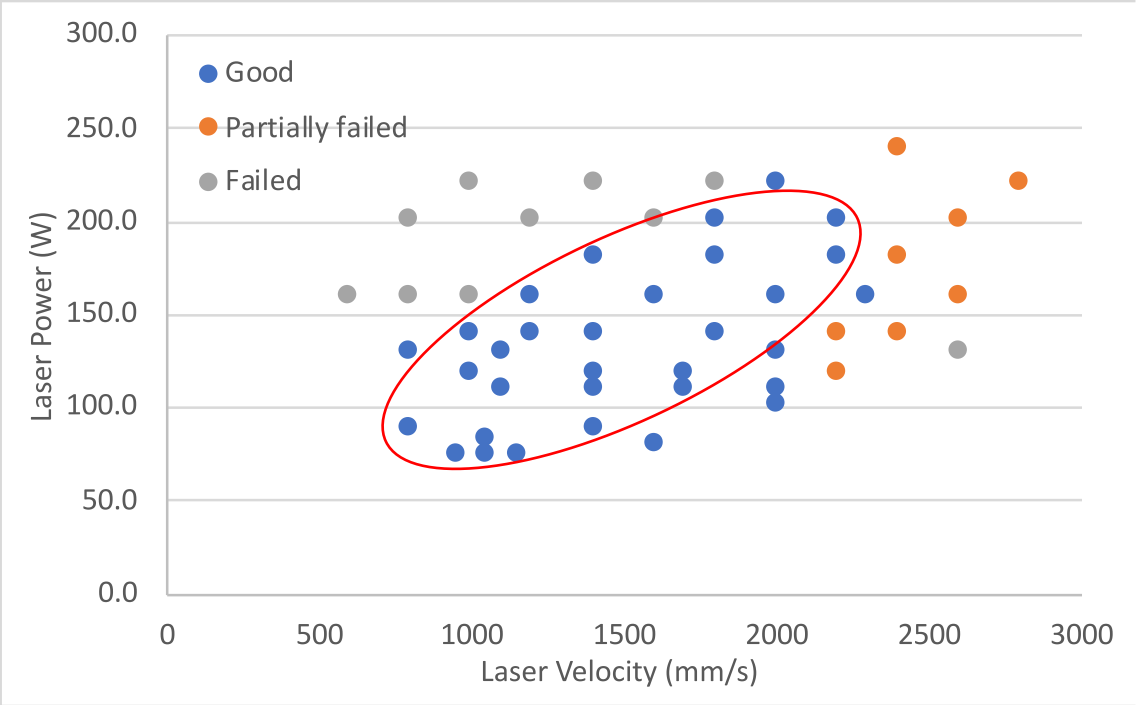

[redacted]

boundaries. The process map showed a band of dog bone arrays that printed, running diagonally through the process map, shown in Figure 66.  The dog bones that failed lied above the band that used higher power settings and slowed velocities.  The dog bones that partially failed used high velocities at all powers.  Process maps for mechanical properties were generated to determine if any properties were maximized in specific regions.

The first mechanical properties analyzed were the unloading Young’s modulus, yield strength, and UTS.  The dog bone array with the highest unloading modulus was 135 GPa fabricated using a laser power of 140 W and velocity 1000 mm/s, about 25 GPa below the baseline wrought sample.  The modulus values were split into five groups, over 120 GPa, 110 to 120 GPa, 100 to 120 GPa, under 100 GPa, and if they failed or could not be tested.  The results showed the dog bone arrays with similar unloading modulus values were grouped on the process map, as seen in Figure 67.  The group of dog bone arrays

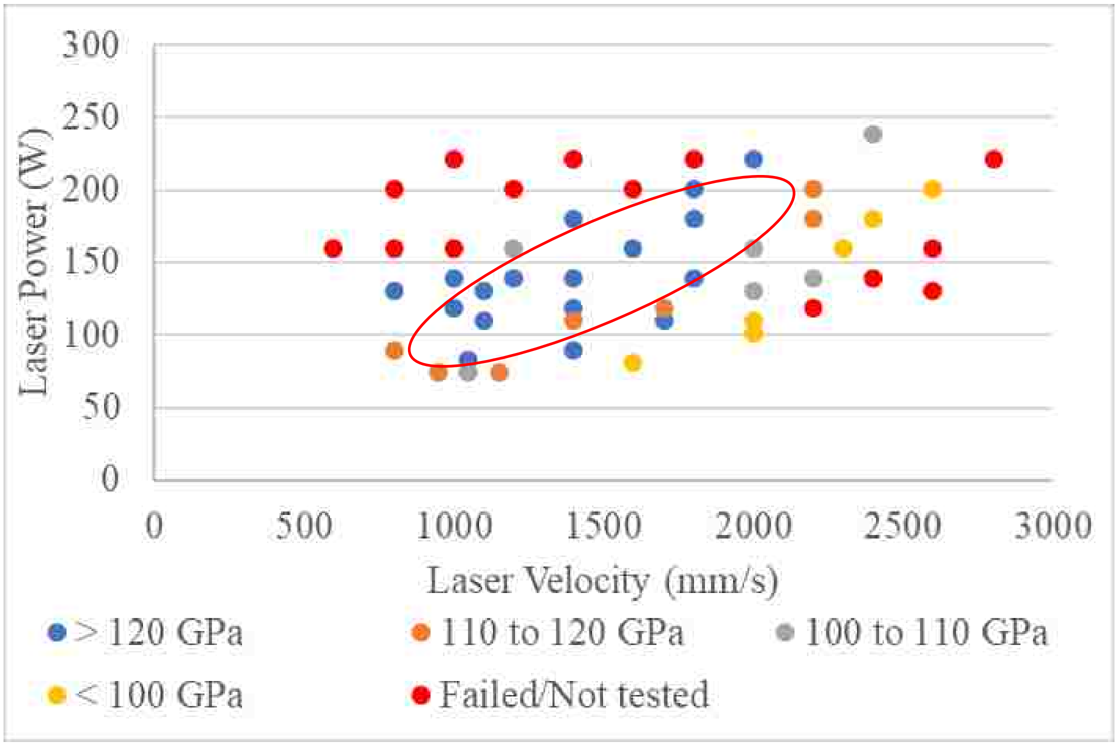

[redacted]

that exhibited over 120 GPa moduli fell on the border of arrays that did not print and none of these arrays had velocities over 2000 mm/s.

Yield strength was the second mechanical property compared using the process map. The dog bone array with the highest yield strength at 457 MPa used 120 W power and 1700 mm/s velocity for fabrication. The wrought 316L provided a yield strength of only 308 MPa and the literature value was even lower at 205 MPa. This showed that while modulus was lower in AM when compared to wrought, the strength was much higher. The yield strength results were again split into five categories, above 400 MPa, 350 to 400 MPa, 300 to 350 MPa, below 300 MPa, and failed/not tested. Where these regions fell on the process map are shown in Figure 68. Again each category provided regions on the process map similar to the unloading modulus results. The region that

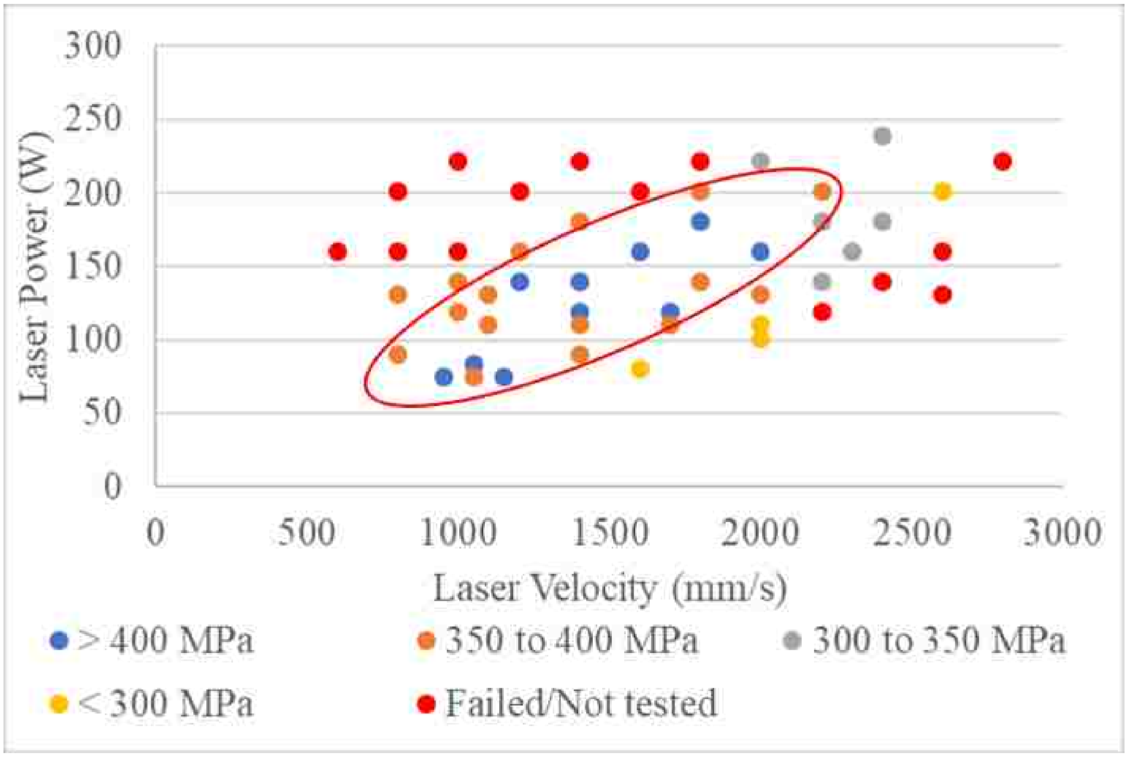

[redacted]

maximized yield strength was found running diagonally through the center of the process map.

The next mechanical property that was compared was ultimate tensile strength (UTS). The array with the highest UTS had a UTS of 584 MPa and used a laser power of 120 W with 1700 mm/s velocity, this array was also had the highest yield. The 584 MPa UTS was lower than the UTS from the wrought sample, 626 MPa, but was higher than the literature value, 515 MPa. The results were again split into five categories for UTS, above 540 MPa, 500 to 540 MPa, 400 to 500 MPa, below 400 MPa, and failed/not tested. The arrays with the highest UTS values once again are located in the center of the process map, as seen in Figure 69. The first three properties compared showed similarities on where they were found on the process map.

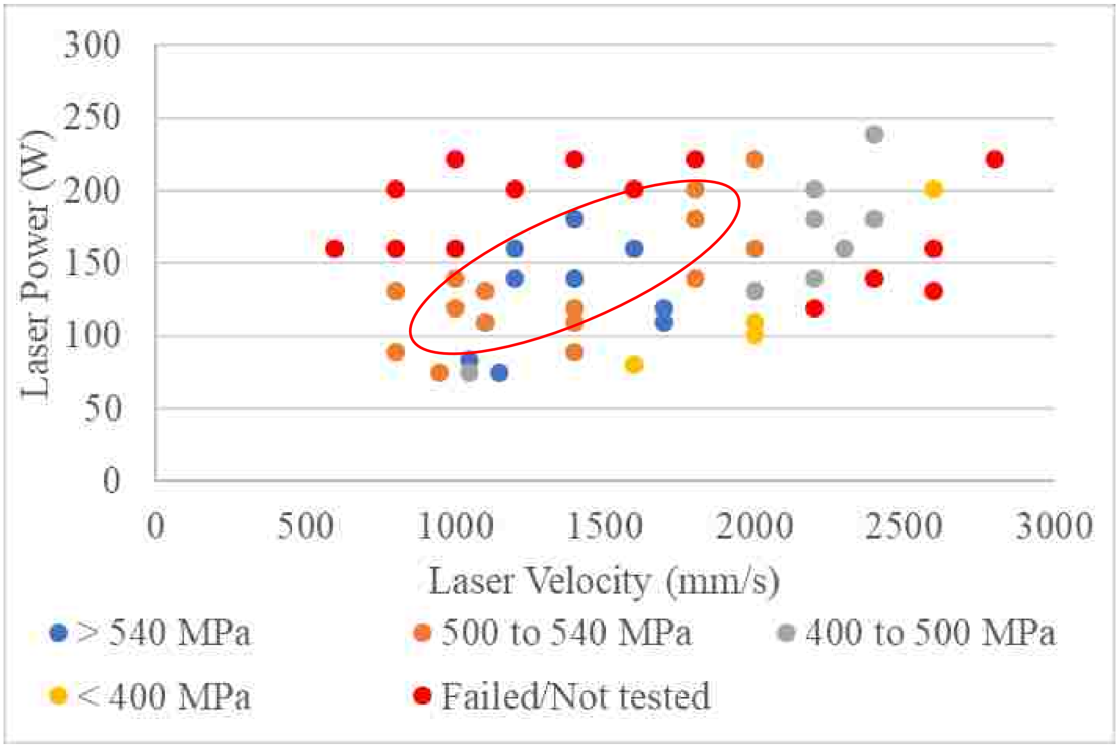

[redacted]

The next mechanical property was uniform elongation or strain at UTS. The array with the highest uniform elongation had a value of 50% and used laser settings of 130 W power with 800 mm/s velocity. This was comparable to the wrought sample which had a value of 52%. The results for all of the arrays from the first three plates were again split up in to five categories, above 38%, 30 to 38%, 20 to 30%, below 20%, and failed/did not print. The arrays with the best uniform elongation values, again, grouped up along an edge of where several dog bone arrays failed, as seen in Figure 70.

The final mechanical property investigated was ductility. The array that was fabricated using 130 W power with 800 mm/s velocity had the highest ductlity at 69%. This value was comparable to the in-house sample that had 70% ductility and out performed literature, which was 60%. Once again the ductility results were divided into five categories for the process map, above 58%, 50 to 58%, 30 to 50%, below 30%, and failed/not tested. The group of arrays with the best ductility were all found grouped

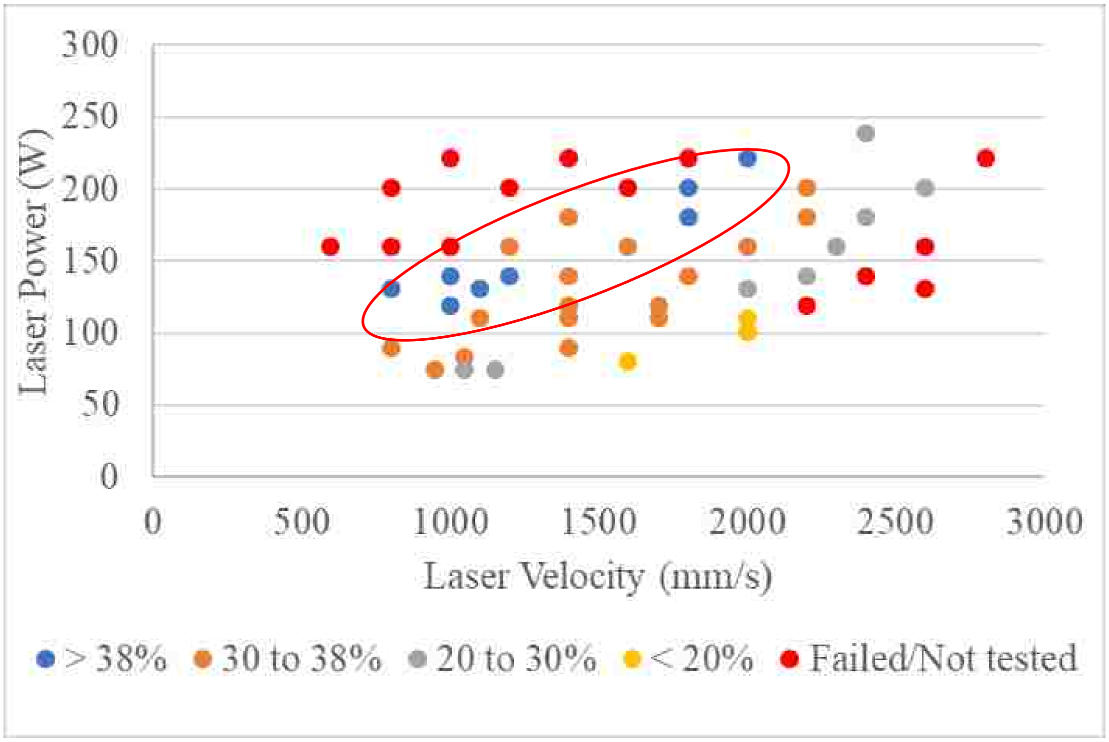

[redacted]

together in a region with laser powers between 110 and 140 W with velocities between

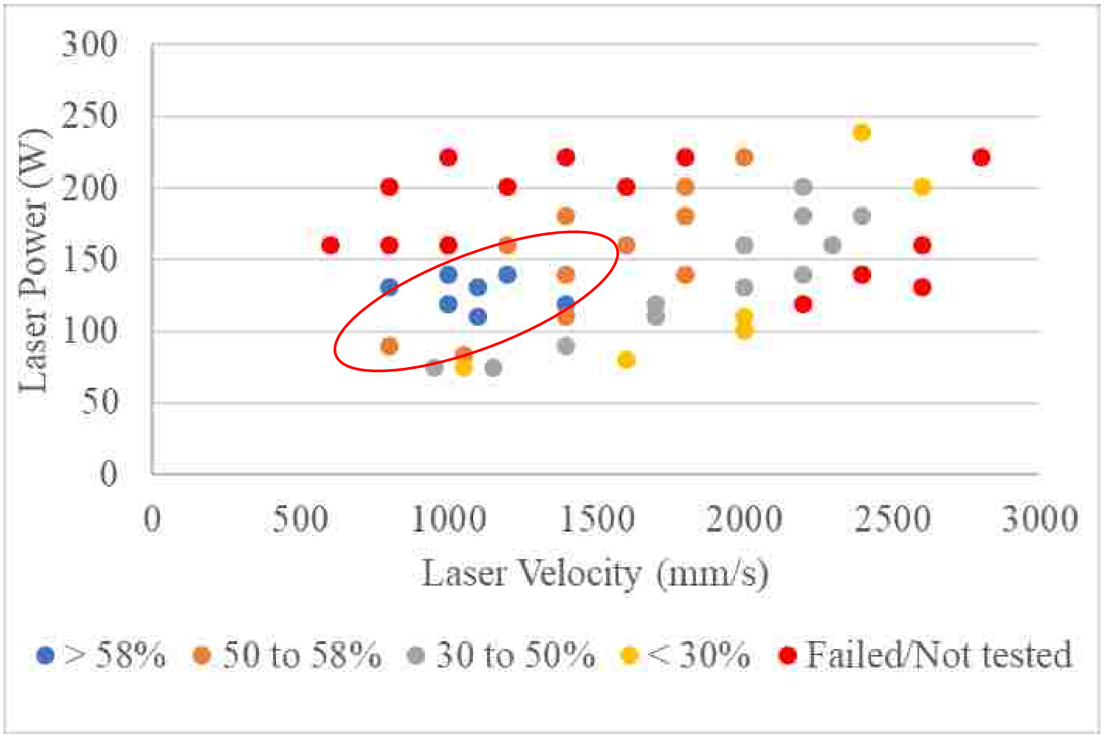

[redacted]

800 and 1400 mm/s, as seen in Figure 71.

To develop a process window, the five mechanical properties were combined in the process space to determine areas of interset. A large printable area was found in the center of the process map, as seen in Figure 72. The majority of the printable region produced arrays with the best unloading modulus and yield strength, only the arrays fabricated using laser settings on edges of the fabricated process space showed a dip in these two properties. The regions that maximized UTS and ductililty were found to partially overlap, the regions are labeled in Figure 72. This region provided an area to explore more and to determine if the results could be reproduced. To test the repeatability, plate #4 was fabricated. Plate #4 used powder from powder lot #3 at a 30.0 µm layer thickness and used corrected colinear start and stop settings.

Plate #4 was fabricated for proof of repeatability and to test out the region that maximized both UTS and ductility. This plate consisted of sixteen dog bone arrays using

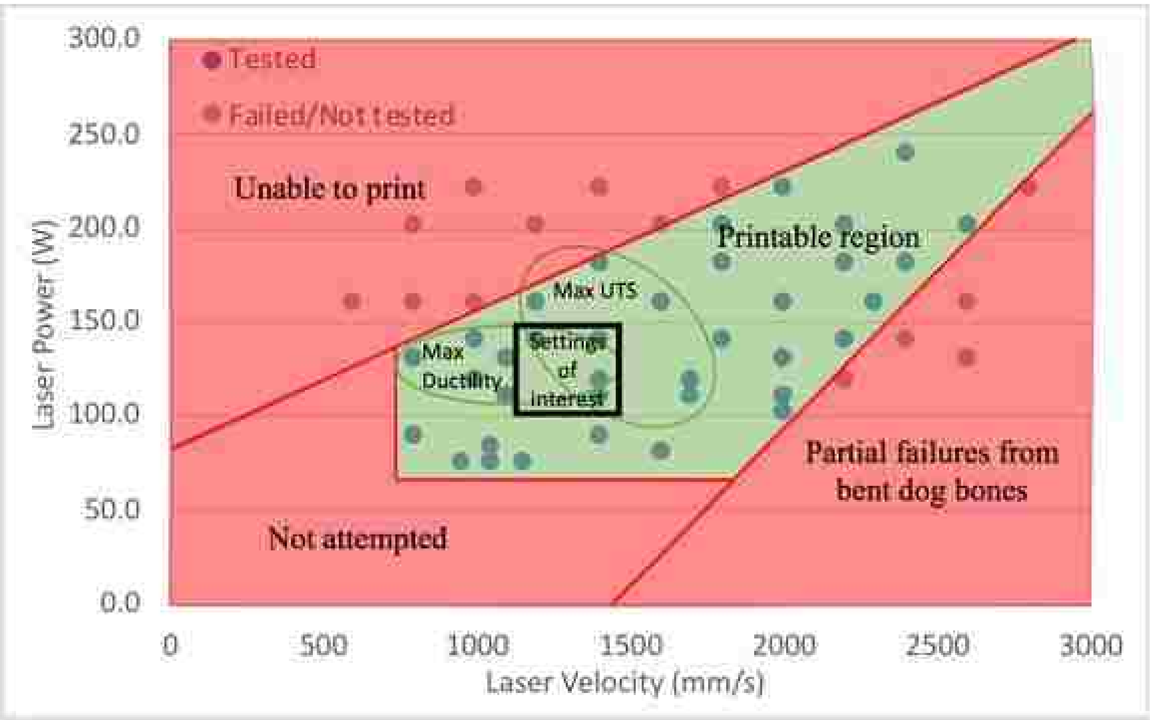

[redacted]

[redacted]

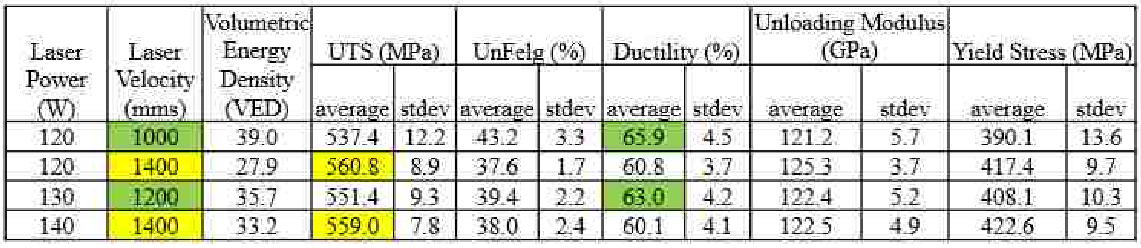

| Laser Power (W) | Laser Velocity (mms) | Volumetric Energy Density (VED) | UTS (MPa) | | UnFelg (%) | | Ductility (%) | | Unloading Modulus (GPa) | | Yield Stress (MPa) | |
|---|---|---|---|---|---|---|---|---|---|---|---|---|
| | | | average | stdev | average | stdev | average | stdev | average | stdev | average | stdev |
| 120 | 🟩 1000 | 39.0 | 537.4 | 12.2 | 43.2 | 3.3 | 🟩 65.9 | 4.5 | 121.2 | 5.7 | 390.1 | 13.6 |
| 120 | 🟨 1400 | 27.9 | 🟨 560.8 | 8.9 | 37.6 | 1.7 | 60.8 | 3.7 | 125.3 | 3.7 | 417.4 | 9.7 |
| 130 | 🟩 1200 | 35.7 | 551.4 | 9.3 | 39.4 | 2.2 | 🟩 63.0 | 4.2 | 122.4 | 5.2 | 408.1 | 10.3 |
| 140 | 🟨 1400 | 33.2 | 🟨 559.0 | 7.8 | 38.0 | 2.4 | 60.1 | 4.1 | 122.5 | 4.9 | 422.6 | 9.5 |

four combinations of laser power and velocity settings, providing four arrays for each set of laser settings. The results were promising, the arrays with the slower velocities maximized ductility (highlighted in green) and the arrays with the faster speeds maximized UTS (highlighted in yellow), shown in Table 7. This was comparable to what was observed in the original three plates and created a desire to explore more of the process map using the corrected colinear start and stop values to determine if more of the process space was repeatable or if the process window would move. To test this theory plate #5 was fabricated.

The main focus of plate #5 was to determine if correcting the colinear start and stop settings would have any effect on mechancal properties. There were twenty arrays selected for this plate mainly to fill out the process space where the colinear start and stop settings may have had an affect, away from 1400 mm/s velocities. Of the twenty arrays four failed and five partially failed, the partial failure arrays were tested where possible. The averages of the four settings from plate #4 were also included on the process maps for plate #5.

The first mechanical property investigated for these two plates was ductility. The array with the highest ductility used a laser power of 120 W with a velocity of 1000 mm/s, the ductility was 66%. This was slightly lower then the highest density from the first three plates, 69%. The region that maximized ductility was found in the same region

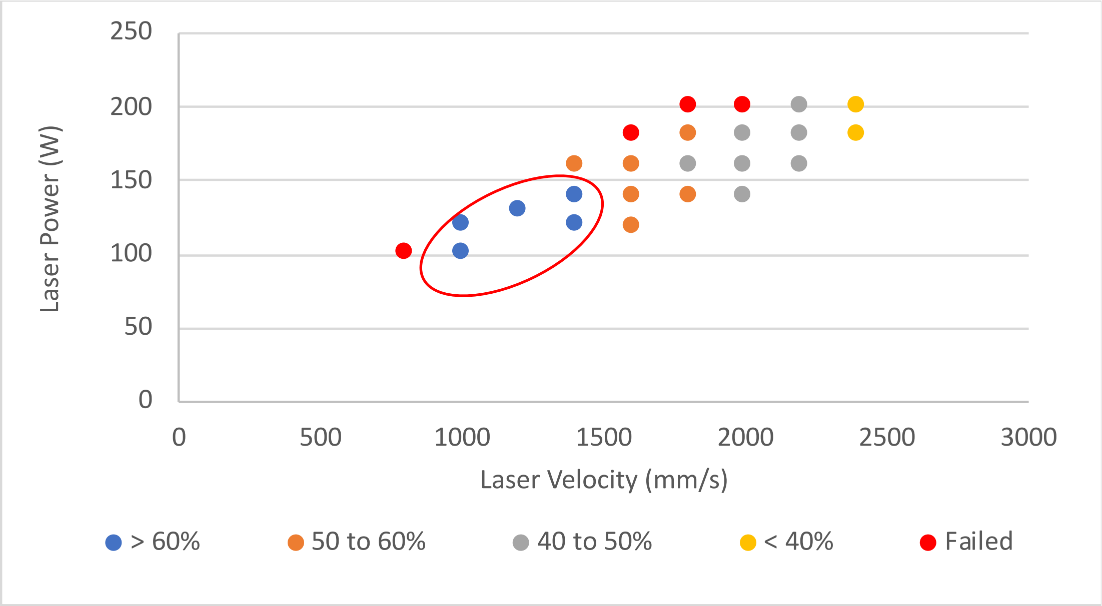

[redacted]

of the process map from the first three plates, as seen in Figure 73. A noticable trend of the reduction in ductility can be seen as laser velocity is increased in these arrays. This showed to maximize ductility lower velocities were required.

The next mechanical property investigated was UTS. The colinear start and stop setting had an effect on the geometry of the parts which was affecting the cross-sectional area of the gauge section of the first three plates. The colinear start and stop settings should have had an impact on the UTS results because of the odd cross-sectional areas from the first three plates. The maximum UTS for plates #4 and #5 was 621 MPa compared to 584 MPa from the first three plates. The array was fabricated using 200 W power at 2200 mm/s velocity and the UTS of 621 MPa was comparable to the wrought sample which had an UTS of 624 MPa. With the colinear start and stop settings corrected the region for maximizing UTS moved to higher velocities, as seen in Figure 73.

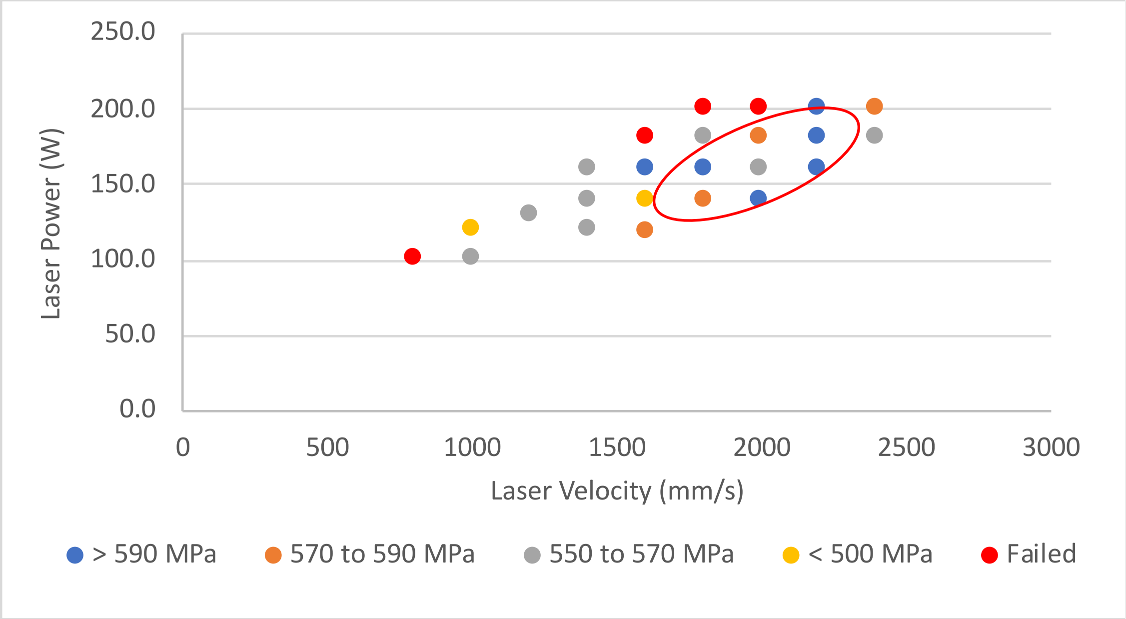

[redacted]

Overall only the mechanical properties that used cross-sectional areas in their calculations where affected by correcting the colinear start and stop settings, the changes in ductility and uniform elongation were not. An example of the fracture surface of dog bones fabricated with 180 W laser power and 220 mm/s velocity is shown in Figure 75. The dog bone on the left did not use the corrected colinear start and stop settings which resulted in a cross sectional area that appeared more like a cross than a square. This cross-sectional geometry made it very difficult for the cameras used by the HTT system to determine an accurate cross-sectional area. The HTT system estimated the the area of the uncorrected dog bone at 1.68 mm$^2$ this is well above the estimated area in the figure of 0.96 mm. This difference is more than likely why there is such a difference in the strength properties. The corrected dog bone, right figure, had a calculated cross sectional area of 1.26 mm$^2$ which was still above the estimated of 1.0 mm from measuring the fracture surface. The estimations could not be considered acurate because

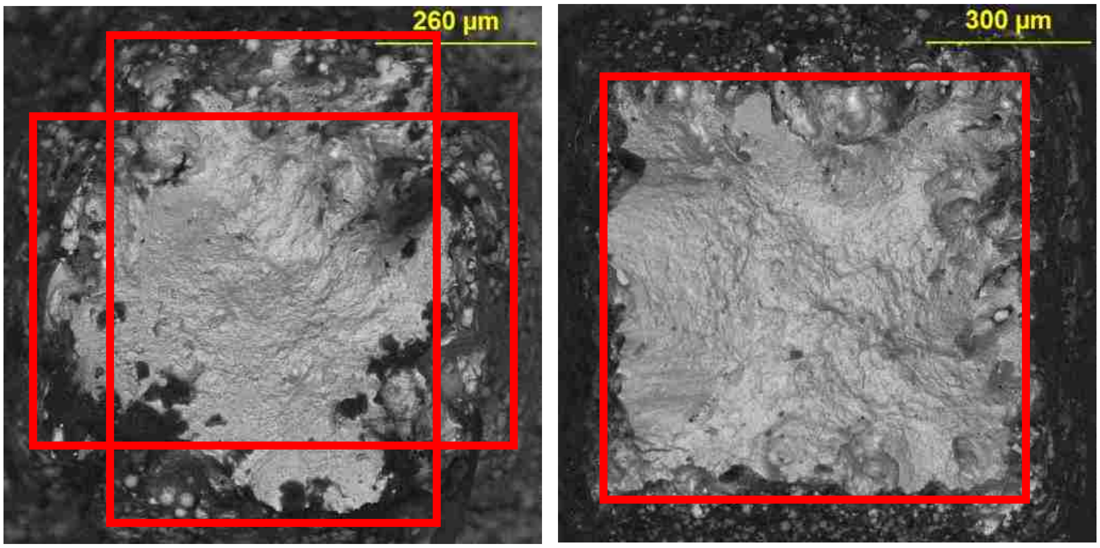

[redacted]

of necking from the tensile tests so they were not used to recalculate the strength propeties.

The comparisons of the arrays with and without the corrected colinear start and stop settings showed the UTS and yield being much higher in the corrected arrays with velocities over 1600 mm/s. The modulus was only affected in the highest velocities, and ductility being minimally affected, these results are shown in Table 8. Understanding the colinear start and stop settings was one of the most successful parts of this study.

[redacted]

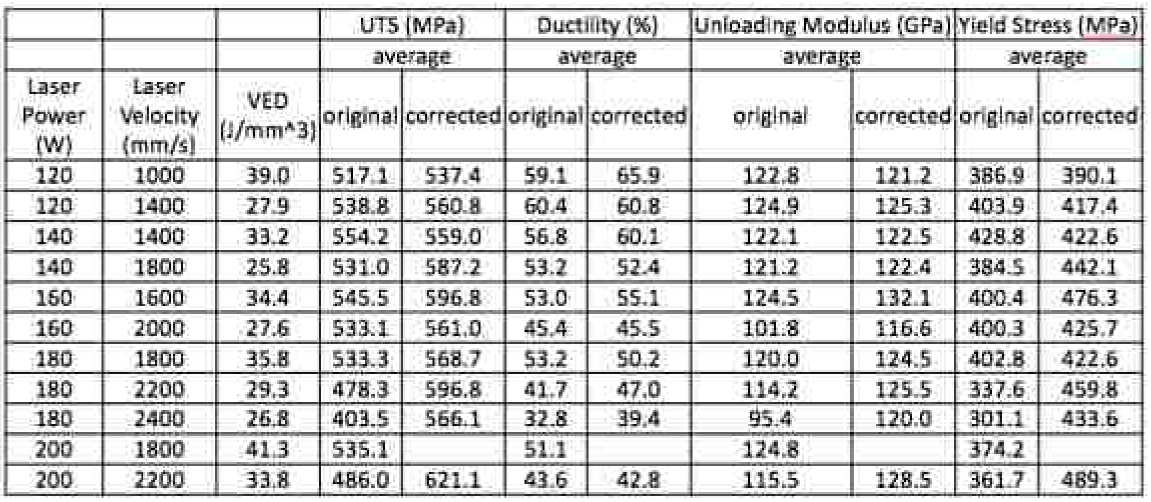

| | | | UTS (MPa) | | Ductility (%) | | Unloading Modulus (GPa) | | Yield Stress (MPa) | |
|---|---|---|---|---|---|---|---|---|---|---|
| | | | average | | average | | average | | average | |
| Laser Power (W) | Laser Velocity (mm/s) | VED (J/mm^3) | original | corrected | original | corrected | original | corrected | original | corrected |
| 120 | 1000 | 39.0 | 517.1 | 537.4 | 59.1 | 65.9 | 122.8 | 121.2 | 386.9 | 390.1 |
| 120 | 1400 | 27.9 | 538.8 | 560.8 | 60.4 | 60.8 | 124.9 | 125.3 | 403.9 | 417.4 |
| 140 | 1400 | 33.2 | 554.2 | 559.0 | 56.8 | 60.1 | 122.1 | 122.5 | 428.8 | 422.6 |
| 140 | 1800 | 25.8 | 531.0 | 587.2 | 53.2 | 52.4 | 121.2 | 122.4 | 384.5 | 442.1 |
| 160 | 1600 | 34.4 | 545.5 | 596.8 | 53.0 | 55.1 | 124.5 | 132.1 | 400.4 | 476.3 |
| 160 | 2000 | 27.6 | 533.1 | 561.0 | 45.4 | 45.5 | 101.8 | 116.6 | 400.3 | 425.7 |
| 180 | 1800 | 35.8 | 533.3 | 568.7 | 53.2 | 50.2 | 120.0 | 124.5 | 402.8 | 422.6 |
| 180 | 2200 | 29.3 | 478.3 | 596.8 | 41.7 | 47.0 | 114.2 | 125.5 | 337.6 | 459.8 |
| 180 | 2400 | 26.8 | 403.5 | 566.1 | 32.8 | 39.4 | 95.4 | 120.0 | 301.1 | 433.6 |
| 200 | 1800 | 41.3 | 535.1 | | 51.1 | | 124.8 | | 374.2 | |
| 200 | 2200 | 33.8 | 486.0 | 621.1 | 43.6 | 42.8 | 115.5 | 128.5 | 361.7 | 489.3 |

Using all the data gathered from the tensile area testing a final process map was constructed. This process map showed there is a large window in the center of the map where dog bones arrays were succesfully fabricated, as shown in Figure 76. The process window did still encompase a wide range of laser powers and velocities for use. The printable region of the process map was even able to be split into two regions, one region that maximized density and the other that maximized UTS.

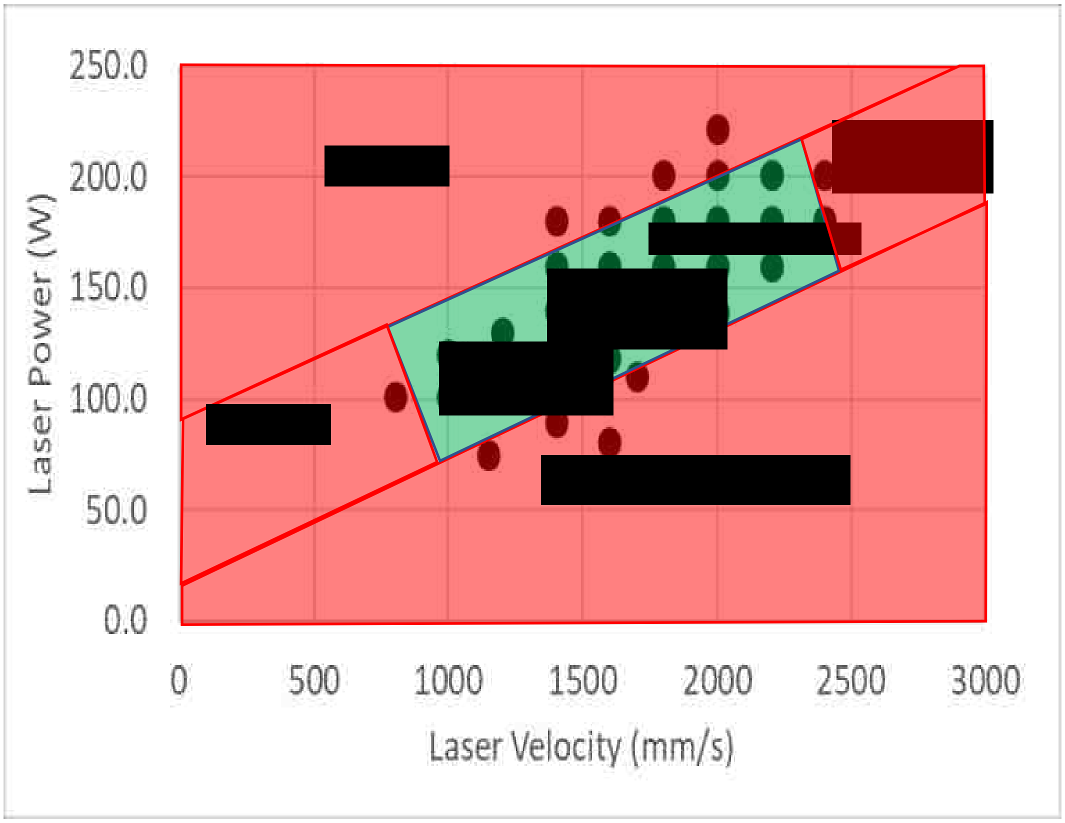

[redacted]

## Section 4.5: Charpy Samples

The final set of experiments included only five samples but were fabricated to capture mechanical properties that hadn't been investigated throughout this study. The Charpy samples provided properties including density, Rockwell B hardness, and Charpy impact. Four of the samples used the same laser settings as tensile plate #4 which was the region of interest for the tensile arrays. The fifth used the updated baseline laser settings provided by the manufacturer to compare the baseline with optimized settings. The updated baseline settings were 113 W laser power and 1400 mm/s velocity. The laser settings used along with the results can be seen in Table 9. Other parameters include powder from lot #1, 1.0 mm focus offset, and a 30.0 μm layer thickness.

The results from these five samples did not show any strong trends between laser settings and properties. The density of the AM samples were nearly idenical at each of the laser setting and were 99% denste compared to literature [25]. The Rockwell B hardness also wasn't affected by the laser settings but did out perfom literature. One of the Charpy tests was different from the others, the sample that used the highest power exhibited the lowest impact strength. The other four settings were within ~5 J and out performed literature by at least 15 J. The lack of samples made it hard to draw any conclusions for the Charpy results but the 99% dense parts showed that these laser settings have been optimized for density.

[redacted]

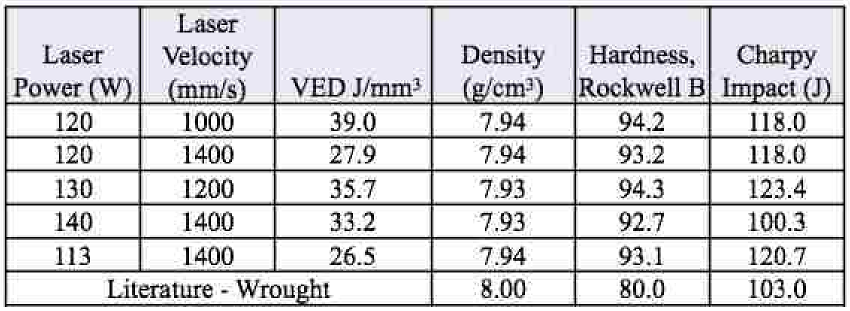

| Laser Power (W) | Laser Velocity (mm/s) | VED J/mm$^3$ | Density (g/cm$^3$) | Hardness, Rockwell B | Charpy Impact (J) |
|---|---|---|---|---|---|
| 120 | 1000 | 39.0 | 7.94 | 94.2 | 118.0 |
| 120 | 1400 | 27.9 | 7.94 | 93.2 | 118.0 |
| 130 | 1200 | 35.7 | 7.93 | 94.3 | 123.4 |
| 140 | 1400 | 33.2 | 7.93 | 92.7 | 100.3 |
| 113 | 1400 | 26.5 | 7.94 | 93.1 | 120.7 |
| Literature - Wrought | | | 8.00 | 80.0 | 103.0 |

# Chapter 5: Model Validation

There were two models introduced back in chapter 2 of this study, the Rosenthal model and the prediction of lack of fusion model. The Rosenthal model was used to predict the melt pool width and depth at various laser power and velocity settings. The prediction of lack of fusion model was used for predicting if laser power and velocity settings would produce a fully dense part. The Rosenthal model was compared to the experimental results from both sets of line scan experiments, on plate and on AM pad. The lack of fusion (density) model was compared using line widths and depths from both the Rosenthal model and the line scan experiments' results. This was used to make comparisons against the density results from the cubes.

The Rosenthal model predicted a heat distribution from a moving heat source which provided a model to compare a single laser pass line scan to. This heat distribution was in the form of a semi-circle which was very comparable to the lines on plate experiments, but the lines on pad produce more of a circular shaped melt pool. The lines on pad also produced lines that were difficult to accurately measure a width and depth of the lines. Both sets of lines did have a cross-sectional area which could accurately be measured so the cross-sectional areas were chosen to make a comparison against the Rosenthal model. Five plots were produced, one for each power setting, plotting melt pool area against the laser velocity, as seen in Figure 77. The comparisons showed at low power, 25 W, the model over predicted the melt pool area. Slower velocities were under predicted by the model, this was because the slower velocities were found to create melt pools that were keyholing. The model predicts a semi-circle which doesn't account for

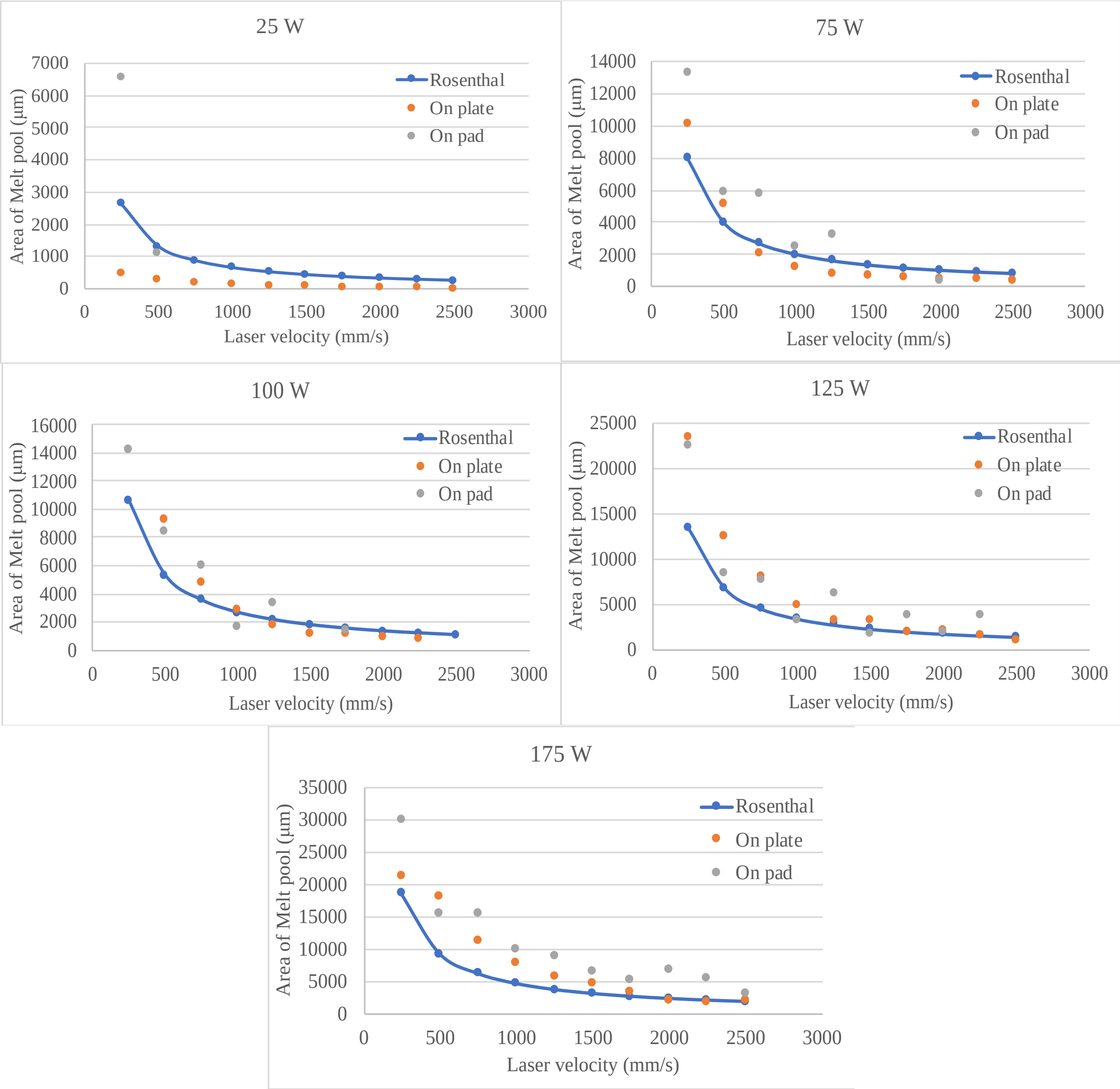

[redacted]

keyholing.  The model did show a similar trend line between the model and the experimental results.  While the Rosenthal model did not accurately predict all the areas, it did show that it could be used as a tool to generate results that could be used as a starting point for process development.

The melt pool widths and depths predicted by the Rosenthal model were used in the density model to predict part density at the various laser settings.  The inputs into the density model included line width and depth, layer thickness, and hatch spacing.  A layer

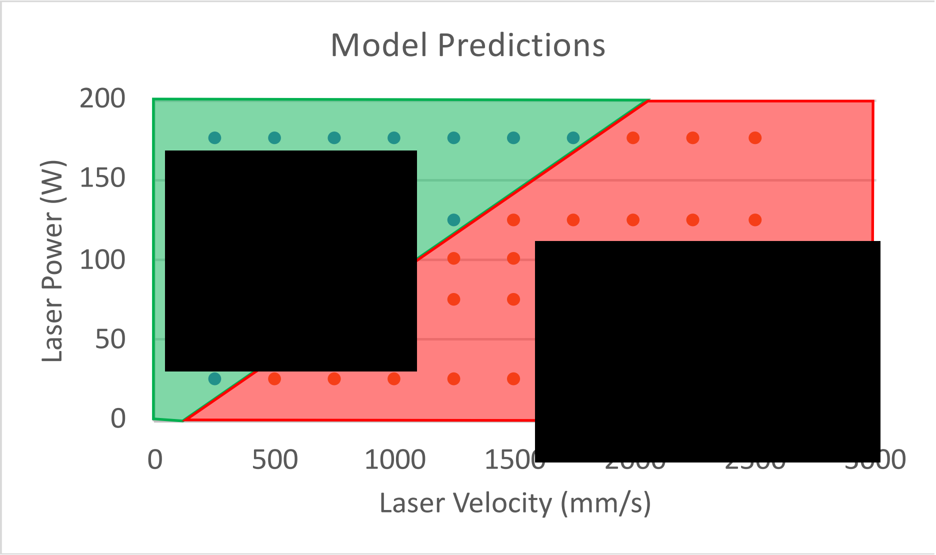

[redacted]

[redacted]

[redacted]

thickness of 30.0 μm and a hatch spacing of 50.0 μm was used. The density model only predicts whether the part is expected to be fully dense or not, it doesn't predict actual density or a percent dense. The results from the model can be seen in Figure 78. The results showed that the baseline laser settings with 107 W power and velocity at 1400 mm/s would not produce a dense part.

Density data was collected from the cube experiments which was compared against the density model. The density results for cube group #2 was used as a comparison for the density model because that group used a layer thickness of 30.0 μm and a hatch spacing of 50.0 μm. Figure 80 shows the comparison from the density model against the experimental results. The black line denotes the separation of the fully and not fully dense predicted parts, the green area was where the cubes were found to be at least 97% dense from the experimental results, and the red area was where the cubes were less than 97% dense. The comparison shows some accuracy in predicting cubes that were at least 97% dense except in low powers.

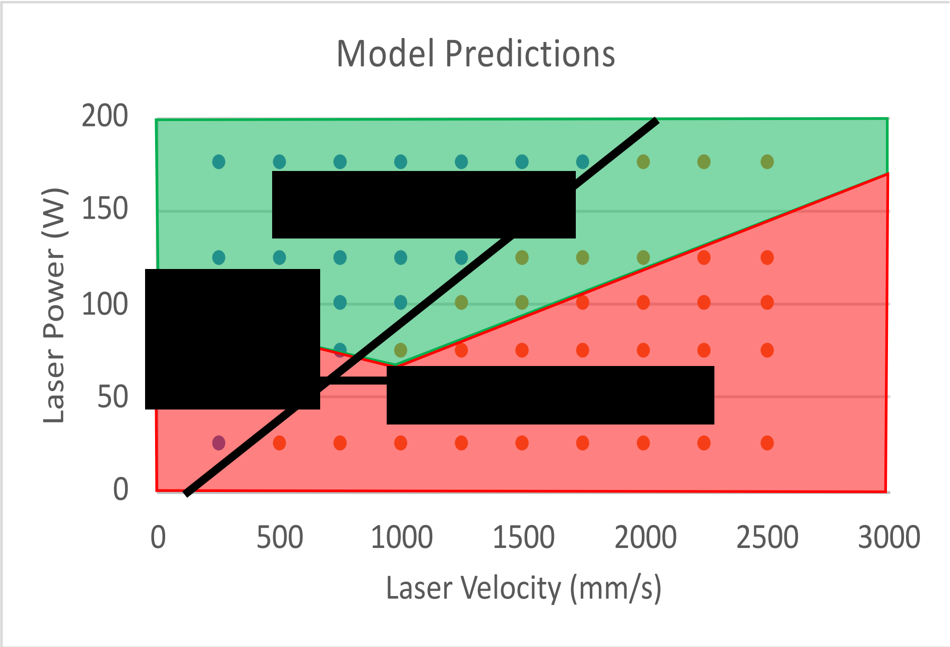

[redacted]

To test if the density model would produce a more accurate prediction, the melt pool widths and depths that were measured from the lines on plate were used as inputs in the model. Using the actual melt pool dimensions was expected to provide a more accurate density prediction and as seen in Figure 79, and it did. While the model was

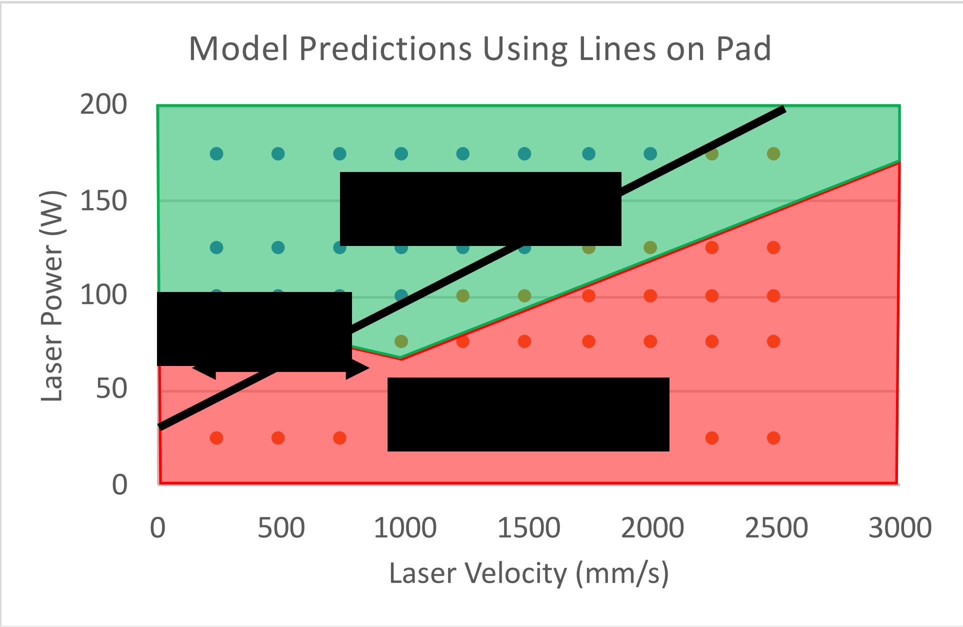

[redacted]

supposed to predict if process settings would fabricate a fully dense part, it was coming close to predicting a 97% dense part. The lines on pad measurements were not used in the density model because of the difficulty in determining accurate measurements. The experimental results provided encouragement that the models could be used as a starting point for process optimization and/or development for other AM printers and other metal powders.

# Chapter 6: Summary of Experimental Results

This study investigated several process variables including laser power, velocity, focus offsets, layer thickness, and powder size. Laser power was measured to determine an accurate value so relying on the manufacturer's percent of maximum laser power was not needed and it was found to be incorrect. The laser beam diameter was then measured to determine a point where it remained constant over time, this provided the zero-focus offset. The powder was analyzed to determine the size differences in the powder lots. These pre-experimental process variable characterizations provided the ability to make recommendations based on the experimental results for this study. The laser velocity was difficult to characterize because of the travel speed of the laser so the velocity was assumed to be accurate. Accuracy in the layer thickness is also difficult to determine to because of the micron height scale, so layer thickness was also assumed to be accurate.

The variable that showed it may have the largest influence of part fabrication was the laser focus offset. The focus offsets were characterized by measuring the laser beam diameter and how it changed over time. The offset with the lowest average diameter and lowest standard deviation was selected to be the zero-offset point, see Figure 10. There were three experiments that investigated the effects of focus offsets including line scans, area pads, and cubes. The lines scans on plate and AM pad investigated eleven different offsets in 0.5 mm increments from 1.5 mm below focus to 3.5 mm above focus at 100 W laser power and 1500 mm/s velocity. The line scan on plate showed the offset did have an influence on the penetration depth of the line which was maximized between 1.0 – 2.0 mm above the focus point, see Figure 27. The metallography for the lines on pad only captured the lines with offsets from 1.5 – 3.5 mm above focus, see Figure 31, and the visual inspection showed the lines above the focal point as being close to continuous. The area pads used five sets of laser power and velocity settings at five different focus offsets to investigate the influence of offsets on surface roughness. The focus offsets were zero to 2.0 mm above focus in 0.5 mm increments. Again, the results showed 1.0 – 2.0 mm provided the best surface roughness values across all the laser settings investigated, see Figure 37. The final experiment investigated the influence of focus offsets on density. Nine cubes were fabricated using the baseline settings at focus offsets from 2.0 mm below focus to 2.0 mm above focus. The results showed that the cube at 2.0 mm above focus had the highest density, but the surface roughness was maximized between 1.0 – 1.5 mm above focus. All these results pointed to the same conclusion, the laser focus offset should be set between 1.0 – 2.0 mm above focus.

The second most influential variable was the laser power. Laser power was investigated in all the experiments in this study. The lines on pad showed there was a minimum amount of power required to fuse a layer of powder to a previous layer. This was shown by only the two slowest velocities of the 25 W lines fused to the AM pad, see Figure 28. The area pads showed laser power had a large influence on the surface roughness. Nearly every pad that had a laser power below 100 W had a $S_a$ value above 15.0 μm, see Figure 34. The cubes also showed a threshold at 100 W laser power. The cubes that used 100 W produced densities over 97% dense and a quality surface finish, see Figure 46. The tensile arrays showed that too much power also had an influence. Too much power caused the gauge sections to swell which caused the array to fail. The limited number of Charpy samples also showed too high of a power had a negative effect on the Charpy impact value, see Table 9. These experimental showed the laser power setting should be at least 100 W with the upper range being selected by taking the velocity into account.

That leads into the next important process variable, laser velocity. Like laser power, laser velocity was investigated in every set of experiments. The line scans showed when keeping laser power constant the melt pools started in a keyholing regime at slow velocities and transition from smooth to balling as velocity is increased, see Figure 25 and Figure 30. In the area pads it was shown slower velocities typically produced pads with poor form. The cube experiments showed when keeping power constant, slow and fast velocities produced cubes with poor finishes with velocities in the middle providing high densities and surface finishes, see Figure 46. The tensile arrays are where the velocities really showed their influence. Slow velocities maximized ductility and fast velocities produced high strength properties, see Figure 76. The limited amount of Charpy samples did not show any velocity influences on the Charpy experiments. These experimental results showed that selected velocities should be part specific, depending on geometry and requested mechanical properties. Laser velocities should also take laser power into account.

The final two variables, layer thickness and powder size, were only investigated in the cube experiments. For layer thickness, the results showed that if a thicker layer thickness is used, laser power should be increased for density to remain constant, see Figure 52. Reducing velocity didn’t show it had more of an impact of density as power did, this provided another data point to support laser power being more influential of a variable over velocity, see Figure 51. For powder size, the only noticeable effect was on the surface finish when all other settings are held constant. The powder with the larger size produced parts with a poor surface finish when compared to parts with the powder with a smaller size. These results showed the laser has the largest influence on part fabrication.

A set of recommended process settings was found to depend on what properties are being requested. The laser focus offset should be set to 1.0 – 2.0 mm above focus, laser power over 110 W, and a velocity 1000 and 1600 mm/s for fabricating a high-density part with a quality finish. If ductility is more important, velocity should be set to 1000 mm/s. If high strength is being requested and ductility is not important the laser power should be near 160 W with a velocity near 2000 mm/s. If strength and ductility is being requested a laser power of 120 – 140 W with a velocity of 1400 - 1600 mm/s should be used.

# Chapter 7: Conclusion and Future Work

## Section 7.1: Conclusion

The focus of this study was to investigate the influence of process variables using an additive manufacturing laser powder bed fusion printer. The influence of several process variables on the physical and mechanical properties of fabricated parts were shown. Nearly 1000 samples were measured and/or tested in this study providing a large data set to support these conclusions.

The first conclusion which was shown was a set of simple models can be used to develop future process studies. The Rosenthal model was shown it can be used to predict melt pool areas on both a flat plate and on an AM pad. Using the melt pool data from the lines on plate, a density model was able to nearly predict 97% dense parts. These models were not 100% accurate but they can provide a starting point for future studies.

The second conclusion was process variables do have an influence on physical properties. Laser powers under 100 W produced parts with rougher surface finishes and low density. Powder particle size also has an influence of on surface finish with the powder with larger particles produced parts with a higher surface roughness. Parts with high density required using a laser power over 100 W but required an increase in power as velocity was increased.

The third conclusion was mechanical properties could be customized using laser settings. It was shown slower velocities, 1000 mm/s, increased ductility and faster velocities, > 2000 mm/s, increased strength. These regions also produced different grain sizes with the low velocities having larger grains and higher velocities having smaller grains. More research is needed to make correlations between the grain sizes and mechanical properties.

## Section 7.2: Future Work

This study covered several types of experiments with many samples tested for physical and mechanical properties, but there is still more to investigate. Laser power, velocity, focus offsets, and layer thickness are not the only process settings that could have been investigated. EBSD provided the microstructure of the cubes but were not fully studied. The Charpy samples were barely introduced and showed some possibilities.

There are at least two other laser settings that may have a large influence on the process. The first is the hatch spacing which was set to be about half of the laser beam diameter, 50.0 μm. A smaller hatch spacing would provide more of an overlap of the laser on each pass. Decreasing hatch spacing could provide more dense parts with a higher surface finish. The other laser setting is scan strategy, this study only used a normal scan. Other scan strategies include hexagons, concentric, and continuous mesh. Hexagon scanning fires the laser in hexagon "islands" to reduce the heat input into the part. Concentric prints in circles and is mainly used for round parts. Continuous mesh fires the laser multiple times on each layer, the second time is at a 90-degree angle compared to the first pass. These other scan strategies need to be investigated to determine if they have an influence on physical and/or mechanical properties.

About 40 cubes were sectioned to have their microstructure investigated by EBSD. This study only visually inspected the grain sizes and orientations to make conclusions on the influence of process variables on microstructure. The raw data from the EBSD images need to be analyzed to determine actual grain sizes to determine if the process settings do have an influence on the microstructure.  EBSD should also be performed on the tensile arrays to determine if the differences in the mechanical properties are influenced by the grain sizes.  Higher quality EBSD images should also be acquired for the ability to measure the dislocation densities of the parts.

Before the five Charpy samples were fabricated there was over one thousand other parts fabricated for testing.  The Charpy block showed multiple tests could be performed on the same sample including surface roughness measurements, density, hardness, and Charpy impact.  These tests can be performed quickly and possibly provide an idea if the process out of bounds.  Future work should include fabricating Charpy blocks across the process space to determine if changes in the process variables have an influence on the test provided by the Charpy samples.

# References

[1] D. L. Bourell, M. C. . Leu, and D. W. Rosen, “Identifying the Future of Freeform Processing 2009,” *Rapid Prototyp. J.*, p. 92, 2009.

[2] C. Kamath, “Data mining and statistical inference in selective laser melting,” *Int. J. Adv. Manuf. Technol.*, vol. 86, no. 5–8, pp. 1659–1677, 2016.

[3] M. Hedges and N. Calder, “Near net shape rapid manufacture & repair by LENS,in: Cost Eff. Manuf. via Net-Shape Process,” *Meet. Proc. RTO-MP-AVT-139*, vol. 2, p. 13, 2006.

[4] W. Frazier, “Direct digital manufacturing of metallic components: vision and roadmap,” *Solid Free Form Fabr. Proc.*, pp. 717–732, 2010.

[5] W. Hofmeister, M. Wert, J. Smugeresky, J. A. Philliber, M. Griffith, and M. Ensz, “Investigating Solidification with the Laser-Engineered Net Shaping (LENSTM) Process,” *JOM*, vol. 51, no. 7, 1999.

[6] T. DebRoy *et al.*, “Additive manufacturing of metallic components – Process, structure and properties,” *Prog. Mater. Sci.*, vol. 92, pp. 112–224, 2018.

[7] M. Grasso and B. M. Colosimo, “Process defects and in situ monitoring methods in metal powder bed fusion: A review,” *Meas. Sci. Technol.*, vol. 28, no. 4, 2017.

[8] M. Tang, P. C. Pistorius, and J. L. Beuth, “Prediction of lack-of-fusion porosity for powder bed fusion,” *Addit. Manuf.*, vol. 14, pp. 39–48, 2017.

[9] W. E. King *et al.*, “Observation of keyhole-mode laser melting in laser powder-bed fusion additive manufacturing,” *J. Mater. Process. Technol.*, vol. 214, no. 12, pp. 2915–2925, 2014.

[10] W. E. Frazier, “Metal additive manufacturing: A review,” *J. Mater. Eng. Perform.*,

vol. 23, no. 6, pp. 1917–1928, 2014.

[11] M. Van Elsen, F. Al-Bender, and J. P. Kruth, “Application of dimensional analysis to selective laser melting,” *Rapid Prototyp. J.*, vol. 14, no. 1, pp. 15–22, 2008.

[12] D. Gu and Y. Shen, “Balling phenomena in direct laser sintering of stainless steel powder: Metallurgical mechanisms and control methods,” *Mater. Des.*, vol. 30, no. 8, pp. 2903–2910, 2009.

[13] U. Scipioni Bertoli, A. J. Wolfer, M. J. Matthews, J. P. R. Delplanque, and J. M. Schoenung, “On the limitations of Volumetric Energy Density as a design parameter for Selective Laser Melting,” *Mater. Des.*, vol. 113, pp. 331–340, 2017.

[14] J. P. Kruth, L. Froyen, J. Van Vaerenbergh, P. Mercelis, M. Rombouts, and B. Lauwers, “Selective laser melting of iron-based powder,” *J. Mater. Process. Technol.*, vol. 149, no. 1–3, pp. 616–622, 2004.

[15] J. L. Beuth *et al.*, “Process Mapping for Qualification Across Multiple Direct Metal Additive Manufacturing Processes,” *Proc. Solid Free. Fabr. Symp.*, pp. 655–665, 2014.

[16] C. Kamath, B. El-Dasher, G. F. Gallegos, W. E. King, and A. Sisto, “Density of additively-manufactured, 316L SS parts using laser powder-bed fusion at powers up to 400 W,” *Int. J. Adv. Manuf. Technol.*, vol. 74, no. 1–4, pp. 65–78, 2014.

[17] D. Wang, Y. Yang, X. Su, and Y. Chen, “Study on energy input and its influences on single-track,multi-track, and multi-layer in SLM,” *Int. J. Adv. Manuf. Technol.*, vol. 58, no. 9–12, pp. 1189–1199, 2012.

[18] Q. S. Wei, X. Zhao, L. Wang, R. Di Li, J. Liu, and Y. S. Shi, “Melting, Effects of the Processing Parameters on the Forming Quality of Stainless Steel Parts by

Selective Laser," *Adv. Mater. Res.*, vol. 189–193, pp. 3668–3671, 2011.

[19] J. Metelkova, Y. Kinds, K. Kempen, C. De Formanoir, and A. Witvrouw, "On the in fl uence of laser defocusing in Selective Laser Melting of 316L," *Addit. Manuf.*, vol. 23, no. April, pp. 161–169, 2018.

[20] A. B. Spierings and G. Levy, "Comparison of density of stainless steel 316L parts produced with selective laser melting using different powder grades," in *In: Bourell D (ed) Symposium, twen- tieth annual international solid freeform fabrication: an additive manufacturing conference. University of Texas at Austin, Austin*, pp. 342–353.

[21] B. Liu, R. Wildman, C. Tuck, I. Ashcroft, Hague, and Richard, "INVESTIGATION THE EFFECT OF PARTICLE SIZE DISTRIBUTION ON PROCESSING PARAMETERS OPTIMISATION IN SELECTIVE LASER MELTING PROCESS," in *International solid freeform fabrication symposium: an additive manufacturing conference. University of Texas at Austin, Austin*, 2011, no. mm, pp. 227–238.

[22] M. Scaggs and G. Haas, "Thermal lensing compensation optics for high power lasers," no. February 2011, p. 79130C, 2011.

[23] D. Rosenthal, "Mathematical Theory of Heat Distribution During Welding and Cutting," *Weld. J.*, vol. 20, no. 5, pp. 220–234, 1941.

[24] ASTM International B962-13, "Standard Test Methods for Density of Compacted or Sintered Powder Metallurgy ( PM ) Products Using Archimedes ' Principle Designation: B962 − 13," *ASTM B. Stand.*, pp. 1–7, 2013.

[25] Matweb, "ASM Aerospace Specifaction Metals Inc." .